UCLA
UCLA Electronic Theses and Dissertations

Title
Mechanisms Regulating PGC Specification and Epigenomic Reprogramming

Permalink
https://escholarship.org/uc/item/57v5t9st

Author
Lowe, Matthew Gregory

Publication Date
2022

Peer reviewed|Thesis/dissertation

eScholarship.org Powered by the California Digital Library
University of California

UNIVERSITY OF CALIFORNIA

Los Angeles

Mechanisms Regulating PGC Specification and Epigenomic Reprogramming

A dissertation submitted in partial satisfaction of the requirements for the degree Doctor of Philosophy in Molecular Biology

by

Matthew Gregory Lowe

2022

© Copyright by
Matthew Gregory Lowe
2022

ABSTRACT OF THE DISSERTATION

Mechanisms Regulating PGC Specification and Sex-Specific Differentiation

by

Matthew Gregory Lowe

Doctor of Philosophy in Molecular Biology

University of California, Los Angeles, 2022

Professor Amander Therese Clark, Chair

Infertility is a broad disorder with numerous causes including physical, genetic and environmental. While techniques are currently in use to address certain causes of infertility, such as *in vitro* fertilization and hormonal therapies, there is currently no treatment option for those who are either unable to make or no longer possess viable gametes. Recently, advances have been made in the development of *in vitro* gametogenesis which, if perfected, promises an option for gametes to be derived from a patient's own tissue. In order to bring this technique to fruition, further research is needed into the mechanics directing the specification and epigenetic reprogramming of the earliest stage of the germline, the primordial germ cells (PGCs).

Mammalian PGCs are specified early in embryonic development and give rise to the entire adult germline. Following specification, PGCs undergo epigenetic reprogramming in order to establish a permissive epigenetic landscape for proper gametogenesis prior to differentiation into either oocyte or spermatogonial progenitors. Any errors in either of these processes can result in the complete loss of the germline and infertility. In order to better understand the mechanisms underlying PGC development, we utilized the *in vitro* PGC-like cell (PGCLC) differentiation to study human PGC specification and PGC-specific conditional knockout mice to

assess epigenetic remodeling. In our studies into specification, we further characterized the differences between mouse and human PGC specification mechanisms. Using CRISPR/Cas9 gene editing we identified that EOMES directs human PGCLC specification, whereas in the mouse this role is accomplished by T. Our exploration into epigenetic reprogramming utilized a Cre/lox driven PGC-specific conditional knockout mouse to assess the role of epigenetic regulatory proteins during PGC differentiation. We used two knockouts, the first being UHRF1 which interacts with DNMT1 to promote DNA methylation maintenance and the second being EED, a key component of PRC2 which adds the repressive H3K27me3. Through this we identified that while UHRF1 appears to play no role in regulating the PGC stage of germline development, it is necessary for the viability of the spermatogonial stem cell population within the adult testes. In the case of EED, we identified that PRC2 is essential for regulating the timing of sex-specific differentiation in PGCs as well as a novel role for H3K27me3 in X chromosome decompensation within the embryonic testis. Finally, we identified a dual enrichment of H3K27me3 and DNA methylation within the promoters of gametogenesis genes at the time of PGC specification from the mouse epiblast. This provides an exciting glimpse into the complex interactions between the epigenetic regulatory networks that direct PGC differentiation. Further work will need to be conducted to identify the extent of these epigenetic regulator interactions in human PGCs and to apply these findings into developing better methods to more accurately recapitulate human PGC differentiation *in vitro*.

The dissertation of Matthew Gregory Lowe is approved.

Patrick Allard

Siavash Kurdistani

Hanna Mikkola

Jesse Zamudio

Amander Therese Clark, Committee Chair

University of California, Los Angeles

2022

Dedication

To my family and friends, both old and new. I could not have accomplished any of this work without the love, support and guidance that you provided throughout these past few years.

Table of Contents

ABSTRACT OF THE DISSERTATION……....ii
Committee Page…….….iv
Dedication……v
Table of Contents……....vi
List of Figures……..……..vii
List of Tables……vii
Acknowledgements……..viii
VITA……..xii

Chapter 1 – Introduction……..1
Importance of the germline……2
Germline Specification……..3
PGC DNA Demethylation…….....5
PGC Chromatin Mark Reorganization……..6
References…….....8

Chapter 2 – Germline Competency of Human Embryonic Stem Cells Depends on Eomesodermin……12
Summary…….....…….13
Introduction……..……..……...14
Material and methods…….……...14
Results ……..…….……...17
Discussion……...……..…….……...21
References…....……...……...23

Chapter 3 – UHRF1 is not Required for Germline Maturation……...……..25
Summary…….....…….26
Introduction……...26
Results…….....…….29
Discussion…….....……...33
Materials and Methods…….....……....36
References…….....……...39

Chapter 4 – EED is Required for Primordial Germ Cell Differentiation in the Embryonic Gonad……..……44
Summary…….....…….46
Introduction……...46
Results…….....…….50
Discussion…….....……...61
Materials and Methods…….....……....68
References…….....……...100

Chapter 5 – Conclusion……..……..……..……...108
References…….....……...112

List of Figures

Figure 2-1: Analysis of ITGA6/EPCAM and TNAP/cKIT populations in human prenatal gonads……....…………………………………………………..…………18
Figure 2-2: Germline competency varies between independent hESC lines……..……..………20
Figure 2-3: TGFb and. WNT signaling are required for PGCLC induction from hESCs..……..……....21
Figure 2-4: EOMES is required for PGCLC induction from hESCs.................……..……......22

Figure 3-1: UHRF1 is not required for embryonic germline proliferation……..……..………...29
Figure 3-2: UHRF1 is not required for XX germline maturation……..……..…………………31
Figure 3-3: UHRF1 required for the maintenance of spermatogonial stem cells……..………...33

Figure 4-1: Graphical Abstract……..……..…………………………………………………..…...79
Figure 4-2: EED regulates PGC number within the embryonic gonads……..……..…………....80
Figure 4-3: EED regulates PGC differentiation in the testis……..……..………………………81
Figure 4-4: EED regulates PGC differentiation in the ovary……..……..……………………....82
Figure 4-5: Gametogenesis genes are co-enriched for H3K27me3 and DNA Methylation in the epiblast……..……..……..……..……..……..……..……..……..……..……..……..…………..83
Figure 4-6: Gametogenesis genes are co-regulated by EED and DNMT1……..……..………..84
Figure 4-7: Model for EED and DNMT1 Co-regulation of Gametogenesis Genes……..……..……..……..……..……..……..……..……..……..……..……..……..85
Figure 4-8: ECKO embryos lose H3K27me3 in PGCs by E11.5……..……..…………...…86
Figure 4-9: Global epigenetic remodeling in PGCs following deletion of EED……..……..……..……..……..……..……..……..……..……..……..……..…….87
Figure 4-10: Loss of EED alters expression of genes but not transposons in PGCs……..……..……..……..……..……..……..……..……..……..……..……...…88
Figure 4-11: Ovarian ECKO PGCs precociously differentiate……..……..……………..…....89
Figure 4-12: Late demethylating promoters are enriched for both H3K27me3 and DNA methylation...……..……..……..………........90
Figure 4-13: Overlapping ECKO and DCKO DEGs show similar regulation..........................91
Figure 4-14: Full western blots……..……………………………………………………....93

List of Tables

Table 2-1: Table of antibodies used...37
Table 2-2: Table of genotyping primers used……..………...39

Table 4-1: Table of antibodies used……..……..……..……..……..……..……..…………....92
Table 4-2: Table of genotyping primers used……..……..………………………………….....92

Acknowledgements

This work would not have been possible without the support and guidance that I received throughout my PhD. I would like to thank my thesis advisor, Dr, Amander Clark, for her boundless enthusiasm for research and willingness to allow me to take my thesis in directions that I found interesting. Even in the worst of times she was always there to provide support and keep me moving forward. Her dedication to research and building a strong and supportive lab environment continue to inspire me to grow as a scientist.

I would also like to thank the members of the Clark lab who contributed to my project, if not physically than emotionally, and helped keep everything moving despite the pandemic. I would first like to thank my rotation mentor, Dr. Di Chen, who has since started his own lab. His ability to conduct high level research, train and manage of a team of high-level scientists on top of maintaining a family life is nothing short of inspiring and I wish him all the best with his future endeavors. I would also like to thank Hunter Hu who taught me everything I know about mouse embryonic microdissection and helped establish the mouse lines used in these experiments. Thank you to Dr. Sissy Wamaitha and Dr. Fei-man Hsu for their support and expertise in all things molecular and computational. I would also like to thank my undergraduate mentee, Isaac Gorgy, for helping me catalogue and image the mountain of slides that we generated. Thank you Dr. Tsotne Chitiashvili for sharing his expertise on the X chromosome and aiding in data analysis. Thank you to Tim Hunt for being the best lab manager that I have ever had the privilege of working with. Thank you Jon DiRusso and Dr. Varsha Desai for the moral support and guidance during our mouse team meetings. Thank you to Drs. Enrique Sosa, Grace Hancock, Erica Pandolfi and Joanna Gell for their advice throughout the PhD. Finally, I would like to thank the past and current lab undergraduates for your enthusiasm towards research:

Ernesto Rojas, Jared Faith, Esme Villavicencio, Marianna Aslanyan, Jill Zimmerman, Yao Chang Tan, Grace Bower, Allison Wang, Shefali Varma Qiu Ya Wu, Aryan Sood, Nicole Agranonik, Alexander Robbins, Mary Jasmine Lara and Amanda Hagen.

I would like to thank my committee members, Drs. Patrick Allard, Siavash Kurdistani, Hanna Mikkola, and Jesse Zamudio for their support and guidance throughout my research. I would especially like to thank Jesse Zamudio who helped me with statistical analysis and for being an excellent mentor during my rotation in his lab. Additionally, I would like to Dr. Jefferey Long for being a wonderful home area director and guiding us through the pandemic. Thank you to Jessica Scholes, Jeffery Calimlim and Felicia Codrea from the BSCRC Flow Cytometry core for their expertise and conversation during experiments. I would also like to thank Dr. Suhua Feng from the BSCRC sequencing core for his guidance on library preparation and sequencing analysis.

Thank you to my family and friends for always being there to provide support and patience when I became a bit carried away discussing my research. No matter how difficult things became throughout my time in graduate school, you were always there as a comforting presence.

Last, but not least, I would like to thank my fellow graduate students. The times that we spent together, both in and outside of lab, were some of the best of graduate school. I hope that all of you can achieve the futures that you are working towards.

Chapter 2 was originally published in Biology of Reproduction. Chen, D., Liu, W., Lukianchikov, A., Hancock, G. V., Zimmerman, J., Lowe, M. G., Kim, R., Galic, Z., Irie, N., Surani, M. A., Jacobsen, S. E., & Clark, A. T. (2017). Germline competency of human embryonic stem cells depends on eomesodermin. *Biology of Reproduction*, *97*(6), 850–861. https://doi.org/10.1093/biolre/iox138. It is reprinted here with permission. This work is supported by the Medical Research Council (MR/P009948/1/MRC), and NIH (R01 HD079546/HD/NICHD, R24 HD000836/HD/NICHD). The authors would like to thank Felicia Codrea and Jessica Scholes for FACS, Jinghua Tang for banking and culturing of the UCLA hESC lines, and Steven Peckman from the Eli and Edythe Broad Center of Regenerative Medicine and Stem Cell Research for critical assistance with human subject and embryonic stem cell review. Human conceptus tissue requests can be made to bdrl@u.washington.edu. SEJ is an investigator of the Howard Hughes Medical Institute.

Chapter 3 is unpublished work performed by Matthew G. Lowe, Zhongxun Hu, Isaac Gorgy, Timothy Hunt, and Amander T. Clark. M.G.L. designed and performed all experiments, maintained the mouse lines and wrote the manuscript. Z.H. and I.G. designed and performed the experiments. T.H. maintained the mouse lines. A.T.C. designed and oversaw all experiments, wrote the manuscript, maintained all university compliances and attained funding for the experiments. The authors would like to thank Felicia Codrea, Jessica Scholes and Jeffery Calimlim from the FACS UCLA BSCRC flow cytometry core and the UCLA MCDB/BSCRC Microscopy Core. Funding for this project provided in part by NIH/NICHD 2 R01 HD058047 and a Ruth L. Kirschstein National Research Service Award GM007185.

Chapter 4 is unpublished work currently under review at Developmental Cell. It reflects work performed by Matthew G. Lowe, Ming-Ren Yen, Fei-man Hsu, Linzi Hosohama, Zhongxun Hu, Tsotne Chitiashvili, Timothy Hunt, Isaac Gorgy, Matthew Bernard, Sissy Wamaitha, Pao-Yang Chen, and Amander T. Clark. M.G.L. designed and performed all experiments, maintained the mouse lines and wrote the manuscript. Z.H. and I.G. designed and performed the experiments. T.C. performed the X/A expression analysis. M.B. and S.W performed the co-IP. L.H. established the mouse lines. T.H. maintained the mouse lines. M.R.Y. and P.Y.C. performed bulk RNA-seq and ChIP-seq analysis. F.M.H. performed the transposon, whole genome bisulfite and single cell RNA sequencing analysis. A.T.C. designed and oversaw all experiments, wrote the manuscript, maintained all university compliances and attained funding for the experiments.

The authors would like to thank Felicia Codrea, Jessica Scholes and Jeffery Calimlim from the UCLA BSCRC flow cytometry core, Dr, Suhua Feng from the UCLA BSCRC Sequencing core, and the UCLA MCDB/BSCRC Microscopy Core. We would also like to thank Dr. Jesse Zamudio for his expert guidance on statistical analyses used throughout this study. Funding for this project provided in part by NIH/NICHD 2 R01 HD058047, a Ruth L. Kirschstein National Research Service Award GM007185, the UCLA Eli and Edythe Broad Center of Regenerative Medicine and Stem Cell Research Training Program and the Rose Hill Foundation Science and Engineering Scholarship. P.Y.C. was supported by grants from Academia Sinica and Ministry of Science and Technology Taiwan (107-2633-B-001-001 and 108-2313-B-001-013-MY3).

VITA

Education

University of Minnesota, Twin Cities — Minneapolis, MN
B.S. Genetics, Cell Biology and Development — 05/2015

University of California, Los Angeles — Los Angeles, CA
Ph.D. Molecular Biology — present

Publications

Lowe MG, Yen MR, Hsu FM, Hosohama L, Hu Z, Chitiashvili T, Hunt T, Gorgy I, Bernard M, Wamaitha S, Chen PY, Clark AT. EED is Required for Primordial Germ Cell Differentiation in the Embryonic Gonad. Currently in resubmission at Developmental Cell.

Crowell P, Fox J, Hashimoto T, Diaz J, Navarro H, Henry G, Feldmar B, **Lowe M**, Garcia A, Wu Y, Sajed D, Strand D, Goldstein A. Expansion of Luminal Progenitor Cells in the Aging Mouse and Human Prostate. Cell Reports. 2019 Aug 6;28(6): 1499-1510. PMID: 31390564

Lowe M, Lage J, Paatela E, Munson D, Hostager R, Yuan C, Katoku-Kikyo N, Ruiz-Estevez M, Asakura Y, Staats J, Qahar M, Lohman M, Asakura A, Kikyo N. Cry2 Is Critical for Circadian Regulation of Myogenic Differentiation by Bclaf1-Mediated mRNA Stabilization of Cyclin D1 and Tmem176b. Cell Reports. 2018 Feb 20;22(8):2118–2132. PMID: 29466738

Chen D, Liu W, Lukianchikov A, Hancock GV, Zimmerman J, **Lowe MG**, Kim R, Galic Z, Irie N, Surani MA, Jacobsen SE, Clark AT. Germline competency of human embryonic stem cells depends on eomesodermin. Biol Reprod. 2017 Dec 1;97(6):850–861. PMID: 29091993

Robinson C, **Lowe M.** Mechanisms and Developmental Roles of Promoter-proximal Pausing of RNA Polymerase II. Journal of Stem Cell Research & Therapy. 2016; 06(03). PMID: 27158559

Lowe M, Hostager R, Kikyo N. Preservation of Epigenetic Memory During DNA Replication. J Stem Cell Res Ther (Edmond). 2016;1(1). PMID: 27158681

https://www.ncbi.nlm.nih.gov/myncbi/matthew.lowe.1/bibliography/public/

Selected Presentations

Lowe MG, Clark AT. "H3K27me3 and DNA Methylation Epigenetically Regulate Primordial Germ Cell Differentiation in the Embryonic Gonad." (2021, September 9). Invited talk at the Molecular Biology Institute Annual Retreat. Los Angeles, CA.

Lowe MG, Yen MR, Hsu FM, Gorgy I, Chitiashvilli T, Bernard M, Hu Z, Hosohama L, Hunt T, Chen PY, Clark AT. "EED Regulates the Timing of Mouse Primordial Germ Cell Differentiation." (2021, June 25). Invited Poster at the International Society for Stem Cell Research Annual Meeting 2021. Virtual.

Lowe MG, Yen MR, Gorgy I, Bernard M, Hu Z, Hosohama L, Hunt T, Chen PY, Clark AT. "EED Regulates Male and Female Mouse Primordial Germ Cell Differentiation." (2020, September 16). Invited Poster at the Cold Spring Harbor Epigenetics and Chromatin 2020 Conference. Virtual.

Selected Honors and Awards

BSCRC-Rose Hill Foundation Training Program	**2021**
BSCRC Training Program	**2020-2021**
BSCRC Microscopy Core Contest Second Prize; UCLA	**2020**
CMB Training Grant	**2018-2020**
MCDB Retreat Poster Prize Winner; UCLA	**2017, 2018**
Graduate Dean's Scholar Award; UCLA	**2017**

Chapter 1

Introduction

Importance of the Germline

The germline is specified early in embryonic development as a handful of cells which will ultimately give rise to the entire adult germline. In mammals, these earliest cells of the germline are known as primordial germ cells (PGCs). Following specification, PGCs will rapidly expand and specialize into either oocyte or spermatogonial precursors based upon sex-specific signals received from the surrounding ovarian or testis somatic tissue, respectively (Ginsburg et al., 1990; Saitou and Yamaji, 2012; Tang et al., 2016). Because the germline is the source of all genetic material for the future generation, following specification PGCs reorganize their epigenome not only to establish a permissive landscape for germline development but to also protect themselves from the developmental cues which they are exposed to in the early embryo (Guibert et al., 2012; Hackett et al., 2013; Hajkova et al., 2002; Hill et al., 2018; Kobayashi et al., 2013; Liu et al., 2014; Seisenberger et al., 2012; Yokobayashi et al., 2013; Zheng et al., 2016). Given this delicate balance, it is not too surprising that any issues which arise during PGC specification or epigenomic reorganization can have catastrophic outcomes not only on fertility but also the health of future generations.

In humans, infertility is defined as the inability to achieve a pregnancy after at least a year of trying. Despite affecting roughly an eighth of all US couples, infertility remains difficult to treat due to the complex nature in which it presents (Hasanpoor-Azghdy et al., 2014; Walker and Tobler, 2022). The causes of infertility are varied, ranging from physical abnormalities in the reproductive system to an inability to produce viable gametes, and affect both men and women equally (Walker and Tobler, 2022). Additionally, an infertility diagnosis can place severe psychological stress upon the affected individual which can damage relationships and increase risk for other health problems (Abbey et al., 1991; Tao et al., 2011). Over the past few decades,

advancements in our understanding of infertility and the germline have led to more accurate diagnosis and the development of new treatment options, such as *in vitro* fertilization (IVF), surgeries and hormonal therapies. These advancements, alongside greater access to reproductive resources, have reduced infertility rates over the past few decades (Chandra and Stephen, 2013; Gnoth et al., 2005). However, despite these successes, assisted reproductive techniques like IVF have proven ineffective in around 40% of couples and there is currently no treatment option available to those who are unable to produce their own gametes (Tao et al., 2011; Walker and Tobler, 2022). Recently, *in vitro* gametogenesis has successfully been performed using mouse induced pluripotent stem cells to derive oocytes completely *in vitro*, however this feat has yet to be fully recapitulated in humans (Hikabe et al., 2016; Yamashiro et al., 2018). Therefore, a better understanding of the mechanisms underlying early germline specification and epigenetic reprogramming is essential to understand the causes of infertility and develop new therapies to better serve those seeking treatment.

Germline Specification

During embryonic development, cells undergo a process of lineage restriction through commitment and differentiation which progressively locks them into specialized cell types capable of carrying out the necessary tasks for organismal survival (Gilbert, 2000). The commitment process takes place in two phases, specification and determination. Specification is when a cell begins to express a distinct transcriptome but is still capable of reversion if given the proper signals, whereas determination is when the cell is fully fate restricted and can no longer revert. While these two processes can happen in quick succession, the mammalian germline is a special case in which PGC commitment occurs over several days (mice) or weeks (human) before determination within the embryonic gonad (Nicholls et al., 2019).

In mice, (m)PGC precursors arise in the proximal posterior epiblast in response to BMP4 and T which induce expression of *Blimp1* by embryonic day (E)6.25 (Aramaki et al., 2013; Hayashi et al., 2007; Ohinata et al., 2005). These precursors become mPGCs by E7.5 when BLIMP1 forms a positive feedback loop with TFAP2C and PRDM14 which reinforces the pluripotency network, represses somatic gene expression and promotes epigenetic reprogramming (Magnúsdóttir et al., 2013). This collectively insulates the newly specified mPGCs from signals directing tissue differentiation during migration towards the genital ridges. In humans (h), the central hPGC transcription factor network is slightly different, constituting BLIMP1, TFAP2C and SOX17 (Irie et al., 2015). Additionally, while it has recently been shown that PRDM14 does play a key role in hPGC differentiation, the targets of PRDM14 are not conserved between species (Sybirna et al., 2020). In chapter 2, we identify a further distinction between the mouse and human PGC specification networks using CRISPR/Cas9 gene editing and an *in vitro* disordered aggregate differentiation model that generates hPGC-like cells (hPGCLCs) from embryonic stem cells (Sasaki et al., 2015). Briefly, we first knockout a gene of interest in embryonic or induced pluripotent stem cells using CRISPR/Cas9 and then differentiate them through a 24 hour incipient mesoderm-like state before dissociating and reaggregating the cells in a 3D culture system for 4 days (Sasaki et al., 2015). From this aggregate, only a handful of hPGCLCs will arise and by comparing the ratio of hPGCLCs to non-hPGCLCs in the aggregate we can determine whether the gene is necessary for hPGC specification. Using this approach, we found that both EOMES and TFAP2C are required to initiate the human PGC specification network whereas mice only require TFAP2C (Chen et al., 2017, 2018).

PGC DNA demethylation

While the PGCLC model is an effective system to study early PGC specification, it fails to properly undergo the epigenetic reprogramming and transcriptome changes seen in later stage PGCs and beyond (Kurimoto et al., 2015; Sasaki et al., 2015). Following specification, mammalian PGCs undergo a wide ranging reorganization of their epigenome (Lesch et al., 2013; Liu et al., 2020, 2014; Ng et al., 2013; Sachs et al., 2013; Seisenberger et al., 2012; Yamaguchi et al., 2013; Yokobayashi et al., 2013). Due to the ethical and practical limitations of studying these processes in humans, much of our knowledge for these events comes from the mouse which closely models what has been observed in hPGC epigenomic reorganization (Tang et al., 2016). Of these changes, the near complete removal of nuclear DNA methylation in a two stage process during the migration and expansion of the mouse PGCs between E7.5 and E12.5 is one of the most profound (Kagiwada et al., 2013; Seisenberger et al., 2012). The first stage involves a genome-wide removal of DNA methylation through a mostly replication coupled process driven by the downregulation of the *de novo* DNA methyltransferases DNMT3A/B as well as UHRF1 which directs the maintenance methyltransferase DNMT1 to the replication forks (Bostick et al., 2007; Kagiwada et al., 2013). Following this initial stage of DNA demethylation, only a few patches of significantly methylated loci remain including transposable elements and a few key CG island containing promoters which regulate gametogenesis genes, termed late demethylators (Seisenberger et al., 2012). During the second stage, alongside continued replication coupled depletion of DNA methylation, a more targeted removal through TET1 which oxidizes 5mC to 5hmC occurs at the late demethylating promoters, completing by E12.5 just prior to sex-specific differentiation of the embryonic gonads and exit from the mPGC stage of germline development (Hackett et al., 2013; Seisenberger et al., 2012; Yamaguchi et al.,

2013). Previously, our lab has used an mPGC-specific conditional knockout mouse to confirm that DNMT1 is essential for the maintenance of DNA methylation at the late demethylating promoters and prevent precocious exit from the mPGC stage (Hargan-Calvopina et al., 2016). Briefly, this mouse model utilizes a *Blimp1* promoter driven *Cre* which will be uniquely expressed in mPGCs upon specification to knockout a floxed gene of interest (Li et al., 2015; Ohinata et al., 2005). However, while we have identified that DNMT1 is essential to maintain DNA methylation at the late demethylating promoters during PGC differentiation, it still remains unclear how it is targeted specifically to these loci. In chapter 3, we used this same approach to create a mPGC-specific UHRF1 conditional knockout mouse in an attempt to answer this question. Despite being downregulated, low levels of UHRF1 protein have been observed in mPGCs concurrent with DNA demethylation (Kagiwada et al., 2013; Seisenberger et al., 2012). While we did not observe a role for UHRF1 in regulating the mPGC stage of germline development, it was found to be essential for the long-term maintenance of sperm production within the adult mouse.

PGC chromatin mark reorganization

In addition to DNA demethylation, PGCs undergo a profound reorganization of their chromatin marks which have also been shown to regulate germline genes (Lesch et al., 2013; Liu et al., 2020, 2014; Ng et al., 2013; Sachs et al., 2013; Yokobayashi et al., 2013). In particular, PRC1.6, a variant of PRC1, has been shown to repress germline genes in mouse embryonic stem cells (Endoh et al., 2017; Liu et al., 2020). In chapter 4, we explore the role of the other polycomb complex PRC2, which adds H3K27me3 that has been shown to be dynamically reorganized following mPGC specification (Kuzmichev et al., 2002; Sachs et al., 2013; Seki et al., 2005, 2007). Much like PRC1 (Yokobayashi et al., 2013) and DNMT1 (Hargan-Calvopina et

al., 2016), we found that PRC2 represses germline genes and prevents precocious exit from the mPGC stage. Additionally, we identified a co-presence of H3K27me3 and DNA methylation in the epiblast at germline genes prior to mPGC specification as well as a role for PRC2 in X chromosome decompensation within the embryonic testis.

References

Abbey, A., Andrews, F.M., and Halrnan, L.J. (1991). Gender's Role in Responses to Infertility. Psychology of Women Quarterly *15*, 295–316. https://doi.org/10.1111/j.1471-6402.1991.tb00798.x.

Aramaki, S., Hayashi, K., Kurimoto, K., Ohta, H., Yabuta, Y., Iwanari, H., Mochizuki, Y., Hamakubo, T., Kato, Y., Shirahige, K., et al. (2013). A Mesodermal Factor, T, Specifies Mouse Germ Cell Fate by Directly Activating Germline Determinants. Developmental Cell *27*, 516–529. https://doi.org/10.1016/j.devcel.2013.11.001.

Bostick, M., Kim, J.K., Estève, P.-O., Clark, A., Pradhan, S., and Jacobsen, S.E. (2007). UHRF1 plays a role in maintaining DNA methylation in mammalian cells. Science *317*, 1760–1764. https://doi.org/10.1126/science.1147939.

Chandra, A., and Stephen, E.H. (2013). Infertility and Impaired Fecundity in the United States, 1982–2010: Data From the National Survey of Family Growth. 19. .

Chen, D., Liu, W., Lukianchikov, A., Hancock, G.V., Zimmerman, J., Lowe, M.G., Kim, R., Galic, Z., Irie, N., Surani, M.A., et al. (2017). Germline competency of human embryonic stem cells depends on eomesodermin. Biol Reprod *97*, 850–861. https://doi.org/10.1093/biolre/iox138.

Chen, D., Liu, W., Zimmerman, J., Pastor, W.A., Kim, R., Hosohama, L., Ho, J., Aslanyan, M., Gell, J.J., Jacobsen, S.E., et al. (2018). The TFAP2C-Regulated OCT4 Naive Enhancer Is Involved in Human Germline Formation. Cell Reports *25*, 3591-3602.e5. https://doi.org/10.1016/j.celrep.2018.12.011.

Endoh, M., Endo, T.A., Shinga, J., Hayashi, K., Farcas, A., Ma, K.-W., Ito, S., Sharif, J., Endoh, T., Onaga, N., et al. (2017). PCGF6-PRC1 suppresses premature differentiation of mouse embryonic stem cells by regulating germ cell-related genes. ELife *6*, e21064. https://doi.org/10.7554/eLife.21064.

Gilbert, S.F. (2000). The Developmental Mechanics of Cell Specification. Developmental Biology. 6th Edition.

Ginsburg, M., Snow, M.H., and McLaren, A. (1990). Primordial germ cells in the mouse embryo during gastrulation. Development *110*, 521–528. .

Gnoth, C., Godehardt, E., Frank-Herrmann, P., Friol, K., Tigges, J., and Freundl, G. (2005). Definition and prevalence of subfertility and infertility. Human Reproduction *20*, 1144–1147. https://doi.org/10.1093/humrep/deh870.

Guibert, S., Forné, T., and Weber, M. (2012). Global profiling of DNA methylation erasure in mouse primordial germ cells. Genome Res *22*, 633–641. https://doi.org/10.1101/gr.130997.111.

Hackett, J.A., Sengupta, R., Zylicz, J.J., Murakami, K., Lee, C., Down, T.A., and Surani, M.A. (2013). Germline DNA Demethylation Dynamics and Imprint Erasure Through 5-Hydroxymethylcytosine. Science *339*, 448–452. https://doi.org/10.1126/science.1229277.

Hajkova, P., Erhardt, S., Lane, N., Haaf, T., El-Maarri, O., Reik, W., Walter, J., and Surani, M.A. (2002). Epigenetic reprogramming in mouse primordial germ cells. Mech. Dev. *117*, 15–23. https://doi.org/10.1016/s0925-4773(02)00181-8.

Hargan-Calvopina, J., Taylor, S., Cook, H., Hu, Z., Lee, S.A., Yen, M.-R., Chiang, Y.-S., Chen, P.-Y., and Clark, A.T. (2016). Stage-Specific Demethylation in Primordial Germ Cells Safeguards against Precocious Differentiation. Dev. Cell *39*, 75–86. https://doi.org/10.1016/j.devcel.2016.07.019.

Hasanpoor-Azghdy, S.B., Simbar, M., and Vedadhir, A. (2014). The emotional-psychological consequences of infertility among infertile women seeking treatment: Results of a qualitative study. Iran J Reprod Med *12*, 131–138. .

Hayashi, K., de Sousa Lopes, S.M.C., and Surani, M.A. (2007). Germ Cell Specification in Mice. Science *316*, 394–396. https://doi.org/10.1126/science.1137545.

Hikabe, O., Hamazaki, N., Nagamatsu, G., Obata, Y., Hirao, Y., Hamada, N., Shimamoto, S., Imamura, T., Nakashima, K., Saitou, M., et al. (2016). Reconstitution *in vitro* of the entire cycle of the mouse female germ line. Nature *539*, 299–303. https://doi.org/10.1038/nature20104.

Hill, P.W.S., Leitch, H.G., Requena, C.E., Sun, Z., Amouroux, R., Roman-Trufero, M., Borkowska, M., Terragni, J., Vaisvila, R., Linnett, S., et al. (2018). Epigenetic reprogramming enables the primordial germ cell-to-gonocyte transition. Nature *555*, 392–396. https://doi.org/10.1038/nature25964.

Irie, N., Weinberger, L., Tang, W.W.C., Kobayashi, T., Viukov, S., Manor, Y.S., Dietmann, S., Hanna, J.H., and Surani, M.A. (2015). SOX17 is a critical specifier of human primordial germ cell fate. Cell *160*, 253–268. https://doi.org/10.1016/j.cell.2014.12.013.

Kagiwada, S., Kurimoto, K., Hirota, T., Yamaji, M., and Saitou, M. (2013). Replication-coupled passive DNA demethylation for the erasure of genome imprints in mice. The EMBO Journal *32*, 340–353. https://doi.org/10.1038/emboj.2012.331.

Kobayashi, H., Sakurai, T., Miura, F., Imai, M., Mochiduki, K., Yanagisawa, E., Sakashita, A., Wakai, T., Suzuki, Y., Ito, T., et al. (2013). High-resolution DNA methylome analysis of primordial germ cells identifies gender-specific reprogramming in mice. Genome Res *23*, 616–627. https://doi.org/10.1101/gr.148023.112.

Kurimoto, K., Yabuta, Y., Hayashi, K., Ohta, H., Kiyonari, H., Mitani, T., Moritoki, Y., Kohri, K., Kimura, H., Yamamoto, T., et al. (2015). Quantitative Dynamics of Chromatin Remodeling during Germ Cell Specification from Mouse Embryonic Stem Cells. Cell Stem Cell *16*, 517–532. https://doi.org/10.1016/j.stem.2015.03.002.

Kuzmichev, A., Nishioka, K., Erdjument-Bromage, H., Tempst, P., and Reinberg, D. (2002). Histone methyltransferase activity associated with a human multiprotein complex containing the Enhancer of Zeste protein. Genes Dev *16*, 2893–2905. https://doi.org/10.1101/gad.1035902.

Lesch, B.J., Dokshin, G.A., Young, R.A., McCarrey, J.R., and Page, D.C. (2013). A set of genes critical to development is epigenetically poised in mouse germ cells from fetal stages through completion of meiosis. Proc Natl Acad Sci U S A *110*, 16061–16066. https://doi.org/10.1073/pnas.1315204110.

Li, Z., Yu, J., Hosohama, L., Nee, K., Gkountela, S., Chaudhari, S., Cass, A.A., Xiao, X., and Clark, A.T. (2015). The Sm protein methyltransferase PRMT5 is not required for primordial germ cell specification in mice. The EMBO Journal *34*, 748–758. https://doi.org/10.15252/embj.201489319.

Liu, M., Zhu, Y., Xing, F., Liu, S., Xia, Y., Jiang, Q., and Qin, J. (2020). The polycomb group protein PCGF6 mediates germline gene silencing by recruiting histone-modifying proteins to target gene promoters. J. Biol. Chem. *295*, 9712–9724. https://doi.org/10.1074/jbc.RA119.012121.

Liu, S., Brind'Amour, J., Karimi, M.M., Shirane, K., Bogutz, A., Lefebvre, L., Sasaki, H., Shinkai, Y., and Lorincz, M.C. (2014). Setdb1 is required for germline development and silencing of H3K9me3-marked endogenous retroviruses in primordial germ cells. Genes Dev. *28*, 2041–2055. https://doi.org/10.1101/gad.244848.114.

Magnúsdóttir, E., Dietmann, S., Murakami, K., Günesdogan, U., Tang, F., Bao, S., Diamanti, E., Lao, K., Gottgens, B., and Surani, M.A. (2013). A tripartite transcription factor network regulates primordial germ cell specification in mice. Nat Cell Biol *15*, 905–915. https://doi.org/10.1038/ncb2798.

Ng, J.-H., Kumar, V., Muratani, M., Kraus, P., Yeo, J.-C., Yaw, L.-P., Xue, K., Lufkin, T., Prabhakar, S., and Ng, H.-H. (2013). In vivo epigenomic profiling of germ cells reveals germ cell molecular signatures. Dev. Cell *24*, 324–333. https://doi.org/10.1016/j.devcel.2012.12.011.

Nicholls, P.K., Schorle, H., Naqvi, S., Hu, Y.-C., Fan, Y., Carmell, M.A., Dobrinski, I., Watson, A.L., Carlson, D.F., Fahrenkrug, S.C., et al. (2019). Mammalian germ cells are determined after PGC colonization of the nascent gonad. Proceedings of the National Academy of Sciences *116*, 25677–25687. https://doi.org/10.1073/pnas.1910733116.

Ohinata, Y., Payer, B., O'Carroll, D., Ancelin, K., Ono, Y., Sano, M., Barton, S.C., Obukhanych, T., Nussenzweig, M., Tarakhovsky, A., et al. (2005). Blimp1 is a critical determinant of the germ cell lineage in mice. Nature *436*, 207–213. https://doi.org/10.1038/nature03813.

Sachs, M., Onodera, C., Blaschke, K., Ebata, K.T., Song, J.S., and Ramalho-Santos, M. (2013). Bivalent Chromatin Marks Developmental Regulatory Genes in the Mouse Embryonic Germline in Vivo. Cell Rep *3*, 1777–1784. https://doi.org/10.1016/j.celrep.2013.04.032.

Saitou, M., and Yamaji, M. (2012). Primordial Germ Cells in Mice. Cold Spring Harb Perspect Biol *4*, a008375. https://doi.org/10.1101/cshperspect.a008375.

Sasaki, K., Yokobayashi, S., Nakamura, T., Okamoto, I., Yabuta, Y., Kurimoto, K., Ohta, H., Moritoki, Y., Iwatani, C., Tsuchiya, H., et al. (2015). Robust In Vitro Induction of Human Germ

Cell Fate from Pluripotent Stem Cells. Cell Stem Cell *17*, 178–194. https://doi.org/10.1016/j.stem.2015.06.014.

Seisenberger, S., Andrews, S., Krueger, F., Arand, J., Walter, J., Santos, F., Popp, C., Thienpont, B., Dean, W., and Reik, W. (2012). The Dynamics of Genome-wide DNA Methylation Reprogramming in Mouse Primordial Germ Cells. Mol Cell *48*, 849–862. https://doi.org/10.1016/j.molcel.2012.11.001.

Seki, Y., Hayashi, K., Itoh, K., Mizugaki, M., Saitou, M., and Matsui, Y. (2005). Extensive and orderly reprogramming of genome-wide chromatin modifications associated with specification and early development of germ cells in mice. Dev. Biol. *278*, 440–458. https://doi.org/10.1016/j.ydbio.2004.11.025.

Seki, Y., Yamaji, M., Yabuta, Y., Sano, M., Shigeta, M., Matsui, Y., Saga, Y., Tachibana, M., Shinkai, Y., and Saitou, M. (2007). Cellular dynamics associated with the genome-wide epigenetic reprogramming in migrating primordial germ cells in mice. Development *134*, 2627–2638. https://doi.org/10.1242/dev.005611.

Sybirna, A., Tang, W.W.C., Pierson Smela, M., Dietmann, S., Gruhn, W.H., Brosh, R., and Surani, M.A. (2020). A critical role of PRDM14 in human primordial germ cell fate revealed by inducible degrons. Nat Commun *11*, 1282. https://doi.org/10.1038/s41467-020-15042-0.

Tang, W.W.C., Kobayashi, T., Irie, N., Dietmann, S., and Surani, M.A. (2016). Specification and epigenetic programming of the human germ line. Nat. Rev. Genet. *17*, 585–600. https://doi.org/10.1038/nrg.2016.88.

Tao, P., Coates, R., and Maycock, B. (2011). The impact of infertility on sexuality: A literature review. Australas Med J *4*, 620–627. https://doi.org/10.4066/AMJ.20111055.

Walker, M.H., and Tobler, K.J. (2022). Female Infertility. In StatPearls, (Treasure Island (FL): StatPearls Publishing), p.

Yamaguchi, S., Hong, K., Liu, R., Inoue, A., Shen, L., Zhang, K., and Zhang, Y. (2013). Dynamics of 5-methylcytosine and 5-hydroxymethylcytosine during germ cell reprogramming. Cell Res. *23*, 329–339. https://doi.org/10.1038/cr.2013.22.

Yamashiro, C., Sasaki, K., Yabuta, Y., Kojima, Y., Nakamura, T., Okamoto, I., Yokobayashi, S., Murase, Y., Ishikura, Y., Shirane, K., et al. (2018). Generation of human oogonia from induced pluripotent stem cells in vitro. Science *362*, 356–360. https://doi.org/10.1126/science.aat1674.

Yokobayashi, S., Liang, C.-Y., Kohler, H., Nestorov, P., Liu, Z., Vidal, M., van Lohuizen, M., Roloff, T.C., and Peters, A.H.F.M. (2013). PRC1 coordinates timing of sexual differentiation of female primordial germ cells. Nature *495*, 236–240. https://doi.org/10.1038/nature11918.

Zheng, H., Huang, B., Zhang, B., Xiang, Y., Du, Z., Xu, Q., Li, Y., Wang, Q., Ma, J., Peng, X., et al. (2016). Resetting Epigenetic Memory by Reprogramming of Histone Modifications in Mammals. Molecular Cell *63*, 1066–1079. https://doi.org/10.1016/j.molcel.2016.08.032.

Chapter 2 – Germline Competency of Human Embryonic Stem Cells Depends on Eomesodermin

Biology of Reproduction, 2017, 97(6), 850–861
doi:10.1093/biolre/iox138
Research Article
Advance Access Publication Date: 30 October 2017

OXFORD

Research Article

Germline competency of human embryonic stem cells depends on eomesodermin†

Di Chen[1], Wanlu Liu[2], Anastasia Lukianchikov[1], Grace V. Hancock[1,2], Jill Zimmerman[1], Matthew G. Lowe[1,2], Rachel Kim[3], Zoran Galic[3,4], Naoko Irie[5,6,7], M. Azim Surani[5,6,7], Steven E. Jacobsen[1,2,3,8,9] and Amander T. Clark[1,2,3,10,*]

[1]Department of Molecular Cell and Developmental Biology, University of California, Los Angeles, California, USA; [2]Molecular Biology Institute, University of California, Los Angeles, California, USA; [3]Eli and Edythe Broad Center of Regenerative Medicine and Stem Cell Research, University of California, Los Angeles, California, USA; [4]Department of Medicine, University of California, Los Angeles, California, USA; [5]Wellcome Trust Cancer Research UK Gurdon Institute, University of Cambridge, Cambridge, UK; [6]Department of Physiology, Development and Neuroscience, University of Cambridge, Cambridge, UK; [7]Wellcome Trust-Medical Research Council Stem Cell Institute, University of Cambridge, Cambridge, UK; [8]Department of Biological Chemistry, University of California, Los Angeles, California, USA; [9]Howard Hughes Medical Institute, University of California, Los Angeles, California, USA and [10]Jonsson Comprehensive Cancer Center, University of California, Los Angeles, California, USA

*__Correspondence:__ Department of Molecular Cell and Developmental Biology, 615 Charles E Young Drive South, University of California Los Angeles, Los Angeles, CA 90095, USA. E-mail: clarka@ucla.edu

†__Grant Support:__ All experiments, with the exception of human hESC derivation, were funded by R01 HD079546 from the Eunice Kennedy Shriver National Institute of Child Health & Human Development (NICHD) (ATC) and supported by Eli and Edythe Broad Center for Regenerative Medicine and Stem Cell Research NIH-NCATS UCLA CTSI Grant Number UL1TR0001881. No NIH funds were used for human embryo culture or hESC derivation. Instead, the derivation of hESC lines was funded by the California Institute for Regenerative Medicine, the UCLA Eli, and Edythe Broad Center of Regenerative Medicine and Stem Cell Research (BSCRC). Di Chen is supported by a training grant from the UCLA BSCRC. Wanlu Liu is supported by Philip J. Whitcome fellowship from the UCLA Molecular Biology Institute and a scholarship from the Chinese Scholarship Council. Human fetal tissue was obtained from the Laboratory of Developmental Biology, University of Washington, Seattle, which is supported by NIH Award Number 5R24HD000836 from the NICHD.

Received 23 October 2017; Accepted 27 October 2017

Abstract

In humans, germline competency and the specification of primordial germ cells (PGCs) are thought to occur in a restricted developmental window during early embryogenesis. Despite the importance of specifying the appropriate number of PGCs for human reproduction, the molecular mechanisms governing PGC formation remain largely unexplored. Here, we compared PGC-like cell (PGCLC) differentiation from 18 independently derived human embryonic stem cell (hESC) lines, and discovered that the expression of primitive streak genes were positively associated with hESC germline competency. Furthermore, we show that chemical inhibition of TGFβ and WNT signaling, which are required for primitive streak formation and CRISPR/Cas9 deletion of Eomesodermin (*EOMES*), significantly impacts PGCLC differentiation from hESCs. Taken together, our results suggest that human PGC formation involves signaling and transcriptional programs associated with somatic germ layer induction and expression of EOMES.

© The Authors 2017. Published by Oxford University Press on behalf of Society for the Study of Reproduction. All rights reserved.
For permissions, please e-mail: journals.permissions@oup.com

Downloaded from https://academic.oup.com/biolreprod/article/97/6/850/4582255 by guest on 21 May 2021

Summary Sentence

EOMES induction in the progenitor cell prior to germ cell formation in vitro from hESCs is required for efficient PGC-like cell formation.

Key words: human, EOMES, primordial germ cells, embryonic stem cells.

Introduction

Primordial germ cells (PGCs) are diploid embryonic progenitor cells that ultimately differentiate into haploid gametes. PGCs are specified, maintained, and differentiated in a step-wise manner, and as a result are responsible for the number and quality of adult gametes. Very little is known about the earliest steps in human PGC differentiation in the embryo. Most of our knowledge comes from the mouse [1, 2], and more recently the nonhuman primate cynomolgus (cyno) macaque [3], rhesus macaque [4], and porcine [5]. Analysis of PGCs from cyno and porcine embryos relative to the mouse strongly suggest that the molecular and cellular events in PGC specification are different. Notably, around the time of PGC specification, cyno and porcine embryos develop morphologically as a bilaminar disk, whereas mouse embryos develop as an egg cylinder. In mouse embryos, PR domain zinc finger protein 1 (PRDM1), also called BLIMP1, transcription factor AP2 gamma (TFAP2C), and PR domain zinc finger protein 14 (PRDM14) constitute the critical tripartite transcription factor network responsible for specifying PGC fate from competent epiblast cells in vivo [6–8] and epiblast-like cells in vitro [9, 10]. In contrast, PRDM14 may not be required for human PGC fate [11], and instead, SOX17 has emerged as a new critical regulator in primates [12]. Therefore, the transcriptional network required for PGC specification within the mammalian class appears to have diversified.

Just as the transcriptional network for PGC specification has changed in different mammalian species, the timing of PGC formation in the peri-implantation embryo may have also diverged. In cyno embryos, PGCs are first identified in the peri-implantation embryo prior to primitive streak formation in an extra embryonic cell layer called the amnion [3]. Notably, the amnion is derived from the inner cell mass/epiblast just prior to primitive streak formation. In porcine embryos, PGC specification begins in the proximal pre-streak epiblast [5], whereas in the mouse embryo, PGC precursors are first identified as a small cluster in the proximal epiblast around the time of primitive streak formation [6, 13, 14]. Therefore, in cyno, mouse, and porcine embryos, where PGC specification has been studied in detail, PGC formation is induced from embryonic progenitors at or just prior to formation of the primitive streak and would therefore be exposed to signaling events that establish the primary germlayers and the primitive streak.

One of the earliest markers of primitive streak is the T-box transcription factor BRACHYURY (T), and in mouse embryos, T functions downstream of Wnt signaling to promote PGC specification. [15]. A second T-box transcription factor eomesodermin (EOMES) is also expressed in the proximal epiblast prior to overt primitive streak formation, becoming restricted to the primitive streak during gastrulation [16]. In the mouse, there is no functional evidence for EOMES in the regulation of PGC development. However, using human-induced pluripotent stem cells (hiPSCs) a recent study indicated that EOMES is required for human PGC-like cell (PGCLC) formation following induced reprogramming [17]. It is not known whether EOMES is required for differentiation of human PGCLCs from human embryonic stem cells (hESCs).

Although transcription factors regulating PGC specification may have diverged between mice and humans [12], the major signaling pathways that specify PGCs have not. Most notably, bone morphogenetic protein 4 (BMP4) is essential for mouse PGC formation in vivo [18] as well as human and cyno PGCLC formation in vitro [5, 11, 12, 19, 20]. In the mouse, BMP4 specifies PGCs from the Wnt3-primed posterior epiblast, with T functioning downstream of WNT to regulate PGC fate [15]. In cyno's, T is expressed in the nucleus of nascent PGCs in the amnion, presumably due to Wnt3A signaling [3], and in porcine embryos, T is expressed in nascent PGCs of the preprimitive-streak embryo. Furthermore, porcine PGC numbers diminish following WNT inhibition [5]. These results suggest a conserved role for Wnt and BMP signaling in mouse, porcine, cyno, and human PGC formation in the embryo.

Human PGCLCs induced from multiple hiPSCs have been used to study the germ cell fate determinants [17, 21]. However, much less is known about the competency across different hESCs. In the current study, we discovered a positive correlation between the expression of primitive streak genes and efficiency of human PGCLC induction from 18 independently derived hESC lines. Using CRISPR/Cas9, we provide direct evidence that the transcription factor EOMES is required for efficient induction of human PGCLCs from hESCs, and lends additional support to the hypothesis that human PGCs are induced from cells in the embryo that express EOMES.

Material and methods

Human fetal samples

Human prenatal testes and ovaries were acquired following elected termination and pathological evaluation after University of California, Los Angeles (UCLA)-Institutional Review Board (IRB) review, which deemed the project exempt under 45 CRF 46.102(f). All prenatal gonads were obtained from the University of Washington Birth Defects Research Laboratory (BDRL), under the regulatory oversight of the University of Washington IRB-approved Human Subjects protocol combined with a Certificate of Confidentiality from the Federal Government. BDRL collected the fetal testes and ovaries and shipped them overnight in HBSS with ice pack for immediate processing in Los Angeles. All consented material was donated anonymously and carried no personal identifiers. Developmental age was documented by BDRL as days post fertilization using a combination of prenatal intakes, foot length, Streeter Stages, and crown-rump length. All prenatal gonads documented with birth defect or chromosomal abnormality, were excluded from this study.

hESC culture

All primed hESC lines were cultured on mitomycin C-inactivated mouse embryonic fibroblasts (MEFs) in hESC media, which is composed of 20% knockout serum replacement (KSR) (GIBCO, 10828-028), 100 μM L-Glutamine (GIBCO, 25030-081), 1× MEM Non-Essential Amino Acids (NEAA) (GIBCO, 11140-050), 55 μM 2-Mercaptoethanol (GIBCO, 21985-023), 10 ng/mL recombinant

Downloaded from https://academic.oup.com/biolreprod/article/97/6/850/4582255 by guest on 21 May 2021

human FGF basic (R&D systems, 233-FB), 1× Penicillin-Streptomycin (GIBCO, 15140-122), and 50 ng/mL primocin (InvivoGen, ant-pm-2) in DMEM/F12 media (GIBCO, 11330-032). All hESC lines were split every 7 days with Collagenase type IV (GIBCO, 17104-019). 4i hESCs were maintained as described before [19]. 4i cells were grown on irradiated MEFs (GlobalStem) in knockout DMEM containing 20% KSR, 2 mM L-glutamine, 0.1 mM NEAA, 0.1 mM 2-mercaptoethanol (all GIBCO), 20 ng/mL human LIF (Stem Cell Institute [SCI]), 8 ng/mL bFGF (SCI), 1 ng/mL TGF-β1 (Peprotech), 3 μM CHIR99021 (Miltenyi Biotec), 1 μM PD0325901 (Miltenyi Biotec), 5 μM SB203580 (TOCRIS bioscience), and 5 μM SP600125 (TOCRIS bioscience). 4i hESCs were split every 3 to 5 days using TrypLE Express (GIBCO). An amount of 10 μM of ROCK inhibitor (Y-27632, TOCRIS bioscience) was used for the first 24 h after passage. All hESC lines used in this study are registered with the National Institute of Health Human Embryonic Stem Cell Registry and are available for research use with NIH funds. Specifically, the following hESC lines were used in this study: UCLA1 (46XX), UCLA2 (46XY), UCLA3 (46XX), UCLA4 (46XX), UCLA5 (46XX), UCLA6 (46XY), UCLA7 (47XX+13), UCLA8 (46XX), UCLA9 (46XX), UCLA10 (46XY), UCLA11 (46XY), UCLA12 (46XX), UCLA13 (46XY), UCLA14 (46XX), UCLA15 (46XX), UCLA16 (46XX), UCLA17 (46XX), UCLA18 (46XX). The derivation and basic characterization (Karyotype and teratoma analysis) of UCLA1–6 were previously reported [22]. UCLA8–10, UCLA14, and UCLA16–18 were reported [23].

Derivation and characterization of ESC lines from human embryos

The following UCLA hESC lines UCLA7 (47XX+13), UCLA11 (46XY), UCLA12 (46XX), UCLA13 (46XY), UCLA15 (46XX) were derived from human embryos according to the methods described [22]. All hESC derivations were performed after human subjects' approval from the UCLA-IRB and following Embryonic Stem Cell Research Oversight committee approval. No NIH funds were used for the derivation or initial characterization (karyotype and teratoma) of hESC lines. Teratoma analysis was performed after Institutional approval by the UCLA Office of Animal Research Oversight. Teratomas were created by injecting of collagenase digested clumps of hESCs into the testicles of male scid/beige C.B.17-Prkdc(scid)Lyst(bg) mice. Prior to injection, hESCs were resuspended in ice-cold matrigel (Corning, 354277), with 3× wells (from a 6-well plate) of colonies injected per testis. Karyotype analysis was conducted by Cell Line Genetics.

Induction of human PGCLCs though incipient mesoderm-like cells from primed hESCs

Human PGCLCs were induced from primed hESCs as described in [19] with some modifications. Day 7 hESCs were dissociated into single cells with 0.05% Trypsin-EDTA (Gibco, 25300-054) and plated onto Human Plasma Fibronectin (Invitrogen, 33016-015)-coated 12-well plate at the density of 200 000 cells/well in 2 mL/well of incipient mesoderm-like cell (iMeLC) media, which is composed of 15% KSR, 1× NEAA, 0.1 mM 2-Mercaptoethanol, 1× Penicillin-Streptomycin-Glutamine (Gibco, 10378-016), 1 mM sodium pyruvate (Gibco, 11360-070), 50 ng/mL Activin A (Peprotech, AF-120-14E), 3 μM CHIR99021 (Stemgent, 04-0004), 10 μM of ROCKi (Y27632, Stemgent, 04-0012-10), and 50 ng/mL primocin in Glasgow MEM (GMEM) (Gibco, 11710-035). iMeLCs were dissociated into single cells with 0.05% Trypsin-EDTA after 24 h of incubation unless otherwise mentioned and plated into ultra-low cell attachment U-bottom 96-well plates (Corning, 7007) at the density of 3000 cells/well in 200 μL/well of PGCLC media, which is composed of 15% KSR, 1× NEAA, 0.1 mM 2-Mercaptoethanol, 1× Penicillin-Streptomycin-Glutamine (Gibco, 10378-016), 1 mM sodium pyruvate (Gibco, 11360-070), 10 ng/mL human LIF (Millipore, LIF1005), 200 ng/mL human BMP4 (R&D systems, 314-BP), 50 ng/mL human EGF (R&D systems, 236-EG), 10 μM of ROCKi (Y27632, Stemgent, 04-0012-10), and 50 ng/mL primocin in GMEM (Gibco, 11710-035). An amount of 100 ng/mL stem cell factor (SCF; PEPROTECH, 250-03), 10 μM SB431542 (Stemgent, 04-0010-10), and 500 ng/μL Dickkopf Wnt Signaling Pathway Inhibitor 1 (DKK1) (R&D systmes, 5439-DK) was added in PGCLC media for some experiments.

Induction of human PGCLCs from 4i hESCs

4i WIS2 cells were dissociated with TrypLE and plated to ultra-low cell attachment U-bottom 96-well plates (Corning, 7007) at the density of 2000–4000 cells/well in 200 μL PGCLC media, which is composed of 15% KSR, 0.1 mM NEAA, 0.1 mM 2-mercaptoethanol, 100 U/mL Penicillin–0.1 mg/mL Streptomycin, 2 mM L-Glutamine, 1 mM Sodium pyruvate, 500 ng/mL BMP4 (R&D Systems) or BMP2 (SCI), 1 μg/mL human LIF (SCI), 100 ng/mL SCF (R&D Systems), 50 ng/mL EGF (R&D Systems), and 10 μM ROCK inhibitor in GMEM (Gibco, 11710-035).

Flow cytometry and fluorescence activated cell sorting

Human prenatal gonads or day 4 aggregates were dissociated with 0.25% trypsin (Gibco, 25200-056) for 5 min or 0.05% Trypsin-EDTA (Gibco, 25300-054) for 10 min at 37°C. The dissociated cells were stained with conjugated antibodies, washed with fluorescence activated cell sorting (FACS) buffer (1% BSA in PBS), and resuspended in FACS buffer accompanying with 7-AAD (BD Pharmingen, 559925). The single cell suspension was analyzed or sorted. The conjugated antibodies used in this study are ITGA6 conjugated with BV421 (BioLegend, 313624), EPCAM conjugated with 488 (BioLegend, 324210), EPCAM conjugated with APC (BioLegend, 324208), tissue nonspecific alkaline phosphatase (TNAP) conjugated with PE (BD Pharmingen, 561433), and cKIT conjugated with APC (BD Pharmingen, 550412).

Real-time quantitative polymerase chain reaction

Sorted cells or cell pellets were lysed in 350 μL of RLT buffer (QIAGEN) and RNA was extracted using RNeasy micro kit (QIAGEN, 74004). Complementary DNA was synthesized using SuperScript II Reverse Transcriptase (Invitrogen, 18064-014). Real-time quantitative polymerase chain reaction (PCR) was performed using TaqMan Universal PCR Master Mix (Applied Biosystems, 4304437) and the expression level of genes-of-interest were normalized to the expression of housekeeping gene GAPDH. The Taqman probes used in this study include GAPDH (Applied Biosystems, Hs99999905_m1), NANOS3 (Applied Biosystems, Hs00928455_s1), PRDM1 (Applied Biosystems, hs01068508_m1), TFAP2C (Applied Biosystems, Hs00231476_m1), SOX17 (Applied Biosystems, Hs00751752_s1), cKIT (Applied Biosystems, hs00174029_m1), DAZL (Applied Biosystems, hs00154706_m1), DDX4 (Applied Biosystems, Hs00251859_m1), SOX9 (Applied Biosystems, Hs01001343_g1), AMH (Applied Biosystems, Hs01006984_g1), DND1 (Applied Biosystems, Hs00832091_s1), T (Applied Biosystems, Hs00610080_m1), CER1 (Applied Biosystems,

Downloaded from https://academic.oup.com/biolreprod/article/97/6/850/4582255 by guest on 21 May 2021

Hs00193796_m1), MIXL1 (Applied Biosystems, Hs00430824_g1), WNT3 (Applied Biosystems, Hs00902257_m1), EOMES (Applied Biosystems, Hs00172872_m1), GSC (Applied Biosystems, Hs00906630_g1), FOXA2 (Applied Biosystems, Hs00232764_m1), POU3F1 (Applied Biosystems, Hs00538614_s1), TCF15 (Applied Biosystems, Hs00231821_m1). For human gonad samples, two technical replicates of real-time quantitative PCR were performed. For hESCs, iMeLCs, and PGCLCs, two to three independent experiments were performed.

Generation of *EOMES* mutant hESC lines

A pair of guide RNA (gRNA) targeting EOMES was designed using crispr.mit.edu, and the corresponding gDNA sequence was cloned into px330 vector [24]. An amount of 4 μg of gRNA pair or 2 μg of pMax-GFP was electroporated into 800 000 UCLA1 cells using P3 Primary Cell 4D-Nucleofector X Kit according to the manufacturer's instructions (Lonza, V4XP-3024). Twenty-four hours after nucleofection, cells were dissociated with Accutase (ThermoFisher Scientific, A1110501) and seeded in low density. A total of 96 individual colonies were picked after 9 days and expanded. Lines were screened for the presence of shorter bands due to deletion. To determine the precise mutations, PCR product from the targeted allele was cloned using Topo-TA cloning (Thermo-Fisher) and analyzed by Sanger sequencing. Two mutant lines were chosen and subcloned before experiments. The gRNA sequences used to target *EOMES* are 5'- GCGGTGTACAGCCGTAACAT and 5'-GTTATCTACACCGAAAGTGC. Karyotyping by Cell Line Genetics was performed before experimentation. GFP-labeled control and EOMES mutant hESCs were made by lentivirus-based transfection of UbiC-GFP-IRES-Puromycin and maintained as stable cell lines with puromycin (1 μg/mL) selection.

Immunofluorescence

Immunostaining paraffin sections or aggregates in whole mount were described previously [25, 26]. For cells cultured on chamber slides, samples were fixed in 4% paraformaldehyde in PBS for 10 min and washed with PBS containing 0.1% Tween 20 and permeabilized with PBS containing Triton X for 10 min. Samples were blocked with 10% donkey serum for 30 min before antibody incubation. The primary antibodies used for immunofluorescence in this study include rabbit-anti-EPCAM (Abcam, ab71916, 1:50), goat-anti-VASA (R&D Systems, AF2030, 1:20), rabbit-anti-cKIT (DAKO, A4502, 1:100), goat-anti-OCT4 (Santa Cruz Biotechnology, sc-8628x, 1:100), rabbit-anti-PRDM1 (Cell Signaling Technology, 9115, 1:100), mouse-anti-PRDM1 (R&D Systems, MAB36081SP, 1:100), rabbit-anti-TFAP2C (Santa Cruz Biotechnology, sc-8977, 1:100), mouse-anti-TFAP2C (Santa Cruz Biotechnology, sc12762, 1:100), rat-anti-ITGA6 (Santa Cruz Biotechnology, sc-80554, 1:100), goat-anti-T (R&D Systems, AF2085, 1:100), goat-anti-SOX17 (Neuromics, GT15094, 1:100), rabbit-anti-EOMES (Abcam, ab23345, 1:100), rabbit-anti- β-CATENIN (Cell Signaling Technology, 9582, 1:100), rabbit-anti-pSMAD2/3 (Cell Signaling Technology, 8828, 1:100). The secondary antibodies used in this study are all from Jackson ImmunoResearch Laboratories including donkey-anti-rabbit-488, donkey-anti-mouse-488, donkey-anti-goat-488, donkey-anti-rat-488, donkey-anti-rabbit-594, donkey-anti-mouse-594, and donkey-anti-goat-594. DAPI is counterstained to indicate nuclei.

RNA-sequencing

Sorted cells or cell pellets were lysed in 350 μL of RLT buffer (QIAGEN), and total RNA was extracted with RNeasy micro kit (QIAGEN, 74004). Total RNA was reverse transcribed and cDNA was amplified using Ovation RNA-Seq System V2 (Nugen, 7102-32) according to manufacturer's instructions. Amplified cDNA was fragmented into ~200 bp by Covaris S220 Focused-ultrasonicators. RNA-sequencing (RNA-seq) libraries were generated using Ovation Rapid Library Systems (Nugen, 0319-32 for index 1-8 and 0320-32 for index 9–16) and quantified by KAPA library quantification kit (Illumina, KK4824). Libraries were subjected to single-end 50 bp sequencing on HiSeq 2000 or HiSeq 2500 sequencer with 4–6 indexed libraries per lane.

RNAseq analysis

Analysis of individual gene expression

Raw reads in qseq format obtained from sequencer were first converted to fastq format with customized perl script. Reads quality were controlled with FastQC (http://www.bioinformatics.babraham.ac.uk/projects/fastqc). High-quality reads were then aligned to hg19 reference genome using Tophat [27] (v 2.0.13) by using "-no-coverage-search" option, allowing up to two mismatches and only keeping reads that mapped to one location. Basically, reads were first mapped to hg19 gene annotation with known splice junction. When reads did not map to the annotated genes, the reads were mapped to hg19 genome. Number of reads mapping to genes were calculated by HTseq [28] (v 0.5.4) with default parameters. Expression levels were determined by RPKM (reads per kilobase of exons per million aligned reads) in R using customized scripts. For RNAseq of published datasets GSE60138 [12], GSM1643143 [19], raw reads were obtained from GEO and then processed exactly the same as described above.

Hierarchical clustering of RNAseq

Raw read counts for each gene obtained from HTseq were preprocessed with DESeq R package [28]. To account for heteroscedasticity between samples, variance stabilizing transformation was first applied to all genes with DEseq. Samples were then hierarchical clustered (hclust function) based on their Euclidian distances (dist function) in R using customized scripts.

Principal component analysis

For principal component analysis (PCA), RPKM for each sample was first calculated. Variance of each genes across samples were then calculated (rowVars function in R). PCA analysis (prcomp function in R) was performed on genes with the top 500 variation across samples. PCA were then plotted with ggplot2 package in R (http://ggplot2.org).

Correlation analysis between samples

Correlation between ITGA6/EPCAM and TNAP/cKIT was calculated and plotted in R. Firstly, RPKM of each ITGA6/EPCAM and TNAP/cKIT RNAseq replicates were calculated. Pearson correlations were then obtained with cor function. Scatter plot was plotted with ggplot2 with linear regression line. Human PGC-enriched genes compared to H9 hESCs were defined by Irie et al. [12] (only genes with at least four fold enrichment in hPGC compared to H9 hESCs were selected). The RPKM of those selected genes were extracted, and heat map was plotted with log2(RPKM+1) values in R using pheatmap package.

Downloaded from https://academic.oup.com/biolreprod/article/97/6/850/4582255 by guest on 21 May 2021

Differential gene expression calling

R DESeq package was used to normalize counts per RefSeq transcripts to evaluate differential expression. For comparison between hESC, iMeLC, mutant hESC, and mutant iMeLC, highly upregulated genes of each sample, with mean log2(fold change) >1 and adjusted P value < 0.05 were selected and plotted as Venn diagram using VennDiagram package in R. Scatter plot of log2(RPKM+1) was plotted in R with ggplot2 package. Log2(Fold change) were colored with different scale.

Analysis of gene expression level and PGCLC induction efficiency

In order to obtain iMeLC-specific genes coexpressing with PGCLC induction efficiency, Spearman correlation of each gene's expression level in iMeLC was calculated with PGCLC induction efficiency. Genes in hESC with RPKM more than 2 were filtered out, while genes with at least 2 RPKM in iMeLC were kept. Gene's expression levels with at least 0.45 correlations to PGCLC induction efficiency were kept. Heat map of log2(RPKM+1) was plotted in R as described above.

Results

ITGA6 and EPCAM can be used to isolate human PGCs from embryonic ovaries but not embryonic testes

Recently, in vitro human PGCLCs were isolated using INTEGRINα6 (ITGA6) and EPCAM following hiPSC differentiation [19]; however, whether ITGA6/EPCAM can be used to isolate in vivo PGCs from human embryos has not been shown. To address this, we examined cells from a pair of human embryonic ovaries at 72 day postfertilization by staining with four antibodies that detect ITGA6, EPCAM, TNAP, and cKIT. cKIT and TNAP were used as a positive control, given that these surface proteins can be used to sort human PGCs from the prenatal embryonic ovary and testis [25, 29]. The labeled cells were divided in two and sorted by FACS gating on either ITGA6/EPCAM or TNAP/cKIT (Figure 1A). We discovered that the percentage of ITGA6/EPCAM double positive cells and TNAP/cKIT double positive cells in the embryonic ovary was comparable (Figure 1A). Furthermore, the ITGA6/EPCAM double positive population was also double positive for TNAP/cKIT. Conversely, the TNAP/cKIT double positive cells were also double positive for ITGA6/EPCAM (Figure 1A). Using real-time PCR, we show that both populations expressed PGC genes at equivalent levels (Figure 1B). We repeated this experiment with a pair of human embryonic ovaries at 94 day, and found a similar result (Figure 1A and B). Therefore, these observations indicate that ITGA6/EPCAM can be used to isolate TNAP/cKIT positive germ cells from the human embryonic ovary and vice versa.

Next, we performed the same analysis using embryonic testes. Unlike the ovary, we discovered that most ITGA6/EPCAM double positive cells are negative for TNAP/cKIT (Figure 1C), and the ITGA6/EPCAM double positive cells have reduced levels of PGC genes relative to the TNAP/cKIT double positive population (Figure 1D). Given that ITGA6 and EPCAM are epithelial markers [30, 31], and PGCs in the embryonic testis are known to be enclosed within epithelial cords [25], we reasoned that ITGA6 and EPCAM double positive cells are a mixture of both germ cells and somatic cells in prenatal testis. To test this, we performed immunofluorescence and real-time PCR and show that ITGA6 and EPCAM are expressed by both PGCs and epithelial Sertoli cells (Figure S1A and B), and the ITGA6/EPCAM double positive population is also enriched in Sertoli cell genes *SOX9* and *AMH* (Figure 1D). Therefore, using prenatal tissues containing PGCs, TNAP/cKIT can be used to sort PGCs from both the embryonic ovary and testis, whereas ITGA6/EPCAM can only be used to sort PGCs from the embryonic ovary.

Next, we performed RNA-seq on sorted ITGA6/EPCAM female PGCs at 89 and 103 day (Figure 1E and F), and compared this to a third sample involving a pair of ovaries collected at 89 d, which were pooled and then stained and sorted separately for ITGA6/EPCAM or TNAP/cKIT (Figure 1E–G, marked by asterisk). We also included a testis at 59 day, which was sorted only using TNAP/cKIT to specifically isolate the male PGCs. Using unsupervised hierarchical clustering (UHC), the sorted PGC samples clustered together forming a distinct group relative to an undifferentiated female hESC line (UCLA1), and a male hESC line (UCLA2) (Figure 1E). Evaluation of candidate genes revealed that all putative PGC samples expressed the early and late stage PGC genes and have acquired a naïve pluripotent signature (Figure S1C). Moreover, the ITGA6/EPCAM and TNAP/cKIT PGCs sorted from the same pair of 89 day embryonic ovaries clustered the closest compared to ITGA6/EPCAM populations sorted from different ovaries (Figure 1E). This result further supports the conclusion that ITGA6/EPCAM and TNAP/cKIT are expressed on the same population of PGCs. To better display the similarities and differences between samples, we performed PCA, and found that the PGCs are well separated from undifferentiated hESCs along the PC1 axis, while the 59-day male TNAP/cKIT PGCs are separated from the other gonadal PGCs along the PC2 axis (Figure 1F). This separation is anticipated to be caused by the 4-week difference in age between male and female samples in this study, as well as gender [32]. Last, we examined the differentially expressed genes (DEGs) between ITGA6/EPCAM and TNAP/cKIT positive cells sorted from the same ovary pair and found very few DEGs as the two transcriptomes are highly correlated with linear regression R squared = 0.98 (Figure 1G). Therefore, we propose that ITGA6/EPCAM and TNAP/cKIT are coexpressed on the same cell population in the embryonic ovary.

Germline competency is associated with the induction of genes required for primitive streak formation

Prior to examining PGCLC differentiation across 18 independently derived UCLA hESC lines with ITGA6/EPCAM/TNAP/cKIT, we first piloted the sorting strategy on the male hESC line UCLA2. We discovered that all ITGA6/EPCAM double positive putative PGCLCs at day 4 of differentiation were positive for TNAP; however, cKIT was not detected on the PGCLC population (Figure S2A). In mice, cKIT is critical for PGC survival, migration, and proliferation [33–35]. In humans, cKIT is present on PGCs from at least week 4 to week 20 of prenatal life postfertilization [25, 29, 32, 36]. Furthermore, analysis of cyno PGCs during gastrulation reveals that *cKIT* RNA is expressed by PGCs at the time of specification [3]. Thus, we reasoned that cKIT is either not translated in early stage human PGCs, or alternatively the conditions for PGCLC induction must be optimized to enable cKIT expression on the cell surface. Given that cKIT is subject to ligand induced endocytosis [37], we removed the ligand SCF from the PGCLC media, and this resulted in ITGA6/EPCAM/TNAP/cKIT positive PGCLCs (Figure S2B and D). To determine if excluding SCF affects germ cell identity, we performed real-time PCR and RNA-Seq of the putative ITGA6/EPCAM positive PGCLCs differentiated with or without SCF (Figure S2C and E). To determine the molecular similarity of PGCLCs generated in primed conditions on MEFs, to those generated from hESCs cultured in 4i on MEFs [12], we

Downloaded from https://academic.oup.com/biolreprod/article/97/6/850/4582255 by guest on 21 May 2021

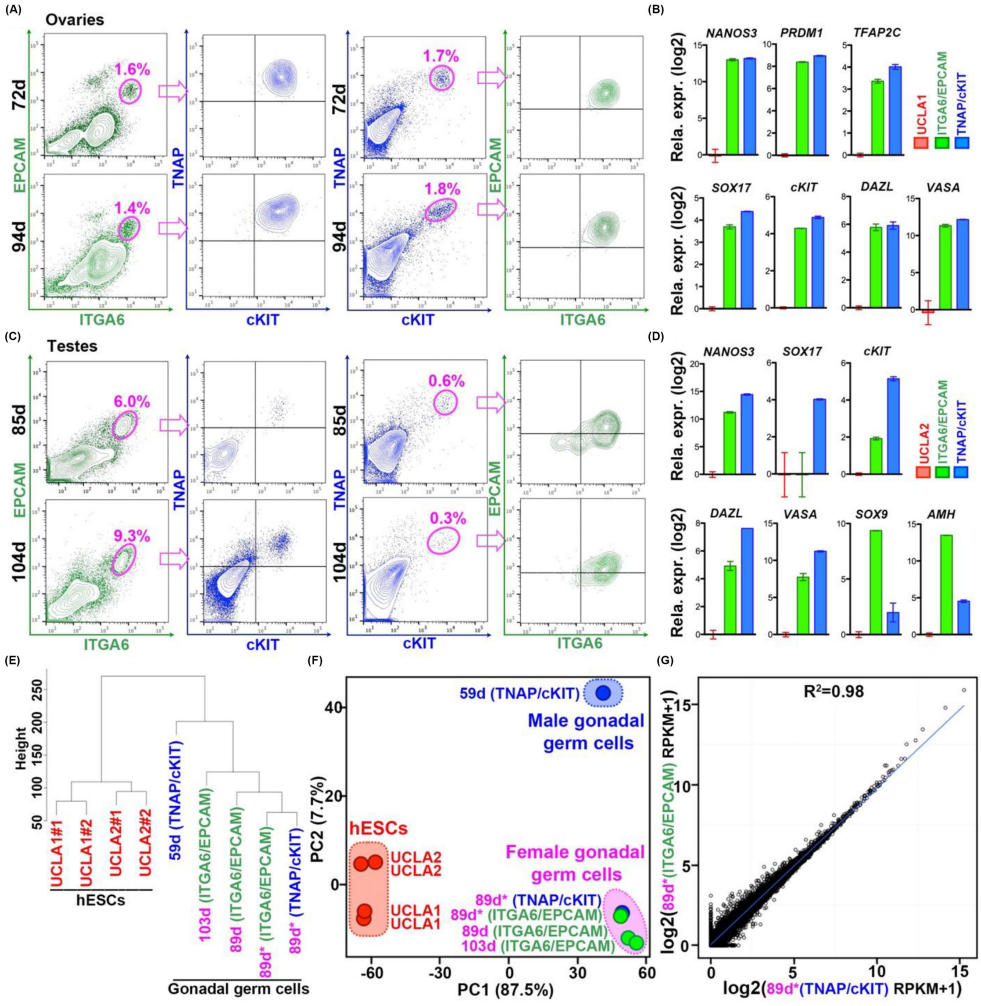

Figure 1. Analysis of ITGA6/EPCAM and TNAP/cKIT populations in human prenatal gonads. (A) Flow cytometry of prenatal ovaries at day (d) 72 and 94 postfertilization stained with antibodies that recognize ITGA6, EPCAM, TNAP, and cKIT. (B) Gene expression of the sorted populations from (A, 72d) by real-time PCR. Expression is normalized to the GAPDH. Fold change is calculated relative to expression levels of each gene in female hESC line UCLA1 (passage 17 (p17) and p18), which was given a value of 1.0. (C) Flow cytometry of prenatal testis at day 85 and 104 postfertilization stained with ITGA6, EPCAM, TNAP, and cKIT. (D) Gene expression of the sorted populations from (C, 85d) by real-time PCR. For each gene examined, its expression is normalized to the GAPDH. Fold change is calculated relative to expression levels of each gene in male hESC line UCLA2 (p11 and p12), which was given a value of 1.0. (E) Unsupervised hierarchical clustering (UHC) of transcriptomes of female hESC line UCLA1 (two biological replicates, p14 and p15), male hESC line UCLA2 (two biological replicates, p13 and p14), TNAP/cKIT positive germ cells from embryonic day 59 testes, ITGA6/EPCAM positive cells from 89d, 103d, and another 89d embryonic ovary. TNAP/cKIT positive cells from 89d ovaries. Asterisk in E–G indicates that the two RNA-seq libraries were made from the same pair of ovaries but sorted with different surface markers. (F) PCA of transcriptomes shown in E. (G) Scatter plot of two transcriptomes made from the same pair of ovaries but sorted with ITGA6/EPCAM (x-axis) and TNAP/cKIT (y-axis).

Downloaded from https://academic.oup.com/biolreprod/article/97/6/850/4582255 by guest on 21 May 2021

differentiated the WIS2 hESC line for 4 days according to the methods of Irie et al. [12] and sorted the TNAP/NANOS3-mCherry PGCLC population. RNA-seq analysis showed that PGCLCs generated from either the primed or 4i cultured hESCs clustered together, and were distinct from the undifferentiated hESCs (Figure S2E and F), indicating that the starting culture media (4i on MEFs versus primed media on MEFs) ultimately yielded PGCLCs with similar transcriptional identities.

Using ITGA6/EPCAM as a sorting approach to analyze PGCLCs, we next examined PGCLC competency of 18 hESC lines, all derived at UCLA from 18 single frozen embryos (Figure 2A). All hESC lines were capable of teratoma formation when injected into severe combined immunocompromized (SCID) beige mice (UCLA1–6 [22]; UCLA8–10, UCLA14, UCLA16–18 [23]; and this study UCLA7, UCLA11–13, and UCLA15: Figure S3A–C). Seventeen out of eighteen hESC lines are karyotypically normal, while UCLA7 has a duplication of chromosome 13 in 100% of cells karyotyped (Figure S3B). We included this cell line in the analysis to determine whether aneuploidy may be associated with alterations in PGCLC potential. It has been previously reported that PGCLC induction efficiency is variable between experiments [12, 19]. In order to minimize variability, we induced PGCLCs from 18 hESC lines simultaneously and repeated this experiment four times to determine the average PGCLC induction efficiency for all 18 lines. All 18 independently derived hESC lines were germline competent. However, UCLA6 consistently exhibited the highest germline potential generating on average 35% PGCLCs at day 4 of aggregate formation, whereas UCLA9 had the lowest germline potential generating on average less than 1% PGCLCs at day 4 (Figure 2A; Figure S3D). The aneuploid UCLA7 female hESC line generated a comparable percentage of PGCLCs to the other female hESC lines in the data set. Meanwhile, we found that male hESC lines on average were more competent for PGCLC induction than female (Figure 2B).

In a recent study using nine hiPSC lines, it was determined that primitive streak genes were associated with PGCLC competency [21]. To determine whether this was also the case for hESCs, we performed RNA-seq on the 18 hESC lines, and the corresponding iMeLCs in biological duplicate. We used the following parameters to define genes whose expression levels in iMeLCs are positively correlated with PGCLC induction efficiency. First, we chose genes that were expressed at low levels or not expressed in hESCs by setting the RPKM value < 2. Second, we used the RPKM value > 2 in at least one of the 18 iMeLC samples to select for genes that are upregulated in at least one of the 18 hESC lines induced to become iMeLCs. Third, we correlated gene expression in iMeLCs with PGCLC induction efficiency, and set the cutoff as >0.45. Based on these parameters, we found 78 genes upregulated from hESCs to iMeLCs that were also positively correlated with resulting PGCLC induction efficiency in the aggregates (Figure 2C). Using gene ontogeny (GO) term analysis of these 78 genes by WebGestalt [38, 39], we discovered that the top term was "formation of primary germ layer" (GO: 0001704), which included seven genes: *EOMES, T, GATA6*, *MIXL1*, *GATA4*, *WLS*, and *LHX1*. These genes are associated with primitive streak formation that are known to be induced by NODAL/ACTIVIN A (TGFβ) and WNT [40].

Signaling pathways that promote primitive streak formation are also required for PGCLC induction

Next, we confirmed the relationship between TGFβ and WNT signaling pathways, and the expression of *T* and *EOMES* in iMeLCs. We performed immunofluorescence and identified nuclear accumulation of phosphorylated SMAD2/3 (pSMAD2/3) (Figure 3A) and β-CATENIN (Figure 3B) in both iMeLCs and hESCs, indicating that these cells are capable of responding to both signaling pathways. We then confirmed expression of T (Figure 3C) and EOMES (Figure 3D) protein by immunofluorescence, and as predicted from the RNA-Seq, T was induced in iMeLCs (Figure 3C), and EOMES protein was expressed in both hESCs and in iMeLCs (Figure 3D).

The correlation of germline competency with TGFβ and WNT signaling, as well as *T* and *EOMES* induction promoted us to test if these molecules are critical for PGCLC formation. To block TGFβ signaling we added SB431542 [41], which inhibits the TGFβ type I receptors ALK5, ALK4, and ALK7, and phosphorylation of SMAD2 and SMAD3. This inhibitor does not block the ALKs or SMADs downstream of BMP4. To block WNT receptor binding, we added DKK1 [42] (Figure 3E). We discovered that the addition of these two molecules prevented the induction of *T* and *EOMES* in iMeLCs despite the presence of ACTIVIN A and GSK3βi in the iMeLC media (Figure 3F). In order to determine if *T* and *EOMES* expression is dependent on TGFβ or WNT, or both, we evaluated *T* and *EOMES* expression in iMeLCs in the presence of either SB431542 or DKK1. We found that *T* and *EOMES* were repressed in the presence of either SB431512 or DKK1 (Figure S4A and B), suggesting the expression of *T* and *EOMES* in iMeLCs requires both TGFβ and WNT signaling. To evaluate the effect on germline competency, we induced PGCLCs in media with or without SB431542 and DKK1 (Figure 3E). We discovered that the PGCLC population was completely abolished when SB431542 and DKK1 were included in the media, despite the presence of exogenous BMP4 and other cytokines known to induce PGCLC fate (Figure 3G). These results suggest that the ability to respond to TGFβ and WNT signaling and potentially the induction of genes associated with primitive streak formation such as *T* and *EOMES* are required for germline induction.

EOMES is required for PGCLC induction

To provide direct evidence for EOMES in PGCLC induction, we used CRISPR/Cas9 to mutate *EOMES* in the UCLA1 hESC line (Figure S4C). We used two independent *EOMES* mutant clones for analysis. By differentiating the *EOMES* mutant and control hESC lines in parallel, we found that the ITGA6/EPCAM double positive PGCLC population was dramatically reduced in the *EOMES* mutant clones (Figure 4A–B). To confirm this result, we also performed immunofluorescence on aggregates and detected PGCLCs by triple staining for TFAP2C, SOX17, and PRDM1. In wild-type control cells, we detected clusters of triple TFAP2C, SOX17, and PRDM1 human PGCLCs (Figure 4C, white dot outlined). However, in the *EOMES* mutant lines, we identified very few triple positive PGCLCs (Figure 4C, white arrowheads). Therefore, our results demonstrate that EOMES is required for PGCLC formation in human, most likely downstream of WNT and TGFβ.

In cyno embryos, nascent PGCs in the amnion are negative for *EOMES* [3]. Similarly, our RNA-seq data show that *EOMES* is not expressed in prenatal PGCs or PGCLCs. Therefore, we hypothesize that EOMES acts either noncell autonomously in the niche to support PGCLC formation, or alternatively EOMES acts cell autonomously in iMeLCs to prime PGC fate. To test this, we made stable GFP lines of control and *EOMES* mutant hESCs. We made iMeLCs and generated PGCLC aggregates containing a mix of GFP and unlabeled cells in a 1:1 ratio. The iMeLC mixtures were composed of GFP-labeled control cells with unlabeled controls (Figure 4D) or

Downloaded from https://academic.oup.com/biolreprod/article/97/6/850/4582255 by guest on 21 May 2021

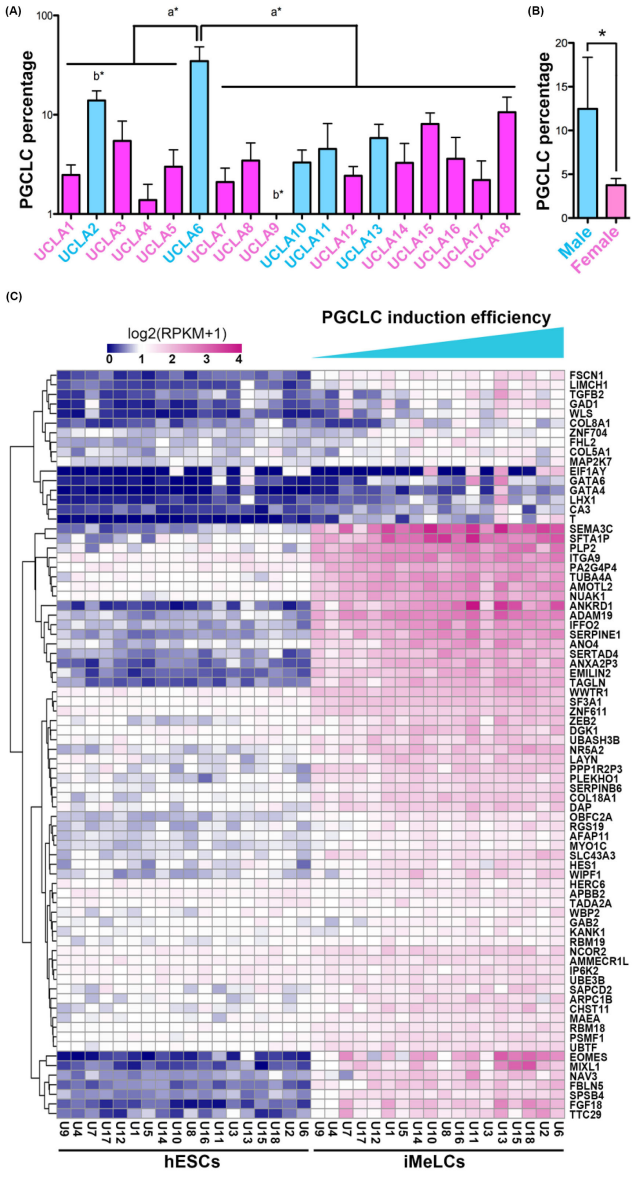

Figure 2. Germline competency varies between independent hESC lines. (A) Average PGCLC induction efficiency at day 4 in aggregates generated from 18 hESC lines (passage numbers ranging from p10 to p22, see experimental procedures for details). Blue represents male and pink represents female. "a∗" indicates the significant difference between UCLA6 and all other cell lines and "b∗" indicates the significant difference between UCLA2 and UCLA9 (tested by ANOVA, $P < 0.0001$). PGCLCs were identified as ITGA6/EPCAM double positive cells. (B) Comparison of day 4 PGCLC induction efficiency from male (blue) and female (pink) hESC lines. "∗" indicates the difference between male and female (t-test, $P < 0.05$). (C) Heat map showing the expression of genes in iMeLCs that positively correlated with PGCLC induction efficiency. Genes are selected as maximal expression <= 2 (RPKM) in hESCs, maximal expression >= 2 (RPKM) in iMeLCs, and correlation coefficient >0.45.

Downloaded from https://academic.oup.com/biolreprod/article/97/6/850/4582255 by guest on 21 May 2021

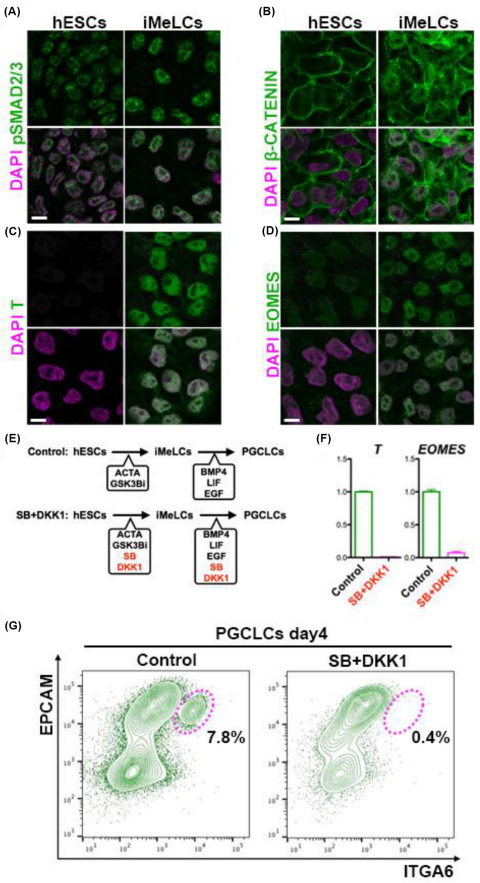

Figure 3. TGFβ and WNT signaling are required for PGCLC induction from hESCs. (A–D) Expression of pSMAD2/3 (A), β-CATENIN (B), T (C), and EOMES (D) in UCLA1 hESCs and iMeLCs. Scale bar: 10 μm. (E) Schematic illustration of PGCLC induction with or without SB431542 (SB) and DKK1. (F) Real-time PCR for *T* and *EOMES* expression at iMeLCs in the presence of SB431542 and DKK1. (G) Flow cytometry showing loss of PGCLC competency in media containing SB431542 and DKK1.

GFP-labeled *EOMES* mutant cells with unlabeled controls (Figure 4E). In the controls, about 45% of the total cells were positive for GFP, and about 35% of the PGCLCs were positive. Therefore, control hESCs with or without GFP both contribute to PGCLC induction (Figure 4D). In contrast, only about 8% of the PGCLCs were induced from GFP-labeled *EOMES* mutant cells, whereas the total cells were composed of about 48% GFP-labeled EOMES mutant cells (Figure 4E). This suggests that EOMES is required cell autonomously to prime PGC fate.

Discussion

In the current study, we prove that PGCLC competency is an inherent property of hESC lines. Together with previous work [11, 12, 19], our study proves that the generation of human PGCLCs in vitro through directed differentiation is not a stochastic event restricted to a small number of hESC or hiPSC lines, but rather a competency that extends to the majority of human pluripotent stem cell lines in vitro regardless of whether they originated from the inner cell mass or through induced reprogramming. We also show that heterogeneity in PGCLC differentiation can provide a unique opportunity to discover conserved and new genes that regulate PGC specification in humans. Heterogeneity in differentiation potential amongst independently derived pluripotent stem cell lines is not unique to the germline, with multiple studies showing that hESC and hiPSC lines each have varying potentials for somatic cell differentiation [43–46]. In these studies, the underlying cause of this heterogeneity is thought to be due to differences in chromatin and DNA methylation in the self-renewing state [45, 46]. The underlying cause of variable germline competency also warrants further investigation.

A recent study using nine hiPSC lines cultured on StemFit also revealed that genes associated with primitive streak formation are associated with germline competency of hiPSCs in vitro [21]. Our study extends this observation by demonstrating that primitive streak gene expression is also associated with germline competency of hESCs, and that functionally, PGCLC competency can be attributed to the appropriate induction of *T* and *EOMES* downstream of TGFβ and WNT signaling. A recent study using hiPSCs revealed that T is not required for hPGCLC specification; therefore, even though *T* is induced and associated with PGCLC competency, *T* itself may not necessary for germline competency in vitro [17].

Unlike T, EOMES has no reported functional role in mouse, cyno, or porcine PGC specification. In mouse, EOMES is required for the cell migration in the primitive streak and *EOMES* loss-of-function mutants fail to undergo germ layer formation [47]. In the current study, we determined that EOMES is critical for human PGCLC specification where EOMES functions cell autonomously. Our RNA-seq data show that EOMES is expressed in iMeLCs but not in PGCLCs or PGCs. Therefore, we hypothesize that EOMES functions before the specification of SOX17 positive PGCs and is associated with germ cell competency of the epiblast/primitive streak. Whether EOMES regulates the migration of iMeLCs and whether the migration of iMeLCs is required for germ cell fate specification require further analysis.

Finally, our work touches on the potential origins of the human germline. In mouse embryos, PRDM1 positive PGC precursors are specified by BMP4 signaling to the Wnt3 primed posterior epiblast around the time of primitive streak formation [6, 15, 48]. In cyno embryos, PGCs were first identified prior to primitive streak formation in an embryonic cell layer called the amnion [3]. In porcine embryos, SOX17 positive PGCs were identified in prestreak epiblasts similar to the mouse [5]. In the current study, we discovered that signaling pathways and transcription factors associated with primitive streak formation (EOMES) regulate competency for SOX17 positive human PGCLC formation. This does not directly refute the origin of PGCLCs as being from the amnion, as the molecular identity of amnion cells is almost completely unknown. Instead, our work demonstrates that embryonic cells with the appropriate competency to respond to TGFβ and Wnt3 in order to induce EOMES are required for human PGCLC formation. Future studies using embryo attachment culture will be necessary to determine the origin of the

Downloaded from https://academic.oup.com/biolreprod/article/97/6/850/4582255 by guest on 21 May 2021

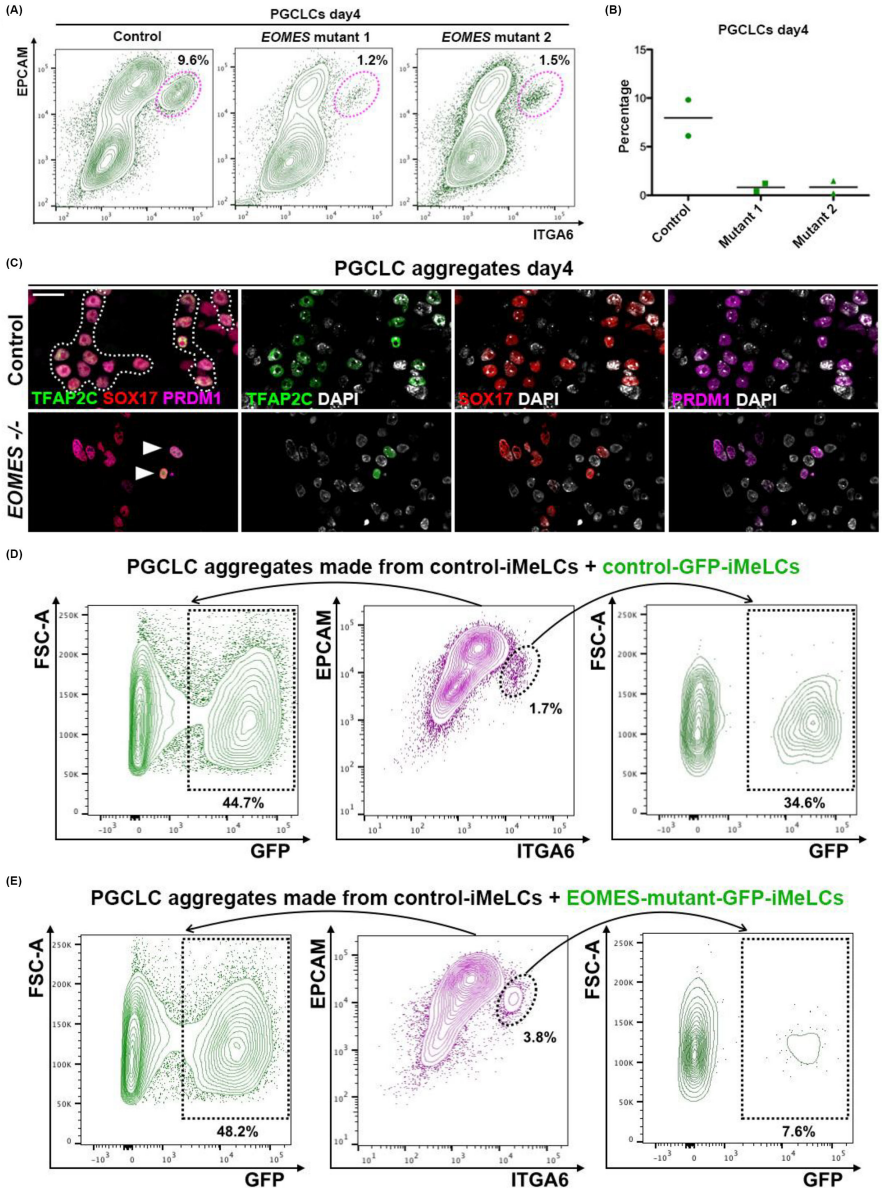

Figure 4. EOMES is required for PGCLC induction from hESCs. (A) Flow cytometry showing reduced PGCLC competency in *EOMES* mutant hESC line. PGCLCs were identified as ITGA6/EPCAM double positive cells. (B) Summary of PGCLC induction percentage from control and two different *EOMES* mutant hESC clones. (C) Control and *EOMES* mutant day 4 aggregates stained with TFAP2C (green), SOX17 (red), PRDM1 (purple), and DAPI (white). White dot outlines TFAP2C/SOX17/PRDM1 triple positive PGCLCs in control. White arrowheads point to rare TFAP2C/SOX17/PRDM1 triple positive PGCLCs in *EOMES* mutant. (D) Flow cytometry analysis of PGCLCs made from mixed iMeLCs (1:1 ratio) made from GFP negative and GFP positive wild-type hESCs. Left panel shows GFP positive cells in all live cells from PGCLC aggregates. Middle panel shows PGCLCs positive for ITGA6 and EPCAM. Right panel shows GFP positive PGCLCs. (E) Same analysis as (D) for PGCLCs made from mixed iMeLCs (1:1 ratio) made from GFP negative wild-type hESCs and GFP positive *EOMES* mutant hESCs.

Downloaded from https://academic.oup.com/biolreprod/article/97/6/850/4582255 by guest on 21 May 2021

human germline, but only if they emerge before the primitive streak given the ethical barrier that our field currently cannot cross.

Supplementary data

Supplementary data are available at *BIOLRE* online.

Figure S1. Germ cell marker expression and optimization of PGCLC induction from hESCs. (A) Human embryonic testis at day 115 section stained with ITGA6 (green), OCT4 (red), and DAPI (blue) by immunofluorescence. Yellow arrowhead points to an OCT4-positive germ cell that is also positive for ITGA6. Purple arrowhead points to an ITGA6-positive germ cell that is negative for OCT4. Scale bar: 10 μm. (B) Human embryonic testis at day 72 section stained with EPCAM (green), VASA (red), and DAPI (blue) by immunofluorescence. Yellow arrowhead points to a VASA-positive germ cell that is also positive for EPCAM. Purple arrowhead points to an EPCAM-positive germ cell that is negative for VASA. Scale bar: 10 μm. (C) Heat map showing the expression of germ cell, somatic cell, and pluripotency genes in transcriptomes shown in Figure 1E.

Figure S2. Generating ITGA6/EPCAM//TNAP/cKIT positive PGCLCs. (A and B) Flow cytometry of day 4 aggregates made with SCF (A) or without SCF (B) from UCLA2 (p13) and stained for ITGA6/EPCAM/TNAP/cKIT. (C) Real-time PCR of the sorted ITGA6/EPCAM positive PGCLCs made from UCLA2 (p13, p14) with SCF (green open columns) or without SCF (purple open columns) and compared to gene expression in ITGA6/EPCAM PGCs at day 72 postfertilization (Figure 1A and B) (green solid columns). Fold change is calculated relative to expression levels of each gene in the UCLA1 hESC line, which was given a value of 1.0. (D) Immunofluorescence of day 4 PGCLC aggregates from UCLA2 (p14) to examine colocalization of OCT4 (red), with cKIT, PRDM1, and TFAP2C (all green). Scale bar: 10 μm. (E) UHC of primed undifferentiated hESCs (UCLA1 p14, p15 and UCLA2 p13, p14), day 4 PGCLCs sorted by FACS using ITGA6/EPCAM (made from UCLA1 p14, p15 and UCLA2 p13, p14) with (plus) and without (minus) SCF, undifferentiated 4i cultured hESCs sorted with TNAP (WIS2) and day 4 PGCLCs sorted by FACS using TNAP/NANOS3-mCherry (made from WIS2). UHC was based on the expression of DEGs between hPGCs and H9 hESCs defined by Irie et al. [12] and Sasaki et al. [19]. U1 and U2 indicate UCLA1 and UCLA2, respectively. Gonadal germ cell libraries analyzed here are the same in Figure 1E. MS: minus SCF. PS: plus SCF. (F) PCA of transcriptomes in (E).

Figure S3. PGCLC induction from 18 pluripotent hESC lines derived at UCLA. (A) Morphology of human embryos used for derivation of hESC lines UCLA7, UCLA11, UCLA12, UCLA13, and UCLA15. All other hESC lines are reported elsewhere. (B) Karyotypes of hESC lines UCLA7, UCLA11, UCLA12, UCLA13, and UCLA15 (from left to right). All other hESC lines are reported elsewhere. (C) Representative images showing teratomas formed by injection of hESC lines UCLA7, UCLA11, UCLA12, UCLA13, and UCLA15 (from left to right) into the testes of SCID-beige mice. All other hESC lines are reported elsewhere. (D) FACS plots of day 4 PGCLCs (sorted with ITGA6/EPCAM) induced from 18 hESC lines through 24 h of iMeLC differentiation.

Figure S4. Evaluation of *T* and *EOMES* in different combination of cytokines and inhibitors and molecular information of *EOMES* mutant alleles. (A) *T* expression in the iMeLCs with different combinations of cytokines and signaling inhibitors. (B) *EOMES* expression in the iMeLCs with different combinations of cytokines and signaling inhibitors. (C) Molecular information of gRNAs for targeting *EOMES* and the resulting *EOMES* mutant alleles in the subline used in this study.

Table S1. List of antibodies used in this study.

Acknowledgments

The authors would like to thank Felicia Codrea and Jessica Scholes for FACS, Jinghua Tang for banking and culturing of the UCLA hESC lines, and Steven Peckman from the Eli and Edythe Broad Center of Regenerative Medicine and Stem Cell Research for critical assistance with human subject and embryonic stem cell review. Human conceptus tissue requests can be made to bdrl@u.washington.edu. SEJ is an investigator of the Howard Hughes Medical Institute.

Conflict of Interest: The authors have declared that no conflict of interest exists.

References

1. Magnusdottir E, Surani MA. How to make a primordial germ cell. *Development* 2014; **141**:245–252.
2. Tang WWC, Kobayashi T, Irie N, Dietmann S, Surani MA. Specification and epigenetic programming of the human germ line. *Nat Rev Genet* 2016; **17**:585–600.
3. Sasaki K, Nakamura T, Okamoto I, Yabuta Y, Iwatani C, Tsuchiya H, Seita Y, Nakamura S, Shiraki N, Takakuwa T, Yamamoto T, Saitou M. The germ cell fate of cynomolgus monkeys is specified in the nascent amnion. *Dev Cell* 2016; **39**:169–185.
4. Clark AT, Gkountela S, Chen D, Liu W, Sosa E, Sukhwani M, Hennebold JD, Orwig KE. Primate primordial germ cells acquire transplantation potential by carnegie stage 23. *Stem Cell Reports* 2017; **9**: 329–341.
5. Kobayashi T, Zhang H, Tang WWC, Irie N, Withey S, Klisch D, Sybirna A, Dietmann S, Contreras DA, Webb R, Allegrucci C, Alberio R et al. Principles of early human development and germ cell program from conserved model systems. *Nature* 2017; **546**:416–420.
6. Ohinata Y, Payer B, O'carroll D, Ancelin K, Ono Y, Sano M, Barton SC, Obukhanych T, Nussenzweig M, Tarakhovsky A, Saitou M, Surani MA. Blimp1 is a critical determinant of the germ cell lineage in mice. *Nature* 2005; **436**:207–213.
7. Yamaji M, Seki Y, Kurimoto K, Yabuta Y, Yuasa M, Shigeta M, Yamanaka K, Ohinata Y, Saitou M. Critical function of Prdm14 for the establishment of the germ cell lineage in mice. *Nat Genet* 2008; **40**:1016–1022.
8. Weber S, Eckert D, Nettersheim D, Gillis AJ, Schäfer S, Kuckenberg P, Ehlermann J, Werling U, Biermann K, Looijenga LH, Schorle H. Critical function of AP-2gamma/TCFAP2C in mouse embryonic germ cell maintenance. *Biol Reprod* 2010; **82**:214–223.
9. Nakaki F, Hayashi K, Ohta H, Kurimoto K, Yabuta Y, Saitou M. Induction of mouse germ-cell fate by transcription factors in vitro. *Nature* 2013; **501**:222–226.
10. Magnúsdóttir E, Dietmann S, Murakami K, Günesdogan U, Tang F, Bao S, Diamanti E, Lao K, Gottgens B, Azim Surani M. A tripartite transcription factor network regulates primordial germ cell specification in mice. *Nat Cell Biol* 2013; **15**:905–915.
11. Sugawa F, Arauzo-Bravo MJ, Yoon J, Kim K-P, Aramaki S, Wu G, Stehling M, Psathaki OE, Hubner K, Scholer HR. Human primordial germ cell commitment in vitro associates with a unique PRDM14 expression profile. *EMBO J* 2015; **34**:1009–1024.
12. Irie N, Weinberger L, Tang WWC, Kobayashi T, Viukov S, Manor YS, Dietmann S, Hanna JH, Surani MA. SOX17 is a critical specifier of human primordial germ cell fate. *Cell* 2015; **160**:253–268.
13. Lawson KA, Hage WJ. Clonal analysis of the origin of primordial germ cells in the mouse. *Ciba Found Symp* 1994; **182**:68–84; discussion 84–91.
14. Tam PP, Zhou SX. The allocation of epiblast cells to ectodermal and germline lineages is influenced by the position of the cells in the gastrulating mouse embryo. *Dev Biol* 1996; **178**:124–132.

Downloaded from https://academic.oup.com/biolreprod/article/97/6/850/4582255 by guest on 21 May 2021

15. Aramaki S, Hayashi K, Kurimoto K, Ohta H, Yabuta Y, Iwanari H, Mochizuki Y, Hamakubo T, Kato Y, Shirahige K, Saitou M. A mesodermal factor, T, specifies mouse germ cell fate by directly activating germline determinants. *Dev Cell* 2013; **27**:516–529.
16. Ciruna BG, Rossant J. Expression of the T-box gene Eomesodermin during early mouse development. *Mech Dev* 1999; **81**:199–203.
17. Kojima Y, Sasaki K, Yokobayashi S, Sakai Y, Nakamura T, Yabuta Y, Nakaki F, Nagaoka S, Woltjen K, Hotta A, Yamamoto T, Saitou M. Evolutionarily distinctive transcriptional and signaling programs drive human germ cell lineage specification from pluripotent stem cells. *Cell Stem Cell* 2017; **21**:517.e5–532.e5.
18. Lawson KA, Dunn NR, Roelen BAJ, Zeinstra LM, Davis AM, Wright CVE, Korving JPWFM, Hogan BLM. Bmp4 is required for the generation of primordial germ cells in the mouse embryo. *Genes Dev* 1999; **13**:424–436.
19. Sasaki K, Yokobayashi S, Nakamura T, Okamoto I, Yabuta Y, Kurimoto K, Ohta H, Moritoki Y, Iwatani C, Tsuchiya H, Nakamura S, Sekiguchi K et al. Robust in vitro induction of human germ cell fate from pluripotent stem cells. *Cell Stem Cell* 2015; **17**:178–194.
20. Kee K, Angeles VT, Flores M, Nguyen HN, Reijo Pera RA. Human DAZL, DAZ and BOULE genes modulate primordial germ-cell and haploid gamete formation. *Nature* 2009; **462**:222–225.
21. Yokobayashi S, Okita K, Nakagawa M, Nakamura T, Yabuta Y, Yamamoto T, Saitou M. Clonal variation of human induced pluripotent stem cells for induction into the germ cell fate. *Biol Reprod* 2017; **96**:1154–1166.
22. Diaz Perez SV, Kim R, Li Z, Marquez VE, Patel S, Plath K, Clark AT. Derivation of new human embryonic stem cell lines reveals rapid epigenetic progression in vitro that can be prevented by chemical modification of chromatin. *Hum Mol Genet* 2012; **21**:751–764.
23. Patel S, Bonora G, Sahakyan A, Kim R, Chronis C, Langerman J, Fitz-Gibbon S, Rubbi L, Skelton RJP, Ardehali R, Pellegrini M, Lowry WE et al. Human embryonic stem cells do not change their X inactivation status during differentiation. *Cell Rep* 2017; **18**:54–67.
24. Cong L, Ran FA, Cox D, Lin S, Barretto R, Habib N, Hsu PD, Wu X, Jiang W, Marraffini LA, Zhang F. Multiplex genome engineering using CRISPR/Cas systems. *Science* 2013; **339**:819–823.
25. Gkountela S, Li Z, Vincent JJ, Zhang KX, Chen A, Pellegrini M, Clark AT. The ontogeny of cKIT+ human primordial germ cells proves to be a resource for human germ line reprogramming, imprint erasure and in vitro differentiation. *Nat Cell Biol* 2013; **15**:113–122.
26. Li Z, Yu J, Hosohama L, Nee K, Gkountela S, Chaudhari S, Cass AA, Xiao X, Clark AT. The Sm protein methyltransferase PRMT5 is not required for primordial germ cell specification in mice. *EMBO J* 2015; **34**:748–758.
27. Trapnell C, Pachter L, Salzberg SL. TopHat: discovering splice junctions with RNA-Seq. *Bioinformatics* 2009; **25**:1105–1111.
28. Anders S, Pyl PT, Huber W. HTSeq–a Python framework to work with high-throughput sequencing data. *Bioinformatics* 2015; **31**:166–169.
29. Tang WWC, Dietmann S, Irie N, Leitch HG, Floros VI, Bradshaw CR, Hackett JA, Chinnery PF, Surani MA. A unique gene regulatory network resets the human germline epigenome for development. *Cell* 2015; **161**:1453–1467.
30. Tamura RN. Epithelial integrin alpha 6 beta 4: complete primary structure of alpha 6 and variant forms of beta 4. *J Cell Biol* 1990; **111**:1593–1604.
31. Trzpis M, McLaughlin PMJ, de Leij LMFH, Harmsen MC. Epithelial cell adhesion molecule. *Am J Pathol* 2007; **171**:386–395.
32. Gkountela S, Zhang KX, Shafiq TA, Liao W, Hargan-Calvopiña J, Chen P, Clark AT. DNA demethylation dynamics in the human prenatal germline. *Cell* 2015; **161**:1425–1436.
33. Loveland KL, Schlatt S. Stem cell factor and c-kit in the mammalian testis: lessons originating from Mother Nature's gene knockouts. *J Endocrinol* 1997; **153**:337–344.
34. Pesce M, Di Carlo A, De Felici M. The c-kit receptor is involved in the adhesion of mouse primordial germ cells to somatic cells in culture. *Mech Dev* 1997; **68**:37–44.
35. Richardson BE, Lehmann R. Mechanisms guiding primordial germ cell migration: strategies from different organisms. *Nat Rev Mol Cell Biol* 2010; **11**:37–49.
36. Guo F, Yan L, Guo H, Li L, Hu B, Zhao Y, Yong J, Hu Y, Wang X, Wei Y, Wang W, Li R et al. The transcriptome and DNA methylome landscapes of human primordial germ cells. *Cell* 2015; **161**:1437–1452.
37. Cruse G, Beaven MA, Music SC, Bradding P, Gilfillan AM, Metcalfe DD. The CD20 homologue MS4A4 directs trafficking of KIT toward clathrin-independent endocytosis pathways and thus regulates receptor signaling and recycling. *Mol Biol Cell* 2015; **26**:1711–1727.
38. Zhang B, Kirov S, Snoddy J. WebGestalt: an integrated system for exploring gene sets in various biological contexts. *Nucleic Acids Res* 2005; **33**:W741–W748.
39. Wang J, Duncan D, Shi Z, Zhang B. WEB-based GEne SeT AnaLysis toolkit (WebGestalt): update 2013. *Nucleic Acids Res* 2013; **41**:W77–W83.
40. Funa NS, Schachter KA, Lerdrup M, Ekberg J, Hess K, Dietrich N, Honorê C, Hansen K, Semb H. β-Catenin regulates primitive streak induction through collaborative interactions with SMAD2/SMAD3 and OCT4. *Cell Stem Cell* 2015; **16**:639–652.
41. Inman GJ. SB-431542 is a potent and specific inhibitor of transforming growth factor-beta superfamily type I activin receptor-like kinase (ALK) receptors ALK4, ALK5, and ALK7. *Mol Pharmacol* 2002; **62**:65–74.
42. Moon RT, Kohn AD, De Ferrari GV, Kaykas A. WNT and beta-catenin signalling: diseases and therapies. *Nat Rev Genet* 2004; **5**:691–701.
43. Feng Q, Lu S, Klimanskaya I, Gomes I, Kim D, Chung Y, Honig GR, Kim K, Lanza R. Hemangioblastic derivatives from human induced pluripotent stem cells exhibit limited expansion and early senescence. *Stem Cells* 2010; **28**:704–712.
44. Hu B-Y, Weick JP, Yu J, Ma L-X, Zhang X-Q, Thomson JA, Zhang S-C. Neural differentiation of human induced pluripotent stem cells follows developmental principles but with variable potency. *Proc Natl Acad Sci USA* 2010; **107**:4335–4340.
45. Bock C, Kiskinis E, Verstappen G, Gu H, Boulting G, Smith ZD, Ziller M, Croft GF, Amoroso MW, Oakley DH, Gnirke A, Eggan K et al. Reference Maps of human ES and iPS cell variation enable high-throughput characterization of pluripotent cell lines. *Cell* 2011; **144**:439–452.
46. Butcher LM, Ito M, Brimpari M, Morris TJ, Soares FAC, Ährlund-Richter L, Carey N, Vallier L, Ferguson-Smith AC, Beck S. Non-CG DNA methylation is a biomarker for assessing endodermal differentiation capacity in pluripotent stem cells. *Nat Commun* 2016; **7**:10458.
47. Russ AP, Wattler S, Colledge WH, Aparicio SA, Carlton MB, Pearce JJ, Barton SC, Surani MA, Ryan K, Nehls MC, Wilson V, Evans MJ. Eomesodermin is required for mouse trophoblast development and mesoderm formation. *Nature* 2000; **404**:95–99.
48. Kurimoto K, Saitou M. Mechanism and reconstitution in vitro of germ cell development in mammals. *Cold Spring Harb Symp Quant Biol* 2015; **80**:147–154.

Downloaded from https://academic.oup.com/biolreprod/article/97/6/850/4582255 by guest on 21 May 2021

Chapter 3

UHRF1 is not Required for PGC Differentiation

Summary

Proper differentiation of the germline is essential for fertility. In mammals, the germline is specified in the early embryo and undergoes major epigenetic remodeling which is hypothesized to facilitate proper gametogenesis. In order to assess the role of Ubiquitin like with PHD and Ring Finger domains 1 (UHRF1) throughout germline differentiation we created a conditional deletion of UHRF1 at the time of specification. Through immunofluorescence and cell sorting, we found that UHRF1 does not regulate the timing of sex-specific differentiation in the embryonic gonads, contribute to global DNA re-methylation of the prospermatogonia in the embryonic testis, or the maturation of the oocytes within the adult ovary. Immunofluorescence of the adult testis revealed that while UHRF1 is not essential for the maintenance of the spermatogonial stem cell population, it is required for the long-term maintenance of this population and spermatogenesis. Thus, we provide the first longitudinal study of the role of UHRF1 in germline differentiation from the time of specification through gametogenesis.

Introduction

In mammals, primordial germ cells (PGCs) are the source of the entire adult germline. In mice, the PGC stage takes roughly seven days beginning with specification from the embryonic epiblast at embryonic day (E) 6.5 and ending at E13.5 following migration and sex-specific differentiation into oogonia or prospermatogonia within the embryonic ovaries and testes, respectively (Ginsburg et al., 1990; Jameson et al., 2012; Saitou and Yamaji, 2012). During migration, the PGCs will undergo a genome-wide depletion of DNA methylation due to a downregulation of the *de novo* DNA methyltransferases 3A and 3B (DNMT3A and DNMT3B) as well as Ubiquitin like with PHD and Ring Finger domains 1 (UHRF1) which is necessary for

directing the maintenance DNA methyltransferase 1 (DNMT1) to the replication forks (Kagiwada et al., 2013; Seisenberger et al., 2012). Despite near complete genome-wide DNA demethylation prior to entry into the genital ridges at E10.5, a few loci still retain significant DNA methylation. These include transposable elements which retain DNA methylation throughout sex-specific differentiation and the promoters of key gametogenesis genes, termed "late demethylators," which slowly lose DNA methylation until becoming fully demethylated prior to sex-specific differentiation (Hargan-Calvopina et al., 2016; Hill et al., 2018; Liu et al., 2014; Saitou and Yamaji, 2012; Seisenberger et al., 2012).

Following sex-specific differentiation, the embryonic oogonia will arrest in meiosis I prophase I and undergo fetal oocyte attrition (FOA) in response to *Line1* expression ending at post-natal day (P) 2 after a majority of oocytes are lost (Malki et al., 2014; Tharp et al., 2020). The remaining oocytes are incorporated into primordial follicles where they will remain until activated (Pisarska et al., 2004). Following follicle activation, the oocytes will undergo global DNA re-methylation and maternal imprinting mediated by DNMT3A as they mature before ovulation (Kaneda et al., 2010; Kobayashi et al., 2012; Lucifero et al., 2004; Smallwood et al., 2011).

In the embryonic testis, the prospermatogonia undergo a similar global DNA re-methylation and paternal imprinting driven by DNMT3A and DNMT3B in coordination with the piRNA machinery and the catalytically inactive DNMT3L (Aravin et al., 2008; Bourc'his and Bestor, 2004; Kato et al., 2007; Suetake et al., 2004). Following DNA re-methylation, the post-natal prospermatogonia will then either migrate towards the basement of the seminiferous tubule and become long lasting spermatogonial stem cells (SSCs) or differentiate into spermatogonia

and ultimately sperm as part of the first wave of spermatogenesis (McLean et al., 2003; Yoshida et al., 2006).

Throughout these processes, from specification to gametogenesis, proper regulation of UHRF1 has been shown to be essential. Despite being downregulated during mouse PGC global DNA demethylation, UHRF1 protein accumulates in the cytoplasm as early as E10.5 when PGCs enter the genital ridges (Seisenberger et al., 2012). Additionally, *Uhrf1* expression increases coincident with sex-specific differentiation at E12.5 (Kagiwada et al., 2013; Seisenberger et al., 2012), suggesting a potential role in DNA re-methylation. Indeed UHRF1 has been shown to be essential for this process in oocytes with knockout resulting in increased hemi-methylated DNA and the improper localization of DNMT1 to the cytoplasm (Cao et al., 2019; Maenohara et al., 2017). Additionally, in the adult testes UHRF1 has been shown to interact with the pachytene piRNA machinery to maintain DNA methylation within the differentiating spermatogonia (Dong et al., 2019; Wang et al., 2015).

Taken together, these studies suggest that UHRF1 is essential throughout germline differentiation. However, a truly longitudinal analysis of its role from the time of specification through gametogenesis has yet to be performed. We evaluated the role of UHRF1 in PGCs by performing a PGC specific conditional deletion of UHRF1 (UCKO) at the time of specification from the epiblast. Through immunofluorescence imaging of gonadal sections and cell sorting we found that UHRF1 is not essential for regulating the timing of PGC sex-specific differentiation. Additionally, while UHRF1 does not appear to be essential for the genomic re-methylation of the prospermatogonia or establishment of the SSC population in the testis, it is necessary for the long-term maintenance of this SSC population. Taken together, this work provides a strong

foundation from which to investigate the loci specific impacts of UHRF1 in DNA methylation at different stages of germline development.

Results

UHRF1 does not regulate PGC differentiation

In order to assess the role of UHRF1 in the germline, we crossed the *Uhrf1f/f* (Obata et al., 2014) allele which has been previously used to study the role of UHRF1 in T cells and the *Blimp1-cre* (BC) (Ohinata et al., 2005) allele to create a PGC specific UHRF1 conditional knockout (UCKO). *Blimp1* is expressed in the PGC precursors prior to specification from the epiblast and this expression is maintained for several days throughout the migration of PGCs ensuring near complete recombination by colonization of the genital ridges at E9.5 (Li et al., 2015; Ohinata et al., 2005). We also crossed in the *Oct4-GFP* (OG) (Lengner et al., 2007) allele to create a GFP reporter to isolate GFP+ PGCs from the embryonic gonads via fluorescent activated cell sorting (FACS) (Figure 1A). Using this approach, we discovered no significant change in GFP+ PGCs isolated from the embryonic ovary or testis at E13.5 (Figure 1B and C). This suggests that UHRF1 is not essential for the migration into and proliferation of either XX or XY PGCs in the embryonic gonads.

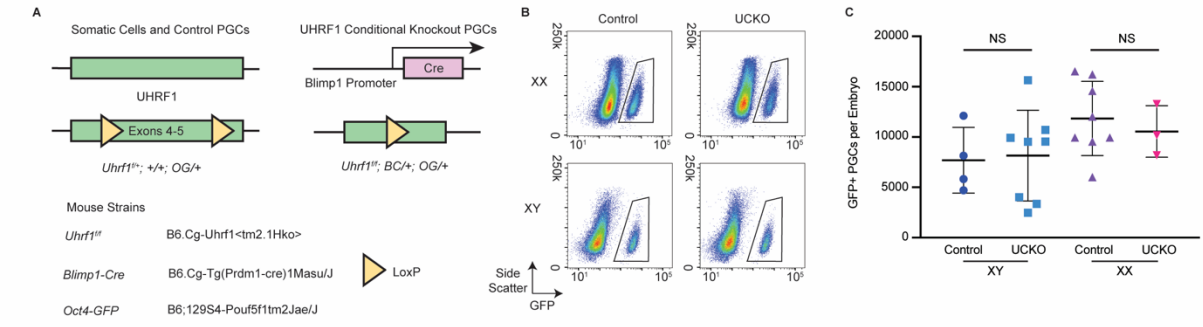

Figure 1: UHRF1 is not Required for Embryonic Germline Proliferation. A) Schematic for UHRF1 conditional knockout used in subsequent experiments. Upon PGC specification, Cre will

be expressed and excise *Uhrf1* exons 4-5 flanked by LoxP sites leading to a UHRF1 conditional knockout. All mouse strains used in this experiment are listed. B) Representative flow cytometry plots from E13.5 XX and XY control and UCKO dissociated gonads. Boxed population of cells represents the quantified GFP+ PGC population. C) Quantification of average PGC number at E13.5 (n=3-8 embryos). Significance was calculated using a two-tailed unequal variance T-test with $P<0.05$ considered significant.

UHRF1 does not regulate embryonic or adult XX germline differentiation

Given that UHRF1 does not play a role in regulating the timing of PGC differentiation in the embryonic gonads, we next wanted to determine if it has a role in the transition from the embryonic to the adult gonads. Therefore, we harvested ovaries at E13.5 and P10, and performed immunofluorescent (IF) staining to detect proper oocyte development. These time points were chosen because they map the exit from the PGC stage into oogonia following sex-specific differentiation (E13.5) (Saitou and Yamaji, 2012) and initiation of folliculogenesis within the adult ovary (P10) (Pisarska et al., 2004). Consistent with our FACs observations, we noticed no difference in the presence or organization of VASA+ UCKO and control XX PGCs within the E13.5 embryonic ovary (Figure 2A). Likewise, at P10 there was no change in the presence of STELLA+ oocytes within the control and UCKO ovaries. During this stage of ovarian development we would expect to see both primordial and primary follicles with loosely associated and a single unbroken layer of FOXL2+ granulosa cells, respectively (Pisarska et al., 2004). Indeed, both control and UCKO oocytes show proper follicular development with both primordial and primary follicles present (Figure 2B). Interestingly, while UHRF1 does not appear to be required for proper oocyte differentiation, it is heavily enriched within cytoplasm of

oocytes following initiation of folliculogenesis.

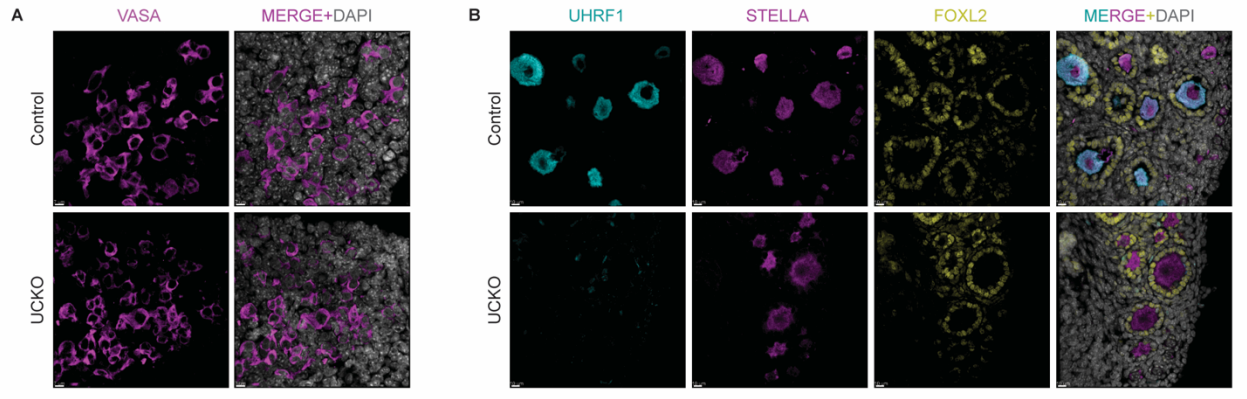

Figure 2: UHRF1 is not Required for XX Germline Maturation. A) Representative IF image of VASA+ PGCs in control and UCKO E13.5 ovaries. Scale bar is 7 µm (n=1). B) Representative IF image of control and UCKO P10 ovaries. STELLA is an oocyte marker, FOXL2 is a marker of the supporting follicle cells. Primordial follicles contain relatively small STELLA+ oocytes and a loose association of FOXL2+ follicle cells. Primary follicles are larger STELLA+ oocytes with a cytoplasm enriched for UHRF1 and ringed by a single layer of FOXL2+ follicle cells. Scale bar is 10 µm (n=3).

UHRF1 is required for maintenance of spermatogonial stem cells

In order to assess the role of UHRF1 in the spermatogenesis, we harvested testes at E13.5, P1, P10 and week 6 and performed immunofluorescent staining. These time points were chosen since they mark the differentiation of PGCs into the prospermatogonial stem cells following completion of sex-specific differentiation (E13.5) (Saitou and Yamaji, 2012), the prospermatogonial stem cells in the postnatal testis prior to the first wave of spermatogenesis (P1) (Shinohara et al., 2001; Yoshida et al., 2006), the spermatogonial stem cells (SSC) and first wave spermatogonia (P10) (Shinohara et al., 2001; Yoshida et al., 2006) and the stable SSC

population (week 6). Much like in the ovary, we saw no change in the gross morphology or localization of PGCs at E13.5 or prospermatogonial stem cells at P1 (Figure 3A). Additionally, there is no change in localization of the SALL4+ SSCs to the basement membrane of the P10 tubule, suggesting that UHRF1 is not essential for surviving first wave spermatogenesis or establishment of the long-term adult SSC population (Hobbs et al., 2012; McLean et al., 2003; Shinohara et al., 2001; Yoshida et al., 2006). However, by week 6 there was a depletion of SALL4+ SSCs within the UCKO testes and a complete lack of VASA+ spermatogonia and round spermatids within the tubules as well as spermatozoa within the lumen (Toyooka et al., 2000). Additionally, the week 6 UCKO testes are undersized and underweight compared to the control testes consistent with a reduction in SSC number and decreased spermatogenesis (Figure 3B) (Pan et al., 2020; Sun et al., 2015; Takada et al., 2021; Xiong et al., 2022). Additionally, we show that UHRF1 is not required for the DNA re-methylation which occurs within the fetal prospermatogonial stem cells (Figure 3C) (Kobayashi et al., 2013; Seisenberger et al., 2012). Taken together we have identified that while UHRF1 has no role in regulating oocyte maturation, it is necessary for the long-term maintenance of SSCs within the testis.

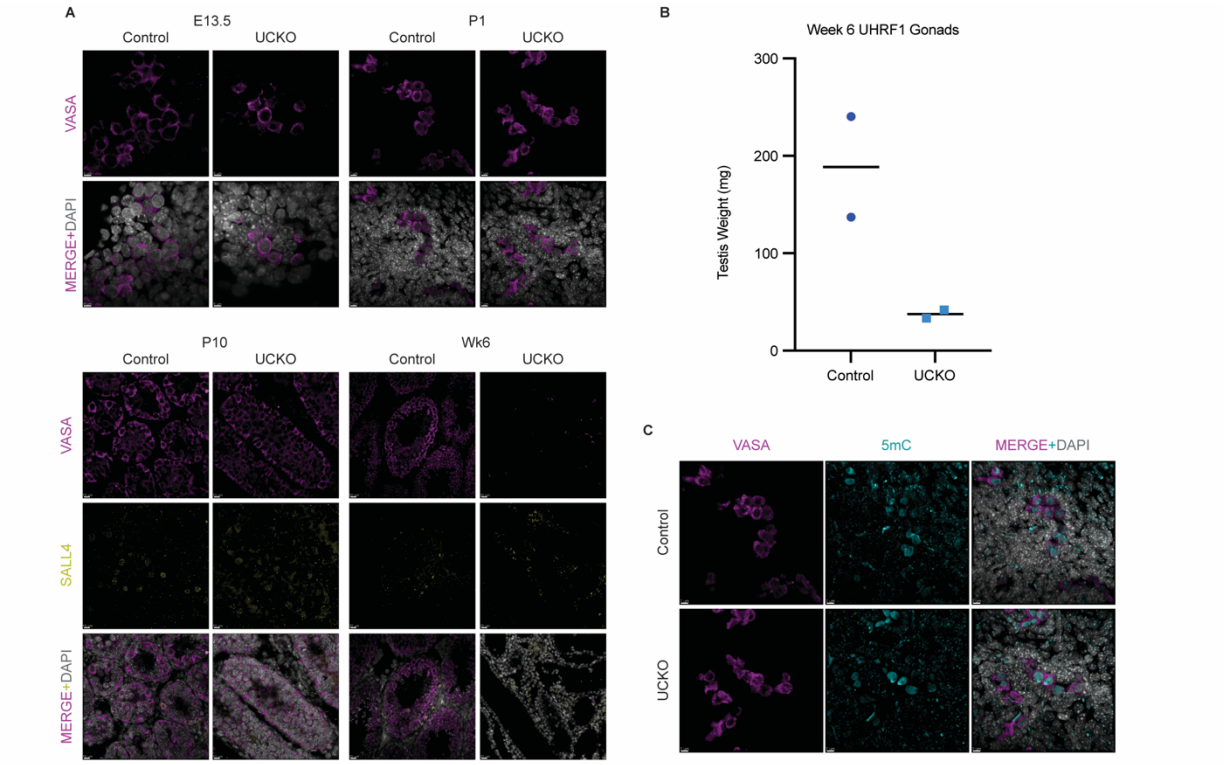

Figure 3: UHRF1 is required for the Maintenance of Spermatogonial Stem Cells. A) Representative IF image of control and UCKO E13.5, P1, P10 and week 6 testes. VASA is a marker of the PGCs at E13.5, prospermatogonial stem cells at P1 and maturing spermatogonia and round spermatids at P10 and week 6. Sall4 is a marker of the spermatogonial stem cells at P10 and week 6. Scale bar is 5 µm at E13.5 (n=2), 7 µm at P1 (n=1), 10 µm at P10 (n=1) and 20 µm at week 6 (n=1). B) Quantified weight of control and UCKO week 6 testes in mg. n=2. C) Representative IF image of 5mC in control and UCKO P1 testes. Scale bar is 7 µm (n=1).

Discussion

In this study, we provide evidence that while UHRF1 plays a key role in regulating the XY adult germline, it is not essential for either the embryonic germline or oocyte differentiation. Through this, we have clarified the role of UHRF1 in regulating the differentiation of the germline from specification to gametogenesis in the mouse.

One of the major findings of this study is that UHRF1 is not essential for the sex-specific differentiation of the embryonic germline. While it has been proposed that the downregulation of *Uhrf1* following specification of the mouse PGCs from the epiblast is essential for global replication coupled DNA demethylation, the continued presence of low levels of UHRF1 protein in the PGC cytoplasm and increased expression during sex-specific differentiation meant that it may still have a role in the embryonic germline (Kagiwada et al., 2013; Seisenberger et al., 2012). The DNMT1 directed maintenance of loci-specific DNA methylation at the late demethylating promoters has been previously shown to be essential to properly regulate the sex-specific differentiation of mouse PGCs (Hargan-Calvopina et al., 2016). Here we show that loss of UHRF1 does not impact the timing of mouse PGC sex-specific differentiation. While we cannot rule out that UHRF1 may play a contributing role in the maintenance of DNA methylation at certain loci, the failure to replicate the phenotype observed in the DNMT1 knockouts suggests that this would be minor.

In the ovary, we saw no appreciable differences between the morphology of the UCKO and control oocytes at P10. Therefore, while UHRF1 protein has been observed in the fetal oocyte and has previously been shown to have a role in regulating *Line1* in spermatogonia, it does not appear to have a similar role in the oocyte (Dong et al., 2019; Malki et al., 2014; Seisenberger et al., 2012). This could be due to the fact that the piRNA machinery, while present in the mouse fetal oocyte, is not essential for the repression of TEs (Taborska et al., 2019). However, whether this non-essential role for piRNAs and UHRF1 holds true for human fetal oocytes remains to be determined and provides an exciting area of future research (Roovers et al., 2015; Tharp et al., 2020). Our findings on the non-essential role of UHRF1 in folliculogenesis has been previously reported (Cao et al., 2019; Maenohara et al., 2017). Using

an oocyte specific *Zp3* promoter driven *Cre*, these studies show that genomic re-methylation and the establishment of maternal imprinting is altered following loss of UHRF1 (Kaneda et al., 2010; Kobayashi et al., 2012; Lucifero et al., 2004; Smallwood et al., 2011). Additionally, aneuploidy and accumulation of DNA damage was observed in the UHRF1 knockout oocytes (Cao et al., 2019; Maenohara et al., 2017). Despite these defects, UHRF1 knockout oocytes can still complete folliculogenesis and become fertilized, arresting at the 2 to 4-cell stage of embryonic development (Cao et al., 2019).

In the XY germline, we observed a re-methylation of the prospermatogonial stem cells prior to birth and the proper establishment of the spermatogonial stem cells before a complete collapse of spermatogenesis by week 6. Despite the fact that DNA re-methylation of the prospermatogonial cells is involves the pre-pachytene piRNA machinery including PIWIL2 which UHRF1 has previously been reported to interact with, UHRF1 does not appear essential for this process (Aravin et al., 2008; Dong et al., 2019). However, we cannot rule out that while we do not see a change in the XY global DNA re-methylation by IF, UHRF1 may still play a role in repressing the TEs and paternal imprinting as was seen in oocytes (Maenohara et al., 2017). Additionally, UHRF1 does not appear essential for the post-natal establishment of the SSC population nor the initiation of first wave spermatogenesis (McLean et al., 2003; Yoshida et al., 2006). However, it is unlikely that these first round spermatogonia ultimately become viable sperm due to the known role of UHRF1 in regulating meiotic chromosome pairing (Pan et al., 2020; Takada et al., 2021; Xiong et al., 2022). Similar to the oocyte, loss of UHRF1 causes aneuploidy as well as a failure to undergo meiotic sex chromosome inactivation ultimately leading to meiotic catastrophe. Intriguingly, UHRF1 also appears essential for the maintenance

of the SALL4+ SSC population and therefore may have a role outside of spermatogenesis. This will require future in order to identify the mechanism by which this occurs.

Taken together, these results have now broadly characterized UHRF1 during the entirety of mouse germline development, from specification through fertilization. However, questions still remain over the exact role in regulating loci specific methylation following sex-specific differentiation, particularly at imprinting control regions and transposable elements.

Methods

Mouse Husbandry

All animal experiments for this study were approved by the UCLA Institutional Animal Care and Use Committee, also known as the Chancellor's Animal Research Committee. All mouse lines were established from strains acquired from either Jackson labs (Oct4-GFP and Blimp1-cre strains) or Riken (UHRF1 strain). Control and UCKO XY and XX embryonic gonads were obtained from crosses between OG; Uhrf1$^{fl/fl}$ (Lengner et al., 2007; Obata et al., 2014) homozygous XX and BC; Uhrf1$^{fl/+}$ heterozygous XY (Ohinata et al., 2005) at E13.5 and postnatal gonads harvested at P1, P10 and week 6. Embryos were staged at E0.5 by the detection of a vaginal plug on the morning after time-mating pairs were established.

Immunofluorescence

Embryonic (E13.5) and postnatal gonads (P1, P10 and wk6) were extracted via microdissection and fixed in 4% paraformaldehyde (Life Technologies) over night at 4˚C. Week 6 testes were weighed prior to fixation. Following fixation, gonads were stored in 70% ethanol until sectioning. Gonads were embedded in paraffin wax and then cut into 5 µm sections. Sections were deparaffinized via immersion in xylene (Fisher Scientific) and rehydrated in an ethanol

series. Antigen retrieval was performed at 95°C in either Tris-EDTA (10mM Trizma base (Sigma), 1mM EDTA (Sigma), 0.05% Tween-20 (Fisher Scientific) at a pH of 9.0) buffer for 40 minutes and then cooled back to room temperature (RT). Sections were washed with 0.2% Tween 20 in PBS (Fisher Scientific) (PBST), permeabilized in 0.5% Triton X-100 (Sigma) in PBS for 20 minutes at room temperature and then washed with PBST. Sections were blocked for 1 hour in 10% donkey serum (Fisher Scientific) in PBST. The primary antibody was added at the manufacturers recommended concentration in 2.5% donkey serum PBST and incubated overnight at 4°C in a humid chamber. Secondary antibody was added at a concentration of 1:200 in 2.5% donkey serum PBST and 1x DAPI (Fisher Scientific) for 1 hour at room temperature. Slides were mounted in Prolong Gold without DAPI mounting media (Invitrogen) and set to cure overnight at room temperature in a dark chamber before being transferred to 4°C for long term storage. All immunofluorescence sections were imaged on a Zeiss LSM 880 microscope as a Z stack which was then processed in Imaris (Bitplane) to trim the Z-stack to a one to two cell thickness (~5 µm) as a maximum intensity projection, adjust individual channels brightness for publication. All immunofluorescence antibodies in Table S1.

Table S1: All antibodies used in this chapter.

Antibodies	Source	Identifier
Goat Polyclonal Anti-MVH	R&D Systems	Cat# AF2030; RRID AB_2277369
Mouse Monoclonal Anti-5mC	Aviva Biosciences	Cat# AMM99021; RRID AB_387479
Rabbit Polyclonal Anti-UHRF1	Santa Cruz	Cat# sc-373750; RRID AB_10947236
Mouse Monoclonal Anti-STELLA	BD Biosciences	Cat# 556003; RRID AB_396287
Goat Polyclonal Anti-FOXL2	Novus Biologicals	Cat# NB100-1277; RRID AB_2106188
Mouse Monoclonal Anti-SALL4	Abcam	Cat# ab57577; RRID AB_2183366
Donkey Polyclonal Anti-Mouse Alexa Fluor 488	Jackson ImmunoResearch	Cat# 715-546-150; RRID AB_2340849
Donkey Polyclonal Anti-Mouse Alexa Fluor 647	Jackson ImmunoResearch	Cat# 715-605-151; RRID AB_2340863
Donkey Polyclonal Anti-Rabbit Alexa Fluor 594	Jackson ImmunoResearch	Cat# 711-585-152; RRID AB_2340621
Donkey Polyclonal Anti-Goat Alexa Fluor 488	Jackson ImmunoResearch	Cat# 705-546-147; RRID AB_2340430
Donkey Polyclonal Anti-Goat Alexa Fluor 594	Jackson ImmunoResearch	Cat# 705-586-147; RRID AB_2340434

Sample Preparation for Flow Cytometry

Embryonic gonads (E13.5) were extracted from the embryos via microdissection and dissociated in 100 µL of 0.05% Trypsin- EDTA (Thermo Fisher Scientific) at 37℃ for 5 minutes with additional minutes added if necessary. Quenched with 200 µL MEF media (10% FBS in DMEM) and spun down at 300xG to pellet the dissociated cells. The pellet was resuspended in 1% BSA (Sigma-Aldrich), passed through the cap strainer into a 5 mL Falcon Corning FACS tube and 1x 7AAD (Fisher Scientific) was added to the solution prior to sorting. Only 7AAD -, GFP+ cells were quantified for statistical analysis. Significance for Flow Cytometry data was calculated via a two-tailed, unequal variance T-test.

Genotyping

The head from each mouse embryo and tail from postnatal pups was collected for genotyping following extraction of the gonad and dissociated in 100 µL Modified Gitschier Buffer and 3 µL (1:33) Proteinase K (Sigma-Aldrich) at 55℃ overnight followed by a 5 minute 95℃ incubation to inactivate the enzyme. The sample was spun down to pellet the undigested debris and 1 µL of the supernatant was used for the genotyping PCR reactions. PCR products were run on a 2% Agarose gel for 1 hour at 100V. For a sexing PCR, XY embryos have two bands at roughly 300 bp and 280 bp, whereas XX only have a single band at 300 bp. Blimp1-cre PCR shows a single band at 200 bp if the transgene is present. Finally, for UHRF1 the control band is at around 150 bp with a larger mutant band at around 300 bp. The sequence oligos is present in Table S2.

Table S2: Genotyping PCR primers used in this chapter.

Primer Name	Primer	Purpose	Sequence
SMCX-1	Forward	Genotyping	CCGCTGCCAAATTCTTTGG
SMCY-1	Reverse	Genotyping	TGAAGCTTTTGGCTTTGAG
Blimp-Cre Transgene	Forward	Genotyping	GCCGAGGTGCGCGTCAGTAC
Blimp-Cre Transgene	Reverse	Genotyping	CTGAACATGTCCATCAGGTTCTTG
Oct4 Control	Forward	Genotyping	GATCACCTGGGGTTTGAGAA
Oct4 Control	Reverse	Genotyping	CAAGGCAAGGGAGGTAGACA
Oct4 Transgene	Forward	Genotyping	CAAGGCAAGGGAGGTAGACA
Oct4 Transgene	Reverse	Genotyping	AGGAACTGCTTCCTTCACGA
UHRF1 fl/fl	Forward	Genotyping	CATCTCTGTACTGACAACTGCACA
UHRF1 fl/fl	Reverse	Genotyping	CTTCAACCACATCTGCTAGGATTC

References

Aravin, A.A., Sachidanandam, R., Bourc'his, D., Schaefer, C., Pezic, D., Toth, K.F., Bestor, T., and Hannon, G.J. (2008). A piRNA pathway primed by individual transposons is linked to de novo DNA methylation in mice. Mol. Cell *31*, 785–799. https://doi.org/10.1016/j.molcel.2008.09.003.

Bourc'his, D., and Bestor, T.H. (2004). Meiotic catastrophe and retrotransposon reactivation in male germ cells lacking Dnmt3L. Nature *431*, 96–99. https://doi.org/10.1038/nature02886.

Cao, Y., Li, M., Liu, F., Ni, X., Wang, S., Zhang, H., Sui, X., and Huo, R. (2019). Deletion of maternal UHRF1 severely reduces mouse oocyte quality and causes developmental defects in preimplantation embryos. The FASEB Journal *33*, 8294–8305. https://doi.org/10.1096/fj.201801696RRRR.

Dong, J., Wang, X., Cao, C., Wen, Y., Sakashita, A., Chen, S., Zhang, J., Zhang, Y., Zhou, L., Luo, M., et al. (2019). UHRF1 suppresses retrotransposons and cooperates with PRMT5 and PIWI proteins in male germ cells. Nat Commun *10*, 4705. https://doi.org/10.1038/s41467-019-12455-4.

Ginsburg, M., Snow, M.H., and McLaren, A. (1990). Primordial germ cells in the mouse embryo during gastrulation. Development *110*, 521–528. .

Hargan-Calvopina, J., Taylor, S., Cook, H., Hu, Z., Lee, S.A., Yen, M.-R., Chiang, Y.-S., Chen, P.-Y., and Clark, A.T. (2016). Stage-Specific Demethylation in Primordial Germ Cells Safeguards against Precocious Differentiation. Dev. Cell *39*, 75–86. https://doi.org/10.1016/j.devcel.2016.07.019.

Hill, P.W.S., Leitch, H.G., Requena, C.E., Sun, Z., Amouroux, R., Roman-Trufero, M., Borkowska, M., Terragni, J., Vaisvila, R., Linnett, S., et al. (2018). Epigenetic reprogramming enables the primordial germ cell-to-gonocyte transition. Nature *555*, 392–396. https://doi.org/10.1038/nature25964.

Hobbs, R.M., Fagoonee, S., Papa, A., Webster, K., Altruda, F., Nishinakamura, R., Chai, L., and Pandolfi, P.P. (2012). Functional Antagonism between Sall4 and Plzf Defines Germline Progenitors. Cell Stem Cell *10*, 284–298. https://doi.org/10.1016/j.stem.2012.02.004.

Jameson, S.A., Natarajan, A., Cool, J., DeFalco, T., Maatouk, D.M., Mork, L., Munger, S.C., and Capel, B. (2012). Temporal Transcriptional Profiling of Somatic and Germ Cells Reveals Biased Lineage Priming of Sexual Fate in the Fetal Mouse Gonad. PLOS Genetics *8*, e1002575. https://doi.org/10.1371/journal.pgen.1002575.

Kagiwada, S., Kurimoto, K., Hirota, T., Yamaji, M., and Saitou, M. (2013). Replication-coupled passive DNA demethylation for the erasure of genome imprints in mice. The EMBO Journal *32*, 340–353. https://doi.org/10.1038/emboj.2012.331.

Kaneda, M., Hirasawa, R., Chiba, H., Okano, M., Li, E., and Sasaki, H. (2010). Genetic evidence for Dnmt3a-dependent imprinting during oocyte growth obtained by conditional knockout with Zp3-Cre and complete exclusion of Dnmt3b by chimera formation. Genes to Cells *15*, 169–179. https://doi.org/10.1111/j.1365-2443.2009.01374.x.

Kato, Y., Kaneda, M., Hata, K., Kumaki, K., Hisano, M., Kohara, Y., Okano, M., Li, E., Nozaki, M., and Sasaki, H. (2007). Role of the Dnmt3 family in de novo methylation of imprinted and repetitive sequences during male germ cell development in the mouse. Human Molecular Genetics *16*, 2272–2280. https://doi.org/10.1093/hmg/ddm179.

Kobayashi, H., Sakurai, T., Imai, M., Takahashi, N., Fukuda, A., Yayoi, O., Sato, S., Nakabayashi, K., Hata, K., Sotomaru, Y., et al. (2012). Contribution of Intragenic DNA Methylation in Mouse Gametic DNA Methylomes to Establish Oocyte-Specific Heritable Marks. PLOS Genetics *8*, e1002440. https://doi.org/10.1371/journal.pgen.1002440.

Kobayashi, H., Sakurai, T., Miura, F., Imai, M., Mochiduki, K., Yanagisawa, E., Sakashita, A., Wakai, T., Suzuki, Y., Ito, T., et al. (2013). High-resolution DNA methylome analysis of primordial germ cells identifies gender-specific reprogramming in mice. Genome Res *23*, 616–627. https://doi.org/10.1101/gr.148023.112.

Lengner, C.J., Camargo, F.D., Hochedlinger, K., Welstead, G.G., Zaidi, S., Gokhale, S., Scholer, H.R., Tomilin, A., and Jaenisch, R. (2007). Oct4 Expression Is Not Required for Mouse Somatic Stem Cell Self-Renewal. Cell Stem Cell *1*, 403–415. https://doi.org/10.1016/j.stem.2007.07.020.

Li, Z., Yu, J., Hosohama, L., Nee, K., Gkountela, S., Chaudhari, S., Cass, A.A., Xiao, X., and Clark, A.T. (2015). The Sm protein methyltransferase PRMT5 is not required for primordial germ cell specification in mice. The EMBO Journal *34*, 748–758. https://doi.org/10.15252/embj.201489319.

Liu, S., Brind'Amour, J., Karimi, M.M., Shirane, K., Bogutz, A., Lefebvre, L., Sasaki, H., Shinkai, Y., and Lorincz, M.C. (2014). Setdb1 is required for germline development and silencing of H3K9me3-marked endogenous retroviruses in primordial germ cells. Genes Dev. *28*, 2041–2055. https://doi.org/10.1101/gad.244848.114.

Lucifero, D., Mann, M.R.W., Bartolomei, M.S., and Trasler, J.M. (2004). Gene-specific timing and epigenetic memory in oocyte imprinting. Human Molecular Genetics *13*, 839–849. https://doi.org/10.1093/hmg/ddh104.

Maenohara, S., Unoki, M., Toh, H., Ohishi, H., Sharif, J., Koseki, H., and Sasaki, H. (2017). Role of UHRF1 in de novo DNA methylation in oocytes and maintenance methylation in preimplantation embryos. PLOS Genetics *13*, e1007042. https://doi.org/10.1371/journal.pgen.1007042.

Malki, S., van der Heijden, G.W., O'Donnell, K.A., Martin, S.L., and Bortvin, A. (2014). A Role for Retrotransposon LINE-1 in Fetal Oocyte Attrition in Mice. Developmental Cell *29*, 521–533. https://doi.org/10.1016/j.devcel.2014.04.027.

McLean, D.J., Friel, P.J., Johnston, D.S., and Griswold, M.D. (2003). Characterization of Spermatogonial Stem Cell Maturation and Differentiation in Neonatal Mice1. Biology of Reproduction *69*, 2085–2091. https://doi.org/10.1095/biolreprod.103.017020.

Obata, Y., Furusawa, Y., Endo, T.A., Sharif, J., Takahashi, D., Atarashi, K., Nakayama, M., Onawa, S., Fujimura, Y., Takahashi, M., et al. (2014). The epigenetic regulator Uhrf1 facilitates the proliferation and maturation of colonic regulatory T cells. Nature Immunology *15*, 571–579. https://doi.org/10.1038/ni.2886.

Ohinata, Y., Payer, B., O'Carroll, D., Ancelin, K., Ono, Y., Sano, M., Barton, S.C., Obukhanych, T., Nussenzweig, M., Tarakhovsky, A., et al. (2005). Blimp1 is a critical determinant of the germ cell lineage in mice. Nature *436*, 207–213. https://doi.org/10.1038/nature03813.

Pan, H., Jiang, N., Sun, S., Jiang, H., Xu, J., Jiang, X., Gao, Q., Li, L., Wu, H., Zheng, H., et al. (2020). UHRF1-repressed 5'-hydroxymethylcytosine is essential for the male meiotic prophase I. Cell Death Dis *11*, 1–17. https://doi.org/10.1038/s41419-020-2333-3.

Pisarska, M.D., Bae, J., Klein, C., and Hsueh, A.J.W. (2004). Forkhead L2 Is Expressed in the Ovary and Represses the Promoter Activity of the Steroidogenic Acute Regulatory Gene. Endocrinology *145*, 3424–3433. https://doi.org/10.1210/en.2003-1141.

Roovers, E.F., Rosenkranz, D., Mahdipour, M., Han, C.-T., He, N., Chuva de Sousa Lopes, S.M., van der Westerlaken, L.A.J., Zischler, H., Butter, F., Roelen, B.A.J., et al. (2015). Piwi Proteins and piRNAs in Mammalian Oocytes and Early Embryos. Cell Reports *10*, 2069–2082. https://doi.org/10.1016/j.celrep.2015.02.062.

Saitou, M., and Yamaji, M. (2012). Primordial Germ Cells in Mice. Cold Spring Harb Perspect Biol *4*, a008375. https://doi.org/10.1101/cshperspect.a008375.

Seisenberger, S., Andrews, S., Krueger, F., Arand, J., Walter, J., Santos, F., Popp, C., Thienpont, B., Dean, W., and Reik, W. (2012). The Dynamics of Genome-wide DNA Methylation Reprogramming in Mouse Primordial Germ Cells. Mol Cell *48*, 849–862. https://doi.org/10.1016/j.molcel.2012.11.001.

Shinohara, T., Orwig, K.E., Avarbock, M.R., and Brinster, R.L. (2001). Remodeling of the postnatal mouse testis is accompanied by dramatic changes in stem cell number and niche accessibility. Proceedings of the National Academy of Sciences *98*, 6186–6191. https://doi.org/10.1073/pnas.111158198.

Smallwood, S.A., Tomizawa, S., Krueger, F., Ruf, N., Carli, N., Segonds-Pichon, A., Sato, S., Hata, K., Andrews, S.R., and Kelsey, G. (2011). Dynamic CpG island methylation landscape in oocytes and preimplantation embryos. Nat Genet *43*, 811–814. https://doi.org/10.1038/ng.864.

Suetake, I., Shinozaki, F., Miyagawa, J., Takeshima, H., and Tajima, S. (2004). DNMT3L stimulates the DNA methylation activity of Dnmt3a and Dnmt3b through a direct interaction. J Biol Chem *279*, 27816–27823. https://doi.org/10.1074/jbc.M400181200.

Sun, F., Xu, Q., Zhao, D., and Degui Chen, C. (2015). Id4 Marks Spermatogonial Stem Cells in the Mouse Testis. Sci Rep *5*, 17594. https://doi.org/10.1038/srep17594.

Taborska, E., Pasulka, J., Malik, R., Horvat, F., Jenickova, I., Matošević, Z.J., and Svoboda, P. (2019). Restricted and non-essential redundancy of RNAi and piRNA pathways in mouse oocytes. PLOS Genetics *15*, e1008261. https://doi.org/10.1371/journal.pgen.1008261.

Takada, Y., Yaman-Deveci, R., Shirakawa, T., Sharif, J., Tomizawa, S., Miura, F., Ito, T., Ono, M., Nakajima, K., Koseki, Y., et al. (2021). Maintenance DNA methylation in pre-meiotic germ cells regulates meiotic prophase by facilitating homologous chromosome pairing. Development *148*, dev194605. https://doi.org/10.1242/dev.194605.

Tharp, M.E., Malki, S., and Bortvin, A. (2020). Maximizing the ovarian reserve in mice by evading LINE-1 genotoxicity. Nat Commun *11*, 330. https://doi.org/10.1038/s41467-019-14055-8.

Toyooka, Y., Tsunekawa, N., Takahashi, Y., Matsui, Y., Satoh, M., and Noce, T. (2000). Expression and intracellular localization of mouse Vasa-homologue protein during germ cell development. Mechanisms of Development *93*, 139–149. https://doi.org/10.1016/S0925-4773(00)00283-5.

von Meyenn, F., Berrens, R.V., Andrews, S., Santos, F., Collier, A.J., Krueger, F., Osorno, R., Dean, W., Rugg-Gunn, P.J., and Reik, W. (2016). Comparative Principles of DNA Methylation Reprogramming during Human and Mouse In Vitro Primordial Germ Cell Specification. Dev Cell *39*, 104–115. https://doi.org/10.1016/j.devcel.2016.09.015.

Wang, Y., Zhu, T., Li, Q., Liu, C., Han, F., Chen, M., Zhang, L., Cui, X., Qin, Y., Bao, S., et al. (2015). Prmt5 is required for germ cell survival during spermatogenesis in mice. Sci Rep *5*, 11031. https://doi.org/10.1038/srep11031.

Xiong, M., Zhou, S., Feng, S., Gui, Y., Li, J., Wu, Y., Dong, J., and Yuan, S. (2022). UHRF1 is indispensable for meiotic sex chromosome inactivation and interacts with the DNA damage response pathway in mice†. Biology of Reproduction ioac054. https://doi.org/10.1093/biolre/ioac054.

Yoshida, S., Sukeno, M., Nakagawa, T., Ohbo, K., Nagamatsu, G., Suda, T., and Nabeshima, Y. (2006). The first round of mouse spermatogenesis is a distinctive program that lacks the self-renewing spermatogonia stage. Development *133*, 1495–1505. https://doi.org/10.1242/dev.02316.

Chapter 4

EED is required for Primordial Germ Cell Differentiation in the Embryonic Gonad

EED is required for Primordial Germ Cell Differentiation in the Embryonic Gonad

Matthew G. Lowe[1,2,3*], Ming-Ren Yen[4,*], Fei-man Hsu[1,3], Linzi Hosohama[1], Zhongxun Hu[1], Tsotne Chitiashvili[1,2,5], Timothy Hunt[1], Isaac Gorgy[1], Matthew Bernard[1,2], Sissy Wamaitha[1], Pao-Yang Chen[4,#], Amander T. Clark[1,2,3,6,#]

1. Department of Molecular Cell and Developmental Biology, University of California, Los Angeles, California, 90095, USA;

2. Molecular Biology Institute, University of California, Los Angeles, California, 90095, USA;

3. Eli and Edythe Broad Center of Regenerative Medicine and Stem Cell Research, University of California, Los Angeles, California, 90095 USA;

4. Institute of Plant and Microbial Biology, Academia Sinica, Taipei City, 11529, Taiwan;

5. Department of Biological Chemistry, University of California, Los Angeles, California, 90095, USA;

6. Jonsson Comprehensive Cancer Center, University of California, Los Angeles, California, 90095 USA

***co-first author**

 # co-senior author

Contact senior author: Amander Clark clarka@ucla.edu

Summary

Development of Primordial germ cells (PGCs) is required for reproduction. During PGC development in mammals, major epigenetic remodeling occurs which is hypothesized to establish an epigenetic landscape for sex-specific germ cell differentiation and gametogenesis. In order to address the role of Embryonic Ectoderm Development (EED) and Histone 3 lysine 27 trimethylation (H3K27me3) in this process, we created a conditional deletion in EED and show that EED is essential for regulating the timing of sex-specific PGC differentiation in both ovaries and testes, as well as X chromosome dosage decompensation in testes. Integrating chromatin and whole genome bisulfite sequencing of epiblast and PGCs, we identified a poised repressive signature of H3K27me3/DNA methylation which we propose is established in the epiblast where EED and DNMT1 interact. Thus, EED joins DNMT1 in regulating the timing of sex-specific PGC differentiation during the critical window when the gonadal niche cells specialize into an ovary or testis.

Introduction

Primordial germ cells (PGCs) are the embryonic progenitors of the germline and their correct epigenetic regulation and sex-specific differentiation is essential for establishing fertility in the adult. In the mouse embryo, the PGC stage of germline development takes around seven days beginning at embryonic day (E) 6.25 with specification of PGCs from the epiblast and ending at E13.5, after the committed PGCs have colonized the embryonic gonad (Ginsburg et al., 1990; Saitou and Yamaji, 2012). In the last 24 hours of PGC development, between E12.5-E13.5, XX and XY PGCs heterogeneously initiate sex-specific differentiation in response to gonadal cues (Jameson et al., 2012). This differentiation is accompanied by locus-specific epigenetic changes

to promoters and enhancers combined with global remodeling of chromatin (Guibert et al., 2012; Hackett et al., 2013; Hajkova et al., 2002; Hill et al., 2018; Kobayashi et al., 2013; Liu et al., 2014; Seisenberger et al., 2012; Yokobayashi et al., 2013; Zheng et al., 2016). Following sex-specific differentiation the germ cells enter cell cycle arrest by E15.5, either in prophase I of meiosis I as XX PGCs become meiotic germ cells, or in G0 cell cycle arrest XY PGCs become pro-spermatogonia (Baltus et al., 2006; Western et al., 2008). It is hypothesized that epigenetic remodeling during the final stages of PGC development is necessary to generate an epigenome conducive to sex-specific differentiation and high-fidelity gametogenesis (Hajkova et al., 2002).

The epigenetic mark trimethylation of lysine 27 on histone 3 (H3K27me3) has long been known to enrich in PGC nuclei following specification from the epiblast (Seki et al., 2005), however little is known about its role in PGC biology. H3K27me3 is generated by polycomb repressor complex 2 (PRC2), composed of the core components Enhancer of Zeste 2 (EZH2), Embryonic Ectoderm Development (EED) and Suppressor of Zeste 12 (SUZ12) (Kuzmichev et al., 2002; Schuettengruber et al., 2017). High levels of EED and SUZ12 are detected in PGC nuclei, concurrent with a global enrichment of H3K27me3 in XY and XX PGCs during development (Mallol et al., 2019; Napoles et al., 2007; Seki et al., 2005). In contrast, while H3K27me3 is initially enriched on the inactive X (Xi) chromosome of XX PGCs at the time of specification, the Xi is rapidly depleted of PRC2 components and H3K27me3 between E8.5 - E9.5 just prior to X chromosome reactivation and repression of the long non-coding RNA X-inactive specific transcript (*Xist*) (Lopes et al., 2008; Mallol et al., 2019; Napoles et al., 2007; Seki et al., 2005; Sugimoto and Abe, 2007). Recent studies have revealed that both the nuclear increase in H3K27me3, and the loss of H3K27me3 from the Xi are dependent upon the transcription factor

Prdm14 (Mallol et al., 2019). After the PGCs have settled into the gonad, H3K27me3 redistributes transiently to the nuclear periphery where it is visualized as a bright ring from E11.5 until the end of PGC sex-specific differentiation (Prokopuk et al., 2017). Nuclear enrichment of H3K27me3 by E9.5 is concurrent with genome wide depletion of DNA methylation, except in locus-specific patches where both H3K27me3 and DNA methylation are identified at CG-island (CGI)-containing promoters of germ cell differentiation genes called "*late demethylators"* (Kobayashi et al., 2013; Seisenberger et al., 2012) or "*germline reprogramming responsive genes*" (GRRs) (Hill et al., 2018) which regulate the timing of PGC differentiation in the embryonic gonad (Hargan-Calvopina et al., 2016) as well as certain transposable elements (TEs) (Liu et al., 2014).

To evaluate locus-specific sites of H3K27me3 enrichment in PGCs at the time of gonadal colonization, chromatin immunoprecipitation (ChIP) followed by sequencing of PGCs isolated at E11.5, E12.5 and E13.5 have revealed that H3K27me3 is enriched at the promoters of genes involved in embryonic and germ cell development, as well as some classes of transposons (Lesch et al., 2013; Liu et al., 2014; Ng et al., 2013; Sachs et al., 2013; Yokobayashi et al., 2013). This promoter enrichment is consistent with other histone modifications that are predicted to synergize with H3K27me3 in PGCs, both in regulating the timing of PGC differentiation as well as maintaining genomic integrity. For example, monoubiquitination at lysine 119 of histone H2A (H2AK119ub1) generated by polycomb repressor complex 1 (PRC1)/RNF2 has been shown to regulate the timing of XX PGC differentiation and entrance into meiosis through regulation of the *Stra8* promoter (Yokobayashi et al., 2013). Addtionally, H3K9me3/SETDB1 and H4R3me2/PRMT5 have broad roles regulating TE repression in PGCs (Kim et al., 2014; Liu et

al., 2014) with H3K9me3 enrichment at some TEs coinciding with both H3K27me3 and DNA methylation (Liu et al., 2014). Repression of TEs throughout germline development is critical because some TEs are still capable of active transposition in mice (Dewannieux et al., 2004; Richardson et al., 2017). Taken together, these studies suggest that H3K27me3 may function in concert with other epigenetic marks to regulate PGC development. However, chemical inhibition of EZH1/2 for 72-hours in *ex vivo* E11.5 gonadal organ culture (Prokopuk et al., 2017, 2018) as well as a hypomorphic mutation in *Eed* (Stringer et al., 2018) had no observable effect on the PGCs despite depletion of H3K27me3.

Given the dynamic nature of H3K27me3 during the course of PGC development *in vivo*, we evaluated the role of EED in PGCs by performing a conditional deletion of EED at the time of PGC specification using Blimp1-Cre (BC). EED is required to add and retain H3K27me3 at nucleosomes, therefore a null deletion in EED causes loss of H3K27me3 from chromatin (Yu et al., 2009). Our work shows that deleting EED and removing H3K27me3 from PGC chromatin regulates the timing of PGC differentiation between E11.5-E13.5, placing H3K27me3 in a synergistic pathway with DNA methylation and H2AK119ub1 in regulating the response of PGCs to the niche during sex-determination. Moreover, we identify a distinct subset of germline promoters within the epiblast uniquely marked with both H3K27me3 and DNA methylation at the time of PGC specification. Finally, our data also reveals that H3K27me3/EED regulates decompensation of X-linked genes in XY PGCs at the end of PGC development (Sangrithi et al., 2017), providing new insights into the phenomenon of X chromosome dosage decompensation in the XY prenatal germline.

Results

Loss of EED Leads to Reduced PGC Number Within the Gonads

To evaluate the role of EED/H3K27me3 in PGCs, we crossed the *Eed*$^{fl/fl}$ (Yu et al., 2009) allele with *Blimp1-Cre* (BC) (Ohinata et al., 2005), to create an EED conditional knockout embryo (ECKO). The *BC* mouse was chosen as *Blimp1 is* expressed in the PGC precursors within the epiblast of mouse embryos and continues to be expressed in PGCs until soon after gonadal colonization (Ohinata et al., 2005) (Figure 1A). In addition, we also crossed the *Eed*$^{fl/fl}$ mice with *Oct4*-GFP (OG) (Lengner et al., 2007) to create a GFP reporter to isolate GFP+ PGCs by fluorescence activated cell sorting (FACS). Using this tool, we performed FACS to isolate *Oct4*-GFP+ PGCs from genital ridges at E10.5 and E11.5 (colonizing PGCs) as well as from the embryonic gonads of XX and XY embryos at E12.5 and E13.5 when H3K27me3 levels are at their highest (Figure 1A and S1A). Using this approach, we discovered a significant reduction in ECKO PGC number compared to controls starting at E11.5 in XX and E12.5 in XY embryos (Figure 1B). Linear regression analysis of PGC number over time shows a distinct difference in doubling time between control and ECKO PGCs, with the effect on XX ECKO PGCs being particularly pronounced (Figure 1C). To evaluate the localization of PGCs within the embryonic gonad at E13.5, we performed immunofluorescence (IF) of embryonic testes and ovaries and show that VASA+ XY ECKO PGCs correctly localize to the AMH+ testis cords (Figure S1B) while XX ECKO PGCs tend to localize into small clusters or nests (Figure S1C). This result indicates that EED regulates the size of the PGC progenitor pool within the gonad between E11.5-E13.5, and does not have an obvious effect on PGC numbers prior to gonadal colonization.

Given the dramatic reduction in PGC number, we next evaluated the presence or absence of H3K27me3 in ECKO and control PGCs at E11.5 and E13.5 using IF. Using the germline transcription factor TFAP2C to mark PGCs (Weber et al, 2010), we show that by E11.5 the vast majority of TFAP2C+ PGCs in ECKO embryos no longer have detectable H3K27me3 (Figure S1D-E). Notably, while the majority of ECKO PGCs do localize properly to the developing gonad, we did observe some rare TFAP2C+ cells still outside the XX embryonic gonad at E11.5 (Figure S1F), which might suggest some developmental delay/mislocalization of ECKO PGCs. However, by E13.5, no VASA+ PGCs were identified outside the embryonic gonad and ECKO PGCs were almost completely depleted of H3K27me3 (Figure 1D-E). Taken together, deleting EED in PGCs leads to loss of H3K27me3 from PGC chromatin by E11.5 and this accompanied by a phenotypic reduction in PGC number between E11.5 and E13.5.

To explore the cause of reduced PGCs at E13.5, we performed IF for the apoptotic marker cleaved PARP (cPARP) (Boulares et al., 1999) and found no significant difference in the fraction of apoptotic PGCs in ECKO embryos relative to control (Figure 1F-G). Additionally, we examined Ki67 which marks cycling cells (Gerdes et al., 1983) and found no significant difference between control and ECKO PGCs at E13.5 (Figure S1G-H). However, it is important to note that Ki67 is still expressed in oocytes initiating meiotic arrest (Traut et al., 2002). This suggests that the reduction in PGC number observed in both sexes by E13.5 is not due to increased apoptosis or entrance into G0.

Given that H3K27me3 becomes enriched in PGCs as DNA methylation is reduced (Seki et al., 2007, 2005), we next evaluated whether loss of EED/H3K27me3 is associated with failure to lose

DNA methylation from the PGC genome by examining 5mC and 5hmC levels using IF. Staining for 5mC in XY and XX ECKO PGCs at E13.5 revealed that global levels of DNA methylation were still depleted in the absence of EED/H3K27me3 (Figure S2A-B). Likewise, the generation of distinct 5hmC foci were also unaffected by loss of EED/H3K27me3 (Figure S2C-D). Therefore, the loss of EED/H3K27me3 does not prevent the global depletion of DNA methylation. In contrast, the active mark H3K27ac was significantly enriched in E13.5 XY PGCs following loss of EED/H3K27me3 consistent with previous reports (Pasini et al., 2010) (Figure S2E-F). While the E13.5 XX PGCs did not have significantly higher H3K27ac signal, they did show a marginal increase and generally had higher H3K27ac signal than XY PGCs.

EED Regulates Precocious Differentiation in the Testis

In order to evaluate whether a deletion of EED in PGCs effects gene expression and identify a mechanism for the reduced PGC number in both sexes, we performed RNA-Seq in XY GFP+ PGCs isolated by FACS from individual embryos at E11.5 and E13.5. Principle component analysis (PCA) of RNA-seq data revealed a major shift in gene expression (PC1) between E11.5 and E13.5 regardless of genotype (Figure 2A). This is expected, and coincides with gonadal niche sex-determination between E11.5-E13.5 which then instructs the PGCs to adopt a sex-specific fate. Additionally, we observed a distinct separation at E13.5 when comparing ECKO and control PGCs along PC2, which indicates a transcriptional shift on account of EED loss. Although ECKO and control PGCs at E11.5 cluster closer together, a small number of significant differentially expressed genes (DEGs) were identified (Table S1), with the vast majority (89%) being upregulated (Figure 2B and Table S1). In order to identify whether the upregulated genes at E11.5 are direct targets of EED/H3K27me3, we evaluated previously published H3K27me3

ChIP-seq data of E11.5 wild-type PGCs (Sachs et al., 2013), and discovered that 81% of upregulated E11.5 XY DEGs are reported to have promoters enriched for H3K27me3. (Figure 2C and Table S1). Therefore, the majority of differentially upregulated genes in the ECKO PGCs are likely to occur as a direct consequence of H3K27me3 loss. Because H3K27me3 is known to also mark TEs in PGCs (Liu et al., 2014), we next assessed whether loss of EED led to an upregulation of TEs at E11.5 and E13.5. We observe a weak positive correlation between up-regulated TE's that are known to be enriched in H3K27me3 (Figure S3A-B), indicating that EED/H3K27me3 does not have a major role in repressing TEs in PGCs.

A recently described phenomenon in the XY germline is X chromosome dosage decompensation, which is initiated at the end of PGC development between E12.5-E14.5 (Sangrithi et al., 2017). Given that *Xist* is not expressed in XY PGCs (McCarrey and Dilworth, 1992), we evaluated whether EED is participating in X chromosome dosage decompensation by examining X chromosome/Autosome (X/A) ratios in XY ECKO and control PGCs (Figure 2D-E). Our data shows that despite there being no significant difference in H3K27me3 promoter abundance between autosomes and the X chromosome in E13.5 XY PGCs (Figure S3C), the X/A ratio in E13.5 ECKO XY PGCs is significantly higher than control (Figure 2D). Using a Hypergeometric test, we discovered that X-linked genes are statistically over-represented amongst the direct targets of EED in XY PGCs at E13.5 (Figure S3D) and that the X-linked genes with known H3K27me3 promoter enrichment appear more sensitive to loss of EED relative to autosomal genes (Figures 2E). Taken together, this data indicates that X chromosome decompensation in the XY germline involves EED/H3K27me3 and that this mode of regulation is likely to be direct.

Similar to E11.5, at E13.5 there is a greater proportion of upregulated genes (59%) in the ECKO PGCs (Figure 2F). Using previously published E13.5 H3K27me3 ChIP-Seq data from FACS isolated PGCs (Liu et al., 2014), we show that approximately half the upregulated DEGs at E13.5 have H3K27me3 promoter enrichment in control PGCs at E13.5; suggesting that depletion of H3K27me3 from chromatin prior to sex-specific differentiation may have indirect or secondary effects on gene expression (Figure 2G and Table S1). Similarly, the vast majority of downregulated DEGs at E11.5 and E13.5 do not contain H3K27me3 and are likely indirect effects of an EED deletion in PGCs (Figures 2C and G). Gene ontology (GO) analysis of the upregulated DEGs at E13.5 revealed an enrichment for genes involved in spermatogenesis and piRNA metabolism (Figure 2H). In contrast, the downregulated DEGs were enriched for GO terms associated with cell cycle and cell division (Figure 2I). Exiting the cell cycle in XY PGCs is a progressive process associated with differentiation into pro-spermatogonia (Western et al., 2008). To confirm that XY PGCs are precociously differentiating downstream of an EED mutation, we performed IF for MILI (PIWIL2) which is expressed in cytoplasmic pi-bodies of pro-spermatogonia (Aravin et al., 2008). Our results show that in the absence of EED, most XY PGCs at E13.5 have MILI in cytoplasmic pi-bodies while only rarely detected in controls (Figure 2J-K). Given the precocious PGC differentiation observed in PGCs at E13.5, combined with the reduction in PGC number at E12.5, we performed single cell RNA sequencing of E12.5 in control and ECKO XY PGCs using SMART-seq to evaluate whether precocious differentiation begins at E12.5 (Figure 2L and S3E). These results show a reduction in *Nanog* levels in about half of the ECKO PGCs indicating preparation for exiting the PGC stage, however *Miwi2 (Piwil4)* was not concomitantly upregulated suggesting that precocious differentiation of XY PGCs into pro-spermatogonia initiates between E12.5 and E13.5. Curiously, we identified de-repression of *Hoxa1* and *Hoxb1* in a small number

of cells which are indicative of somatic gene expression. Finally, some rare ECKO XY PGCs also exhibited an increased in *Stra8*, a gene required for meiotic initiation (Baltus et al., 2006). However, this was not a major phenomenon, occurring in only 6/26 ECKO PGCs (Figure S3E). Taken together these results suggest that EED is necessary to prevent precocious differentiation of XY PGCs into pro-spermatogonia following sex specific differentiation of the gonadal niche, and that EED participates in the XY PGC X chromosome dosage decompensation at E13.5.

EED Regulates Precocious Differentiation in the Ovary

Given that XX PGC numbers were reduced in the ovaries of ECKO embryos, we next turned to the hypothesis that similar to RNF2/PRC1 (Yokobayashi et al., 2013), EED/PRC2 regulates XX PGC differentiation timing. Following deletion of *Rnf2*, the meiotic initiator *Stra8,* is precociously upregulated driving entrance of XX PGCs into meiosis (Yokobayashi et al., 2013). To evaluate whether EED/PRC2 functions upstream of PRC1 in PGCs, we performed IF for the PRC1 deposited epigenetic mark monoubiquitin of lysine 119 on histone 2A (H2AK119ub1) (de Napoles et al., 2004) at E13.5 (Figure S4A-B). Through this, we show that global H2AK119ub1 enrichment is not altered in XX and XY PGCs despite the absence of EED/HK27me3.

In order to evaluate how loss of EED may affect X chromosome dosage compensation in XX PGCs, we performed RNA sequencing of FACS isolated OG+ PGCs from XX ECKO and control embryonic ovaries at E11.5. This data showed that deletion of EED had no effect on PGC X-chromosome dosage compensation (Figure 3A) and only weak effects on TE expression at E11.5 (Figure S3F). Analysis of autosomal genes revealed a relatively small number of DEGs at E11.5, the majority which were upregulated (81%) (Figure 3B and Table S1). In particular, *Stra8* was

upregulated and genes associated with proliferative PGCs (*Pecam1 and Klf5*) were downregulated (Figure 3C-D) (Saitou and Yamaji, 2012). Similar to XY PGCs (Figure 2), analysis of H3K27me3 ChIP-Seq data sets (Sachs et al., 2013) revealed that the majority of upregulated DEGs (78%) at E11.5 were known to have promoter enrichment of H3K27me3, and thus are likely direct targets of EED (Figure 3E and Table S1). Given that after E11.5 H3K27me3 levels are reduced at the *Stra8* locus in wild type XX PGCs (Figure 3F) and the key role that *Stra8* plays in regulating XX PGC entrance into meiosis, this suggests a potential role for H3K27me3 in regulating meiotic initiation.

In order to evaluate PGC identity in ECKO and control PGCs at E12.5, we performed single cell RNA-seq using SMART-seq (Figure 3G and S4C-D). This result confirms that *Stra8* de-repression has begun by E12.5 in all ECKO XX PGCs with heterogenous upregulation of the meiotic marker Synaptonemal Complex Protein 3 *Sycp3* and *Meioc* which marks prophase I meiosis I arrested PGCs (Soh et al., 2017). Furthermore, the down regulation of *Nanog* and *Tfap2c* indicates exit from mitosis and entrance into meiosis. Intriguingly, like XY PGCs, we also observed upregulation of the somatic patterning genes *Hoxa1* and *Hoxb1* in some ECKO meiotic PGCs (Figure S4C). Through a comparison with recently published 10x single cell sequencing of PGCs (Zhao et al., 2020) we found that control E12.5 PGCs in our data set correlated with E12.5 PGCs from (Zhao et al., 2020) (Figure S4D). In contrast, the E12.5 ECKO PGCs showed a stronger correlation to E14.5 PGCs consistent with precocious differentiation (Figure S4D).

Finally, to confirm that XX PGCs are precociously entering into meiosis, we used IF to evaluate the meiotic marker SYCP3, and show that the majority of ECKO PGCs at E13.5 are SYCP3+

(Figure 3H-I). In summary, the reduction in PGC number in XX and XY embryos between E11.5 and E13.5 is due to precocious differentiation of PGCs which involves exit from the mitotic cell cycle and formation of meiotic oocytes or pro-spermatogonia respectively.

Some Gametogenesis Genes are Co-Enriched for H3K27me3 and DNA Methylation in the Epiblast

Given that H3K27me3 in PGCs could be inherited from the epiblast cells at the time of PGC specification as well as through enrichment in PGC chromatin after specification, we next compared H3K27me3 promoter abundance in the epiblast at E6.5 (Yang et al., 2018) to PGCs at E11.5 (Sachs et al., 2013). Using a $\geq$2-fold cut-off, we identified 3,783 promoters with H3K27me3 enrichment in both E6.5 epiblasts and E11.5 PGCs, referring to these promoters as "*pre-existing*" under the assumption that H3K27me3 in the E6.5 epiblast was likely maintained following PGC specification (Figure 4A and S5A-B). Additionally, we identified 2,852 promoters in PGCs that were significantly enriched with H3K27me3 at E11.5, but not at E6.5, which we call "*acquired*" with the assumption that H3K27me3 is acquired at these sites during PGC differentiation.

Given that EED regulates the timing of PGC differentiation similar to DNMT1, we next explored a potential relationship between H3K27me3 and DNA methylation in the context of the pre-existing or acquired promoter categories. Using whole genome bisulfite sequencing (WGBS) data sets from E6.5 epiblast and E11.5 PGCs (Seisenberger et al., 2012), we examined average DNA methylation levels in the pre-existing and acquired H3K27me3 promoter categories (Figure 4B). Because PRC2 recognizes unmethylated CpG rich sequences (Heeringen et al., 2014; Mendenhall et al., 2010) and DNA methylation and H3K27me3 tend to be mutually exclusive (Bartke et al.,

2010; King et al., 2016; Li et al., 2018), we hypothesized that promoters in the epiblast containing pre-existing H3K27me3 should in general also be hypomethylated and indeed this is the case (Figure 4C). In contrast, promoters that acquired H3K27me3 in PGCs were hypermethylated in the E6.5 epiblast and became hypomethylated at E11.5 in PGCs. This is consistent with previously published work showing that loss of DNA methylation can cause spreading of H3K27me3 (van Mierlo et al., 2019; Murphy et al., 2013). Evaluating CpG content of these promoters based on the criteria of (Mohn et al., 2008), revealed that the majority of pre-existing H3K27me3 promoters are categorized as high and intermediate CpG content (HCP, ICP) whereas promoters that acquired H3K27me3 in PGCs corresponded to low (LCP) and ICP (Figure 4D). This fits well with previous work showing that high CpG content is typically associated with low levels of DNA methylation and high levels of H3K27me3 (Chen et al., 2018; Mendenhall et al., 2010). Taken together, this analysis reveals that the retention and acquisition of promoter H3K27me3 is inversely correlated with DNA methylation as PGCs differentiate.

Given that the late demethylators and GRRs contain significant DNA methylation at E6.5 despite being categorized as ICP and HCP (Hill et al., 2018; Seisenberger et al., 2012) we predicted that they might acquire H3K27me3 following PGC specification. To address this, we evaluated the late demethylating promoters identified by (Seisenberger et al., 2012), 45% of which exhibit H3K27me3 promoter methylation in E11.5 PGCs (Sachs et al., 2013) (Figure S5C). Categorizing these promoters with H3K27me3 revealed that while some are acquired as predicted, a greater proportion (60%) had pre-existing H3K27me3. Repeating this analysis for the GRR promoters identified by (Hill et al., 2018), we also found that (60%) were marked by H3K27me3, and the vast majority of the marked promoters (80%) were pre-existing (Figure S5D). We next examined

the extent that late demethylating promoters are enriched for H3K27me3 via scatterplot (Figures S5E) and observed a similar pattern to what was seen in all promoters (Figure S5A). GO analysis of the late demethylating promoters containing H3K27me3 at E11.5 identified categories of genes involved in meiotic cell cycle, spermatogenesis and piRNA metabolic process (Figure 4E). Critically, these are the same GO groups regulated by DNMT1 in PGCs (Hargan-Calvopina et al., 2016) suggesting a potential connection between H3K27me3 and DNA methylation in regulating PGC development.

Given that PGCs lose DNA methylation after specification from the epiblast, we predicted that the relationship between DNA methylation and H3K27me3 likely begins in the epiblast. Evaluating methylation levels of the late demethylating promoters at E6.5 (Seisenberger et al., 2012) revealed that pre-existing promoters of late demethylating genes also begin with high levels of DNA methylation in the epiblast (Figure 4F, S5E-F). This subgroup of pre-existing H3K27me3 promoters that are also enriched in DNA methylation includes critical germline genes such as *Stra8* and *Dazl* (Figure S5E). Analyzing the CpG content of late demethylating promoters with pre-existing H3K27me3 and high levels of DNA methylation (Figure 4F and S5F, red box) mostly correspond to promoters with ICP and HCP (Figure 4G). Taken together, these results suggest a potential functional relationship between EED/H3K27me3 and DNMT1 in PGC development.

Gametogenesis Genes are Coregulated by EED and DNMT1

In order to characterize a potential relationship between EED and DNMT1, we re-analyzed the DNMT1 PGC conditional knockout (DCKO) bulk RNA-seq data set at E13.5 (Hargan-Calvopina et al., 2016) and discovered that 69% of the upregulated DEGs in the E13.5 XY DCKO PGCs have

promoters enriched in H3K27me3 (Liu et al., 2014) (Figure 5A and table S1). We then compared the overlapping upregulated DEGs between the E13.5 XY DCKO and ECKO PGC after filtering out genes which are only expressed in both data sets and discovered that 60% of DCKO upregulated genes at E13.5 are also upregulated in ECKO XY PGCs (Figure 5B-C and S6A). This overlapping set of DEGs are significantly enriched for GO terms involved in gametogenesis (Figure 5D) and the CpG content of their promoters is mostly ICP and HCP (Figure 5E).

Given the overlap, we next asked whether EED/H3K27me3 is required to maintain DNA methylation at these promoters. To achieve this, we performed WGBS of control and ECKO GFP+ PGCs isolated from embryos at E10.5 and E11.5 using FACS (Figure S6B). E10.5 and E11.5 were chosen because this is the time when late demethylators still have observable levels of DNA methylation, whereas at E13.5 late demethylators have fully demethylated. This result shows that loss of EED in PGCs is accompanied by a reduction in global levels of DNA methylation at E10.5 (Figure 5F). However, at a promoter level, we did not observe a significant difference in DNA methylation between control and ECKO PGCs at E11.5 in selected late demethylating, overlapping DEG promoters (Figure 5G and S6C). Therefore, our data suggest that DNA methylation at late-demethylating promoters in PGCs is not dependent upon EED.

To examine a potential relationship between EED and DNMT1 in the epiblast, we performed native co-immunoprecipitation (co-IP) to evaluate the endogenous interaction between EED and DNMT1. For this experiment we used Epiblast Like cells (EpiL6/9/22 1:16:00 PMCs) which are equivalent to the epiblast of post-implantation embryos competent for PGC specification (Hayashi et al., 2011), and mouse embryonic stem cells (ESCs) cultured in serum +LIF (Figures 5H-I and

S6D). Our results show when using EED for IP (Figure 5H-I) DNMT1 and EED interact. Additionally, we also detect EZH2 and DNMT1s binding partner UHRF1 in the EED IP pulldowns with no detectable signal in the IgG negative control. EED is known to have multiple isoforms (Bracken et al., 2006; Liu et al., 2019; Montgomery et al., 2007) and regardless of whether EpiLC or ESCs were used, we selectively enriched for a shorter isoform (~45 kDa) when blotting for EED in the IP experiments with the EED antibody. Interestingly, when performing the reciprocal pull down with DNMT1 antibody in serum +LIF ESCs, we also selectively pull down the shorter EED isoform alongside UHRF1 (Figure S6D). Taken together we identified a unique subset of gametogenesis genes which are enriched for both H3K27me3 and DNA methylation in the E6.5 epiblast prior to PGC specification, where we also see an interaction between EED and DNMT1. From this result, we propose a model by which this epigenetic signature is established in the epiblast and maintained throughout PGC development to regulate PGC differentiation timing (Figure 6).

Discussion

In this study, we show that EED is essential to regulate the timing of PGC differentiation between E11.5-E13.5, and X chromosome dosage decompensation in XY PGCs at E13.5. Through this, we identified a functional role for EED in PGC development before E13.5. Additionally, we show a relationship between DNMT1/DNA methylation and EED/H3K27me3 that begins prior to PGC specification in the epiblast to regulate repression of gametogenesis genes. Collectively, our data further clarifies the epigenetic landscape that regulates PGC differentiation and identifies a new mechanism for regulating X chromosome decompensation in XY germ cells at E13.5.

One of the major findings in the current study is the direct role for EED in X chromosome decompensation in E13.5 XY PGCs. X chromosome compensation in XX cells is regulated by the long noncoding RNA *Xist* as well as H3K27me3, which becomes dynamically re-distributed during the process of X-chromosome reactivation in XX PGCs. During X reactivation, H3K27me3 is simultaneously removed from the Xi chromosome in XX PGCs, while becoming globally enriched in the nucleus of PGCs in both sexes between E8.5-E9.5 (Mallol et al., 2019; Napoles et al., 2007; Seki et al., 2005). Here, we show that loss of EED in XX PGCs does not lead to an increase in the X/A ratio at E11.5, indicating that loss of EED does not have a major impact on X-linked gene expression in XX PGCs prior to sex-determination. Instead, we found that EED had a role in X chromosome decompensation during the transition of XY PGCs to pro-spermatogonia, with X-linked genes in XY PGCs being significantly more sensitive to loss of EED at E13.5 than H3K27me3 marked genes on autosomes. Future studies aimed at the role of X chromosome decompensation in regulating the biology of pro-spermatogonia, establishment of long-term self-renewing spermatogonia and spermatogenesis are warranted.

Despite the well-known complex dynamics of H3K27me3 global enrichment during PGC development (Figure 1A), chemical inhibition of EZH1/2 using *ex vivo* embryonic gonadal organ cultures suggested that EZH1/2 does not regulate PGC number (Prokopuk et al., 2017, 2018). This was confirmed by a recent manuscript involving an EZH2 conditional knockout which showed no loss of PGCs before E13.5, and instead a reduction in PGC number, together with TE de-repression from E16.5 (Huang et al., 2021). A direct comparison of EED and EZH2 null mutant phenotypes in mouse intestinal villus cells revealed that a EZH2 null phenotype is less

severe than the EED null phenotype (Jadhav et al., 2020). This supports the finding that a more severe phenotype is to be anticipated when deleting EED compared to EZH2, which in our study involved the emergence of a PGC phenotype between E11.5-E12.5 in the EED null mutant embryos.

Conditional deletion of *Dnmt1* in PGCs leads to a substantial increase in *Stra8* RNA by E13.5 and precocious entry into meiosis (Hargan-Calvopina et al., 2016). Conversely, deletion of Ten eleven translocation 1 (*Tet1)* which oxidizes 5mC to 5hmC results in delayed entrance into meiosis (Yamaguchi et al., 2013). Given that *Stra8* was not significantly induced in *Dnmt1* conditional knockout PGCs at E11.5, this result implies that other facultative repressors shield *Stra8* from precocious expression until E11.5. One of these repressors was previously identified as PRC1/RNF2 which represses *Stra8* in XX PGCs at E11.5 (Yokobayashi et al., 2013). Here, we show that EED (a binding partner of PRC1 proteins) is also necessary to repress *Stra8* in XX PGCs at E11.5. Intriguingly, a conditional deletion of Eed (this study) and *Ezh2* (Huang et al., 2021) in PGCs has no effect on the global levels of H2AK119ub1 in PGC nuclei. Similarly, loss of Rnf2 does not affect the global levels pf H3K27me3 (Yokobayashi et al., 2013). This indicates that while the global enrichment of H3K27me3 and H2AK119ub1 in PGC nuclei are not dependent upon one another, they appear to localize at certain promoters to co-regulate key loci such as *Stra8*. Given that EED and DNMT1 both act at the *Stra8* promoter, we asked whether EED is functionally required to maintain DNA methylation at the gametogenesis late-demethylating promoters in PGCs. Our data shows that EED is not required to maintain DNA methylation at the late demethylating promoters, suggesting that DNMT1 may utilize other chromatin binding partners or chromatin signatures to maintain DNA methylation at

gametogenesis genes following PGC specification. Taken together, our data indicates that at least three repressive epigenetic modifications converge on the *Stra8* promoter to regulate expression timing in PGCs (DNMT1/DNA methylation, EED/H3K27me3 and RNF2/H2AK119ub1).

Although EED is not required to maintain DNA methylation at gametogenesis promoters in PGCs, future studies could evaluate whether DNA methylation is involved in maintenance of EED/H3K27me3 at gametogenesis promoters in PGCs. UHRF1 protein is repressed in PGCs, therefore maintenance DNA methylation is not thought to be the mechanism by which DNMT1 functions in PGCs. Recent work has shown that DNMT1 has *de novo* methyltransferase activity when targeted to regions with densely methylated CGs maintaining DNA methylation in a "neighborhood" dependent manner (Haggerty et al., 2021; Wang et al., 2020). There are two major forms of DNA methylation at gametogenesis promoters in PGCs, 5-methylcytosine (5mC) and 5-hydroxymethyl cytosine (5hmC) (Hackett et al., 2013). TET1, the enzyme that oxidizes 5mC to 5hmC is known to recruit PRC2 to high CpG content regions (Wu et al., 2011). Therefore, it is tempting to speculate that the presence of 5hmC at gametogenesis promoters in PGCs enables the enrichment of H3K27me3 at these sites through PRC2.

Our data shows that the co-enrichment of DNA methylation and H3K27me3 at gametogenesis promoters begins in the epiblast, before PGC specification. To address the relationship between EED and DNMT1 in pluripotent cells prior to PGC specification we used native co-IP in ESCs and EpiLCs to show that EED and DNMT1 interact, providing a potential mechanism for the coordinated activity of EED and DNMT1 in the epiblast. A caveat to these studies is that the native IP interaction is weak. This could mean that DNMT1 and EED interact in only a small

fraction of protein complexes, or that this interaction is indirect. In addition, a second unexpected finding was that the shorter isoform of EED was preferentially pulled down in the Co-IPs using the EED and the DNMT1 antibody. Different isoforms of EED have previously been described (Bracken et al., 2006; Cao et al., 2014; Liu et al., 2019) and are known to incorporate into a functional PRC2 complex (Montgomery et al., 2007). However, the relevance of the shorter isoform in the putative EED/DNMT1 interaction is not known. In ESCs repression of gametogenesis genes is regulated by PCGF6, a component of the PRC1.6 complex (Endoh et al., 2017; Zhao et al., 2017). In this cellular context, PCGF6 recruits the histone modifying enzymes G9A/GLP to deposit H3K9me2 at gametogenesis promoters (Liu et al., 2020). PRC2 components interact with G9A/GLP in undifferentiated ESCs (Mozzetta et al., 2014), and DNMT1 recognizes H3K9me2 through its interaction with UHRF1 (Rothbart et al., 2012). Since we see an interaction between EED, DNMT1 and UHRF1 in ESCs, we propose that this interaction occurs at promoters of gametogenic genes in the epiblast in order to establish a gametogenesis signature that is sustained in PGCs through continual recruitment of PRC2.

In summary, EED is required to prevent precocious PGC differentiation in response to sex-specific developmental signals during sex determination in the embryonic ovary and testis. Our results identify an expanded role for EED during PGC development beyond what was previously reported for EZH2 and provides an exciting glimpse into the complex epigenetic regulatory networks that govern PGC development, beginning in the epiblast.

Limitations of the Study

In order to show that DNMT1 and EED interact in the epiblast we used an *in vitro* model of the epiblast called Epiblast-Like Cells (EpiLC). While EpiLCs have a similar transcriptome to the post-implantation mouse epiblast, and can specify PGC-like cells *in vitro* (Hayashi et al., 2011), EpiLCs themselves are not generated in an egg cylinder embryo. In addition, this work revealed that EED is not responsible for maintaining DNA methylation at gametogenesis promoters following PGC specification *in vivo*. It remains to be determined whether the reciprocal is true.

Acknowledgements

The authors would like to thank the UCLA BSCRC flow cytometry core, the UCLA BSCRC Sequencing core, and the UCLA MCDB/BSCRC Microscopy Core. We would also like to thank Dr. Jesse Zamudio for his expert guidance on statistical analyses used throughout this study. Funding for this project provided by NIH/NICHD 2 R01 HD058047, a Ruth L. Kirschstein National Research Service Award GM007185, the UCLA Eli and Edythe Broad Center of Regenerative Medicine and Stem Cell Research Training Program and the Rose Hill Foundation Science and Engineering Scholarship. P.Y.C. was supported by grants from Academia Sinica and Ministry of Science and Technology Taiwan (107-2633-B-001-001 and 108-2313-B-001-013-MY3).

Author Contributions

M.G.L. designed and performed all experiments, maintained the mouse lines and wrote the manuscript. Z.H. and I.G. designed and performed the experiments. T.C. performed the X/A expression analysis. M.B. and S.W performed the co-IP. L.H. established the mouse lines. T.H. maintained the mouse lines. M.R.Y. and P.Y.C. performed bulk RNA-seq and ChIP-seq analysis.

F.M.H. performed the transposon, whole genome bisulfite and single cell RNA sequencing analysis. A.T.C. designed and oversaw all experiments, wrote the manuscript, maintained all university compliances and attained funding for the experiments.

Declaration of Interests

The authors declare no competing interest.

Data Availability

RNA-sequencing results have been uploaded to GEO and are available at GSE139413.

Resource Availability

Lead Contact

Further information and requests for resources and reagents should be directed to and will be fulfilled by the Lead Contact, Amander Clark (clarka@ucla.edu).

Materials Availability

All unique/stable reagents generated in this study are available from the lead contact with a completed materials transfer agreement.

Data Availability

All sequencing data generated in this study have been uploaded to GEO and are available at GSE139413. All previously published data used can be found in publicly available repositories at the accession numbers listed in the key resources table.

Experimental Model and Subject Details

All animal experiments for this study were approved by the UCLA Institutional Animal Care and Use Committee, also known as the Chancellor's Animal Research Committee. All mouse lines were established from strains acquired from Jackson labs. Control and ECKO XY and XX embryos were obtained from crosses between OG; *Eed*$^{fl/fl}$ (Lengner et al., 2007; Yu et al., 2009) homozygous XX and BC; *Eed*$^{f/l+}$ heterozygous XY (Ohinata et al., 2005) at E10.5, E11.5, E12.5 and E13.5. Embryos were staged at E0.5 by the detection of a vaginal plug on the morning after time-mating pairs were established.

Method Details

Immunofluorescence

Aorta-gonad-mesonephros (AGM) (E11.5) and gonads (E13.5) were extracted from the embryos via microdissection and fixed in 4% paraformaldehyde (Life Technologies) over night at 4˚C. Following fixation, gonads were stored in 70% ethanol until sectioning. Gonads were embedded in paraffin wax and then cut into 5 μm sections. Sections were deparaffinized via immersion in xylene (Fisher Scientific) and rehydrated in an ethanol series. Antigen retrieval was performed at 95˚C in either Tris-EDTA (10mM Trizma base (Sigma), 1mM EDTA (Sigma), 0.05% Tween-20 (Fisher Scientific) at a pH of 9.0) or Citrate (10 mM Sodium Citrate (Sigma), 0.05% Tween 20 at PH of 6) buffer for 40 minutes and then cooled back to room temperature (RT). Sections were washed with 0.2% Tween 20 in PBS (Fisher Scientific) (PBST), permeabilized in 0.5% Triton X-100 (Sigma) in PBS for 20 minutes at room temperature and then washed with PBST. Sections were blocked for 1 hour in 10% donkey serum (Fisher Scientific) in PBST. The primary antibody (Table S3) was added at the manufacturers recommended concentration in 2.5% donkey serum

PBST and incubated overnight at 4˚C in a humid chamber. Secondary antibody (Table S3) was added at a concentration of 1:200 in 2.5% donkey serum PBST and 1x DAPI (Fisher Scientific) for 1 hour at room temperature. Slides were mounted in Prolong Gold without DAPI mounting media (Invitrogen) and set to cure overnight at room temperature in a dark chamber before being transferred to 4˚C for long term storage. All immunofluorescence sections were imaged on a Zeiss LSM 880 microscope as a Z stack which was then processed in Imaris (Bitplane) to trim the Z-stack to a one to two cell thickness (~5 μm) as a maximum intensity projection, adjust individual channels brightness for publication and quantify the images as described below.

For immunofluorescence staining, presence vs. absence of a mark was determined by identifying the TFAP2C+ (E11.5) or VASA+ (E13.5) PGCs and quantifying the amount of PGCs positive for the given mark by eye. The number of dual positive PGCs was divided by the total number of TFAP2C+/VASA+ PGCs to calculate the ratio for a set of sections. For all IF analysis, sections were analyzed from n≥3 embryonic mice of the appropriate condition. >50 PGCs were quantified for all analyses except the ECKO XX (>10 PGCs per sample) and E11.5 sections (>20 PGCs per sample) due to limited PGC cell number per section. Quantification of H3K27ac signal intensity within the PGC nucleus was performed in Imaris by first creating spots over the nuclei of VASA+/DAPI+ PGCs and VASA-/DAPI+ somatic cells. Mean H3K27ac signal intensity was measured over these spots and normalized for each image by taking the ratio of VASA+ PGC average nuclear signal over VASA- somatic nuclear signal. For the MILI analysis, due to higher background signal a mask over the VASA channel was created and then all MILI signal not under the mask was set to zero in order to only look at MILI signal within PGC cytoplasm.

Significance for all IF data was calculated between ECKO and control via a two tailed, unequal variance T-test.

Sample Preparation for FACS

Aorta-gonad-mesonephros (AGM) (E10.5 and E11.5) and gonads (E12.5 and E13.5) were extracted from the embryos via microdissection and dissociated in 100 μL of 0.05% Trypsin-EDTA (Thermo Fisher Scientific) at 37˚C for 5 minutes with additional minutes added if necessary. Quenched with 200 μL MEF media (10% FBS in DMEM) and spun down at 300xG to pellet the dissociated cells. The pellet was resuspended in 1% BSA (Sigma-Aldrich), passed through the cap strainer into a 5 mL Falcon Corning FACS tube and 7AAD (Fisher Scientific) was added to the solution prior to sorting. Only 7AAD -, GFP+ cells were sorted and used for further analysis. For bulk RNA sequencing, cells were sorted into 300 μL of RLT buffer (Qiagen) in a 1.5 mL Eppendorf tube and stored at -80 ˚C until library prep. For single cell RNA sequencing, individual XY and XX GFP+ cells were sorted into 2 μL of 0.2% Triton X-100 and 40 u/μL RNaseOut (Invitrogen) into a 96 well plate. Plates were sealed, spun down at 300xG for 1 minute and stored at -80˚C until library prep. For whole genome bisulfite sequencing, all PGCs from XX E10.5 and E11.5 embryos were sorted into 0.2 mL PCR tubes containing 10 μL M-Digestion Buffer (Zymo) and 1 μL Proteinase K (Zymo), spun down and stored at -80˚C until library prep.

Significance for FACS data was calculated via a two-tailed, unequal variance T-test. Linear regression analysis was performed based on the assumption that the rate of division across the PGC population in the gonad would be consistent and therefore linear on a log2 scale.

Genotyping

The head from each mouse embryo was collected for genotyping following extraction of the gonad and dissociated in 100 μL Modified Gitschier Buffer and 3 μL (1:33) Proteinase K (Sigma-Aldrich) at 55˚C overnight followed by a 5 minute 95˚C incubation to inactivate the enzyme. The sample was spun down to pellet the undigested debris and 1 μL of the supernatant was used for the genotyping PCR reactions. PCR products were run on a 2% Agarose gel for 1 hour at 100V. For a sexing PCR, XY embryos have two bands at roughly 300 bp and 280 bp, whereas XX only have a single band at 300 bp. Blimp1-cre PCR shows a single band at 200 bp if the transgene is present. Finally, the EED PCR has a control band at around 300 bp with a larger mutant band at around 350 bp. The sequence of all genotyping oligos is present in Table S4.

Bulk RNA-sequencing Analysis

Bulk RNA Libraries were made from sorted cells of the E11.5 XY and XX as well as E13.5 XY embryos. The cell lysate in RLT was thawed on ice and cleaned up using a Qiagen RNeasy Micro RNA kit. Following cleanup, the samples were converted to cDNA following the Ovation RNA-seq System V2 protocol (Nugen). 4.5 μL of RNA + 0.5 μL of ERCC (Thermo Fisher Scientific) spike in was converted to cDNA and purified with Agencourt RNAclean XP beads (Beckman Coulter). cDNA was amplified via the SPIA reaction, cleaned up using the Qiagen MinElute Reaction Cleanup Kit and eluted in 50 μL low EDTA TE buffer. Purified cDNA was quantified via Qubit and then sonicated into 200 bp fragments using a Covaris. Sonicated cDNA was purified using a Qiagen MinElute Reaction Cleanup Kit and eluted in 10 μL Low EDTA TE buffer. 8 μL of eluted cDNA was indexed using the Ovation Rapid DR Multiplex System with

the indices L9-16. Following final repair, the indexed cDNA was purified using Agencourt RNAclean XP beads and eluted in 11 μL low EDTA TE buffer. Indexed libraries were quantified using the Kapa Library Quantification Kit for Illumina platforms (KAPA Biosystems). Libraries were submitted for sequencing in a single lane and sequenced as follows, E13.5 XY on the Illumina 2500 as single end 50 bp, E11.5 XX on the Illumina Hiseq 4000 as paired end 100 bp and the E11.5 XY on the Novaseq as paired end 50 bp.

The bulk RNA-sequencing reads were aligned to the mouse reference genome mm9 using HISAT2 (Kim et al., 2015) and mappability for each sample can be found in Table S5. The mRNA read counts of genes were computed using HTSeq (Anders et al., 2015). Genes that are expressed (read counts > 0) in at least one replicate in both control and ECKO are included for analysis. Normalization for sequencing depth and differential gene analysis was performed using edgeR (Robinson et al., 2010). Only genes with RPKM ≥10 in at least one sample after normalizing for sequencing depth were analyzed. Genes with ≥2-fold difference in expression and FDR < 5% were considered differentially expressed. Gene ontology analysis was performed using DAVID (Huang et al., 2009). All DEGs for bulk RNA-sequencing can be found in Table S1.

For the comparison of the E13.5 XY EED and DNMT1 conditional knockout upregulated DEGs, the RNA-sequencing datasets were first trimmed to remove all genes which are not expressed (read counts >0) in at least one replicate in both the control and mutant from each condition. Only genes with RPKM ≥10 in at least one samples after normalizing for sequencing depth were analyzed. Genes with ≥2-fold difference in expression and FDR <5% were considered

differentially expressed. This ultimately led to a loss of 55 upregulated ECKO DEGs relative to the EED only analysis. Gene ontology analysis was performed using DAVID (Huang et al., 2009).

X Chromosome and TE Expression analysis

X chromosome over autosome expression ratio was calculated by dividing the mean RPKM normalized to sequencing depth of all X chromosome genes by the mean of all somatic genes. A two tailed, unequal variance T-test was then used to assess significance between the X/A ratio of control and ECKO PGCs. A hypergeometric test was used to evaluate the enrichment of the de-repressed genes with H3K27me3 in each chromosome. The test uses the hypergeometric distribution to calculate statistical significance of the enrichment of de-repressed gene promoters with H3K27me3 among all expressed genes on each chromosome. A p-value < 0.01 was considered to be statistically significant.

For TE analysis, raw reads were trimmed with cutadapt 1.18 (Martin, 2011) and trimmed reads with less than 30 bp were discarded. Retained reads were aligned to mm9 with STAR 2.7.0 (Dobin et al., 2013) setting --outFilterMultimapNmax 1000 --outSAMmultNmax 1. Reads aligned to TE were counted by multiBamCov in bedtools (Quinlan and Hall, 2010). RPKM was calculated by edgeR (Robinson et al., 2010).

Single Cell RNA-sequencing Analysis

Single cell libraries were prepared according to the Smart-seq v4 library prep kit (Takara). Prior to the kit, plates were thawed and brought to 11.5 μL with 1 mM DNTP (Invitrogen) in nuclease

free water. Kit protocol was followed exactly for reverse transcription. Following conversion, the libraries were amplified for 22 cycles and then purified using Agencourt Ampure XP beads (Beckman Coulter). The profile of each cDNA library was confirmed using a HS D5000 tape on an Agilent 2200 TapeStation. XX and XY cells were indexed following the Nextera XT DNA library prep kit and indexed with primer sets A and D (Illumina), respectively. Indexed libraries were pooled and purified using Agencourt XP beads and eluted in low EDTA TE buffer. The size profile of the purified eluate was confirmed using a D1000 tape on an Agilent 2200 TapeStation. The pooled libraries were multiplexed and sequenced on the Novaseq as paired end 100 bp.

Raw scRNA-sequencing reads were trimmed with cutadapt 1.18 (Martin, 2011). Trimmed reads with less than 30 bp were discarded. Retained reads were aligned to mm9 with STAR 2.7.0 (Dobin et al., 2013). Reads aligned to exons were counted by featureCount 2.0.1 (Liao et al., 2014) from the Subread package. Cells with at least 2000 genes and 0.8M reads were kept for further analysis. Downstream analyses including k-means clustering, DEG finding, and dimension reduction were performed with R packages SC3 (Kiselev et al., 2017) and Scater (McCarthy et al., 2017) and plotted with ggplot2 (Wickham, 2016). All DEGs for scRNA-sequencing can be found in Table S1.

Whole Genome Bisulfite Sequencing Analysis

Samples were thawed and brought to 20 μL with nuclease free water. Genomic DNA isolation and bisulfite conversion was performed as per the EZ DNA Methylation-Direct Kit (Zymo). Following desulfonation, samples were indexed following the Pico Methyl-seq Library Prep Kit

(Zymo) with a few modifications due to the low input cell number. For the initial amplification, only 1 μL of primer was added. Additionally, during library amplification 10 PCR cycles were performed. Following indexing and purification, samples were run on the Agilent 2200 TapeStation to ensure proper size profile using a D1000 tape and then sequenced on a Novaseq as paired end 100 bp.

Raw WGBS reads were trimmed with cutadapt 1.18 (Martin, 2011) and trimmed reads with less than 30 bp were discarded. Retained reads were aligned to mm9 with BS-Seeker 2 (Guo et al., 2013). Duplicated reads were removed from .bam file with picard_tools (Broad Institute, 2020). Cytosines and reverse complimented guanines with coverage ≥ 4 were retained and calculated for average CG methylation level.

Promoter Methylation Analysis

The E6.5 and E11.5 whole genome bisulfite sequencing datasets were downloaded from European Nucleotide Archive under the accession number ERP001953 (Seisenberger et al., 2012). The reads were mapped against the mouse reference genome mm9 using BS-Seeker 2 (Guo et al., 2013). Genome-wide DNA methylation profiles were generated by determining methylation levels for each cytosine in the genome. The methylation level per cytosine serves as an estimate of the percentage of cells that have a methylated cytosine at a specific locus. We only included cytosines that are covered by at least three reads. The promoter region is defined as the region between -2,000 bp<TSS<+500 bp. Methylation over a promoter region was calculated for each CG in the region and then these individual values were averaged to give a representative

value for the promoter region. Analysis of all promoters based on %CG methylation can be found in Table S2.

H3K27me3 and CpG Classification

ChIP-seq data of H3K27me3 in mouse Epiblast at E6.5 was downloaded from GSE104243 (Yang et al., 2018), H3K27me3 in mouse PGCs at E11.5 was downloaded from GEO accession GSE46396 (Sachs et al., 2013), and H3K27m3 in mouse PGCs at E13.5 was downloaded from GEO accession GSE60377 (Liu et al., 2014). Reads were aligned to the mouse reference genome mm9 using bowtie2 (Langmead and Salzberg, 2012) and the uniquely aligned reads were retained using SAMtools (Li et al., 2009). The E6.5, E11.5 and E13.5 ChIP-seq data were compared between H3K27me3 ChIP-seq and their corresponding control (input or H3) at promoters (-2000 to +500 of TSS) using edgeR (Robinson et al., 2010). The comparison considered the control, replicates, and statistical significance. The promoters with q-value < 0.05 and fold-change ≥ 2 are considered as H3K27me3 enriched promoters. The promoters on the sex chromosomes were excluded from this analysis. Presence or absence of an H3K27me3 enriched promoter at E6.5 and E11.5 was used to classify the promoters into one of four categories. CpG classification for all promoters was performed according to (Weber et al., 2007), updating the CpG cutoffs for the mouse genome as per (Mohn et al., 2008). Analysis of DEGs based on H3K27me3 promoter content can be found in Table S1 and all promoters in Table S2. Analysis of all promoters CpG content can be found in Table S2.

Significance for the distribution of %CG methylation within the pre-existing late demethylating promoters was determined by first classifying all promoters as either “High” (≥mean%) or

"Low" (<mean%) for the time point. Hypergeometric testing was performed to identify enrichment or depletion for %CG methylation within the pre-existing or acquired promoters relative to their abundance within the genome at a given embryonic time point. Additionally, hypergeometric testing was used to identify the enrichment for each CpG content category (LCP, ICP, HCP) within the pre-existing and acquired promoters using the relative distribution in all promoters as the population.

Native Co-Immunoprecipitation

Mouse embryonic stem cells (ESC) were cultured in serum +Lif. EpiLC were differentiated from mouse embryonic stem cells cultured in 2i +Lif conditions following the Hayashi et al., 2011 protocol. 3 million cells were harvested in cold PBS and lysed with 130 mM NaCl, 1% NP-40 (Sigma), 1 mM EDTA (Thermo), and 25 mM Hepes (Thermo) in the presence of 1x HALT protease inhibitor cocktail (Invitrogen). Lysate was agitated for 30 minutes on a rotator at 4˚C and then centrifuged at 4˚C to pellet the cellular debris. Supernatant was precleared with protein G dynabeads (Thermo). Pulldown was performed by adding 500 µg of protein lysate to 5 µg of rabbit anti-DNMT1 (ab188453), mouse anti-DNMT1 (NB100-56519) or mouse anti-EED (05-132) antibody (Table S3) bound to protein A (rabbit) or G (mouse) dynabeads at 4˚C for 1 hour on a rotator. A species matched negative control IgG (Mouse (5415) or Rabbit (ab27478)) was performed in parallel using 500 µg of the same input. Following incubation, beads were washed with lysis buffer 3 times. Beads were then resuspended in 40 µL 1x LDS (Thermo) and 1x NuPAGE reducing agent (Thermo) and boiled for 10 minutes at 95˚C to release the protein. 10 µL (1/4) of eluted IP supernatant was loaded onto a 4-12% Bis-Tris gel (Thermo) alongside 5 µg input and 10 µL (1/4) of eluted IgG supernatant. Proteins were transferred to a PVDF membrane

using the Biorad Trans-Blot Turbo system, blocked with TBST+5% milk for 30 minutes, cut into strips and then exposed to appropriate primary antibodies (Table S3) at 4˚C. The strips were then washed with TBST for 5 minutes 5 times, blocked for 10 minutes with TBST+5% milk and then incubated with secondary antibodies (Table S3) in TBST+5% milk for 1 hour at room temperature on a rocker. Membranes were washed in TBST for 5 minutes 5 times, exposed to ECL reagent (Thermo) and then imaged using a BioRad Chemidoc. For all co-IP analysis, an independent replicate is considered an independent pulldown. All replicate and uncropped blots can be found in document S1.

Quantification and Statistical Analysis

Statistical tests and cutoffs used for each analysis are reported in each methods subsection. All information on replicate numbers and error bars is present in the figure legends and methods. $p<0.05$ was considered significant for all tests, except in bulk RNA sequencing results which were considered significant if the FDR was <0.05 and X chromosome Hypergeometric testing where a $p<0.01$ was considered significant.

Figures and Legends

Graphical Abstract

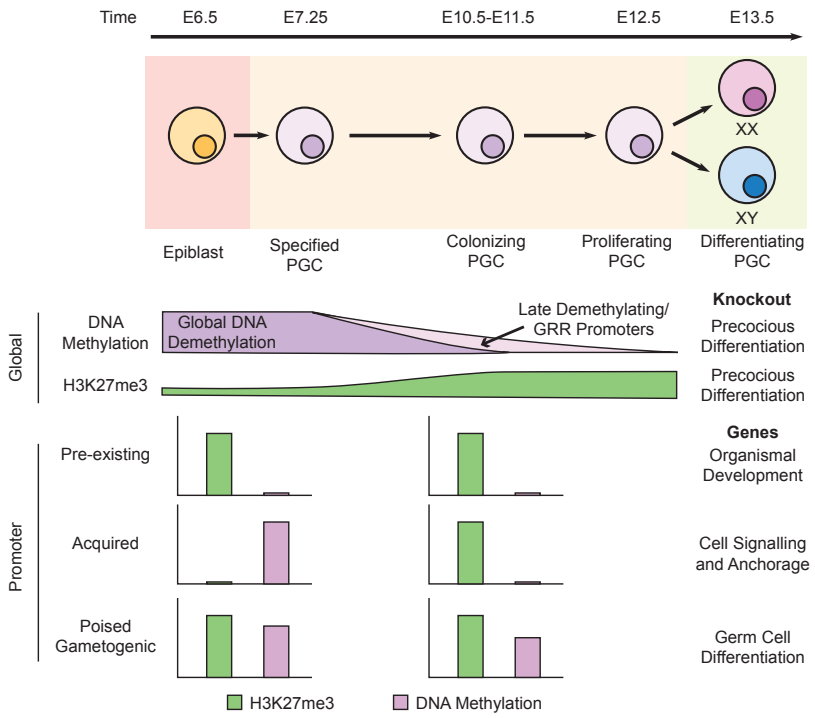

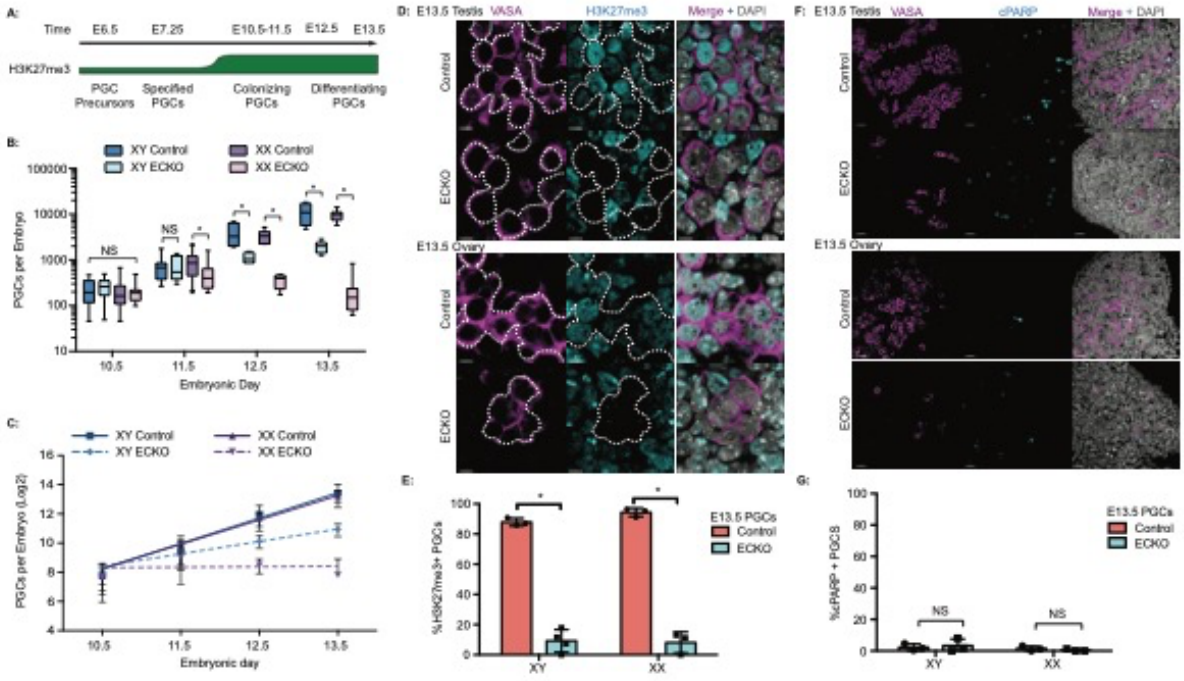

Figure 1: EED regulates PGC number within the embryonic gonads. A) Schematic of PGC differentiation and the global changes of H3K27me3 in epiblast and PGC nuclei from E6.5-E13.5. B) Quantification of average PGC number at E10.5 (n=15-17 embryos), E11.5 (n=8-24 embryos), E12.5 (n=4-7 embryos) and E13.5 (n=6-8 embryos). C) Linear regression analysis of PGC number in B. D) Representative IF image of H3K27me3 at E13.5 in control and ECKO embryonic gonads. VASA marks PGCs. White dashed lines surround PGCs. Scale bar is 5 mm. E) Ratio of H3K27me3+ PGCs from D. F) Representative IF image of cPARP at E13.5 in control and ECKO embryonic gonads. VASA marks PGCs. Scale bar is 10 mm. G) Ratio of cPARP+ PGCs from F. Significance was calculated using T-test in all panels. * is $p<0.05$. All error bars are ± standard deviation. For all IF, n=3 embryos. See also Figures S1 and S2.

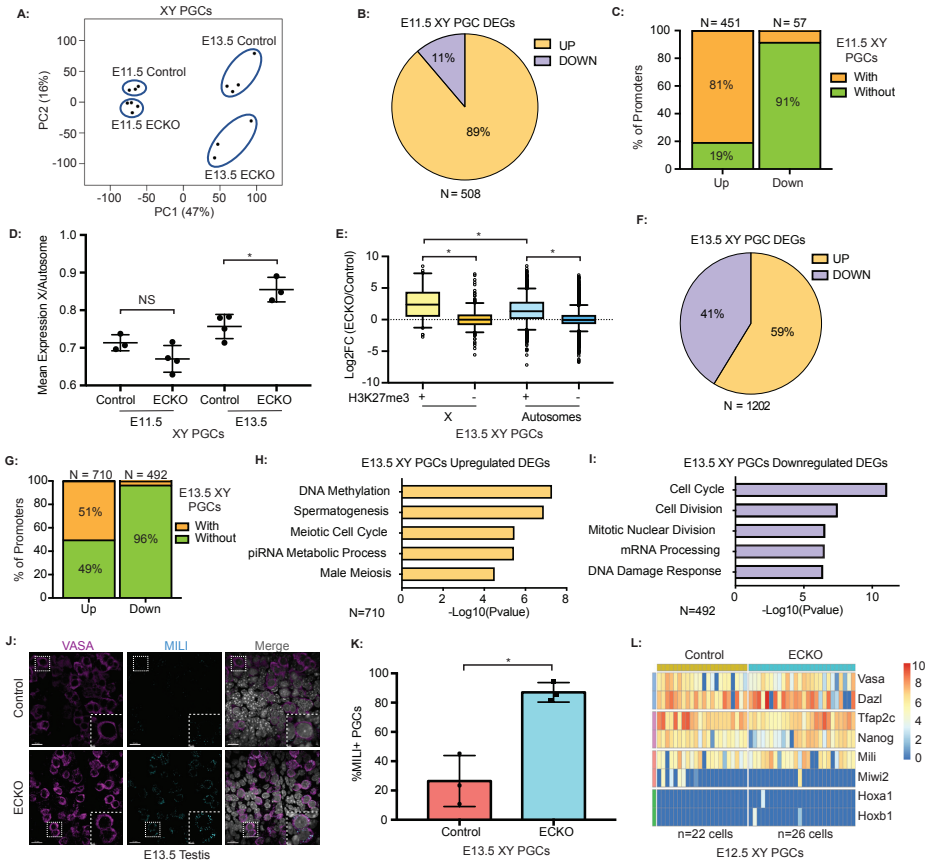

Figure 2: EED regulates PGC differentiation in the testis. A) PCA plot of RNA-Seq data generated from GFP+ XY PGCs isolated at E11.5 and E13.5. B) Percentage of up and down regulated DEGs at E11.5. C) Percentage of DEGs from B with and without H3K27me3 promoter enrichment in wild-type PGCs at E11.5 (Sachs et al., 2013). D) X-chromosome to autosome expression ratio (X/A) at E11.5 and E13.5. E) Differential log2 fold change in gene expression on the X chromosome and autosomes at E13.5 with (+) and without (-) promoter H3K27me3 enrichment (Liu et al., 2014). F) Percentage of up and down regulated DEGs at E13.5. G) Percentage of DEGs from E with and without promoter H3K27me3 enrichment in wild type PGCs at E13.5 (Liu et al., 2014). H/I) Gene ontology of up (H) and down regulated (I) DEGs at E13.5. Values are calculated based on the -Log10(p-value). DEG number denoted below each plot. J) Representative IF of MILI in control and ECKO embryonic testes at E13.5. VASA marks PGCs. Scale bar is 10 mm. Inset of select nuclei shown in white dashed box with scale bar of 2 mm. K) Ratio of MILI+ PGCs from J. L) Heatmap of selected germ cell marker gene expression from single GFP+ PGCs FACS isolated at E12.5. Blue is germline identity, Purple is early PGC genes, Red is piRNA genes and Green is somatic genes. Color is assigned based on log normalized read counts. Significance was calculated using a T-test. * is $p<0.05$. All error bars are ± standard deviation. For IF, n=3 embryos. See also Figure S3.

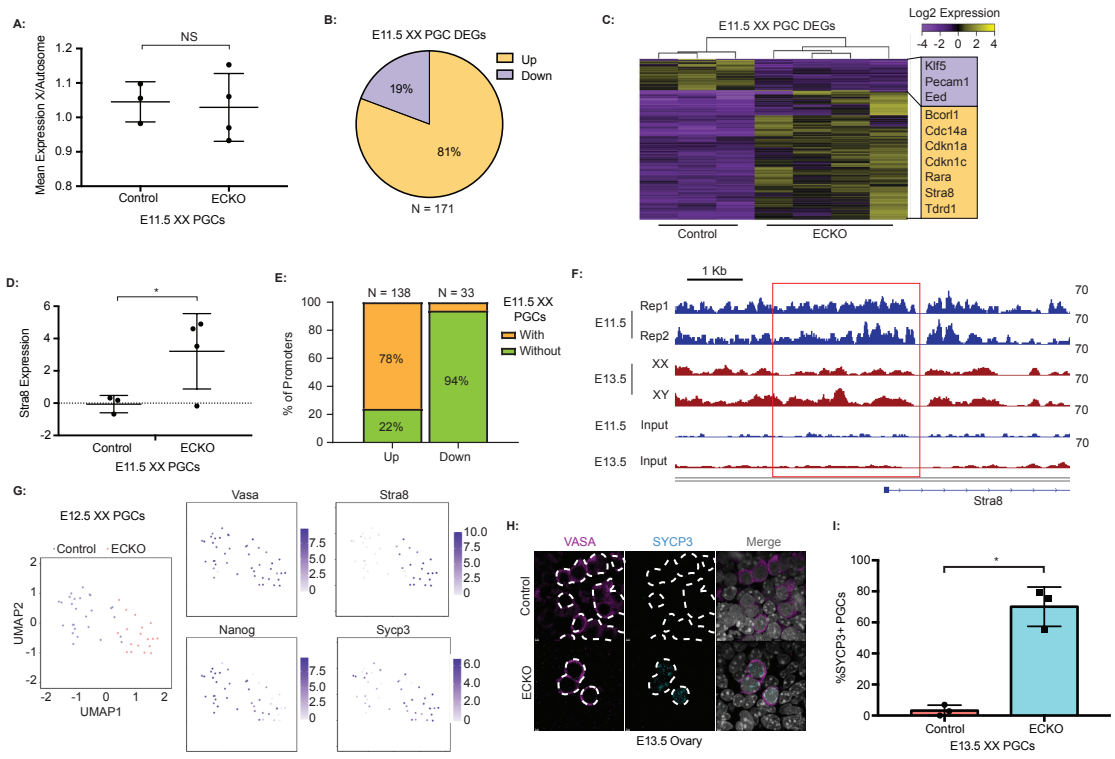

Figure 3: EED Regulates PGC Differentiation in the Ovary. A) Mean X/A expression ratio in XX PGCs at E11.5. B) Percentage of up and down regulated DEGs at E11.5. C) Heatmap of the 171 DEGs at E11.5. Selected up and downregulated DEGs are displayed. D) *Stra8* Log2 fold change expression of E11.5 control and ECKO PGC replicates. E) Percentage of DEGs at E11.5 with or without promoter H3K27me3 in PGCs (Sachs et al., 2013). F) Genome browser track for H3K27me3 at the *Stra8* promoter at E11.5 (Sachs et al., 2013) and E13.5 (Liu et al., 2014). Promoter region boxed in red (-2 to +0.5 kb). G) UMAP of GFP+ FACS isolated single PGCs analyzed using Smart-seq. Feature plots for the PGC marker *Ddx4* (*Vasa*), the meiotic initiator *Stra8*, the pluripotency marker *Nanog* and the meiotic protein *Sycp3* are highlighted. H) Representative IF of SYCP3 at E13.5. VASA marks PGCs. White dashed lines surround PGCs. Scale bar = 2 mm. n=3 embryos. I) Ratio of SYCP3+ PGCs from H. Significance was calculated using a T-test. * is $p<0.05$. All error bars are ± standard deviation. See also Figures S3 and S4.

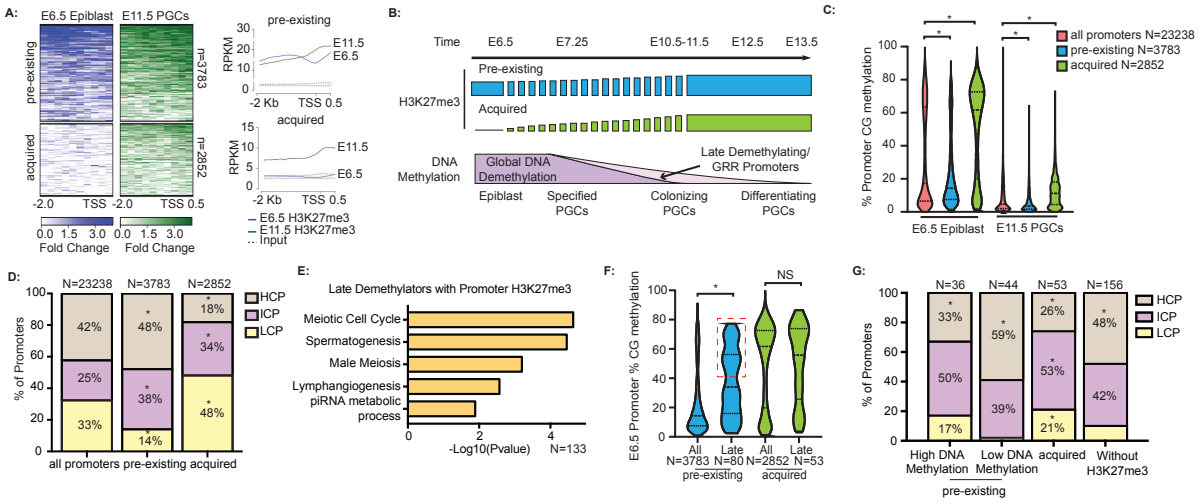

Figure 4: Gametogenesis genes are co-enriched for H3K27me3 and DNA Methylation in the epiblast. A) Heatmaps of H3K27me3 promoter (-2 to +0.5 kb) enrichment at E6.5 (Yang et al., 2018) and E11.5 (Sachs et al., 2013). Acquired promoters gain H3K27me3 by E11.5 in PGCs compared to E6.5 epiblast. Pre-existing promoters have H3K27me3 in both E6.5 epiblast and E11.5 PGCs. Metaplots for each category are presented. B) Schematic of the gain of promoter H3K27me3 in the pre-existing and acquired subsets with dashed bars showing predicted gains in H3K27me3. The average DNA demethylation of the genome (global) and late demethylating/GRR promoters DNA demethylation are below in purple (Seisenberger et al., 2012). C) %CG methylation (Seisenberger et al., 2012) at E6.5 and E11.5 in promoters defined as either having pre-existing or acquired H3K27me3. Significance within a given time point was calculated via Hypergeometric testing. D) Promoter CpG content analysis of pre-existing or acquired promoters. High, intermediate and low CpG content were defined as described in the methods. E) Gene ontology of the late demethylating promoters with H3K27me3 at E11.5 (Sachs et al., 2013). F) %CG methylation of promoters at E6.5 (Seisenberger et al., 2012) with pre-existing or acquired H3K27me3. Pre-existing promoters with high CG methylation (40%) outlined in red. Significance was calculated using T-Test. G) Promoter CpG content analysis of pre-existing promoters with 40% CG methylation (high) or <40% CG methylation (low) at E6.5 (Seisenberger et al., 2012), acquired promoters and all promoters without H3K27me3 at E6.5 (Yang et al., 2018). * is $p<0.05$. See also Figure S4.

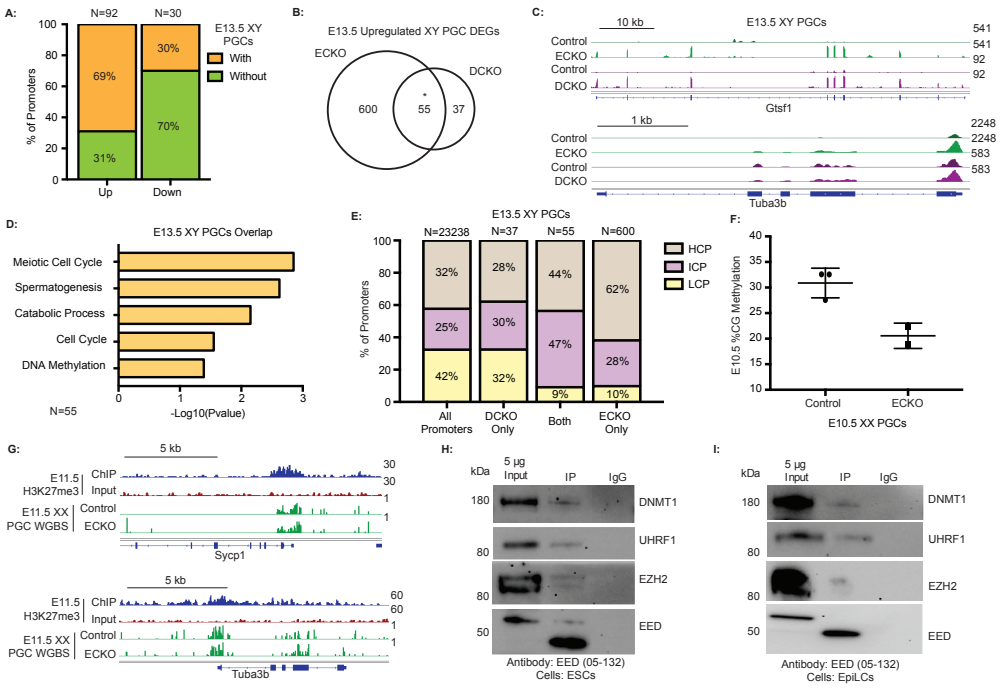

Figure 5: Gametogenesis genes are co-regulated by EED and DNMT1. A) Percentage of up and down regulated DEGs from E13.5 XY DCKO embryos (Hargan-Calvopina et al., 2016) with and without promoter H3K27me3 (Liu et al., 2014). B) Overlap in upregulated DEGs in XY E13.5 ECKO and DCKO conditions. Significance was calculated via hypergeometric testing. * is $p<0.05$. C) Representative RNA-sequencing tracks from overlapping DEGs in the DCKO (Hargan-Calvopina et al., 2016.) and ECKO data sets D) Gene ontology of the overlapping DEGs in the XY ECKO and DCKO conditions. Values are calculated based on the -Log10(p-value) and DEG number denoted below the plot. E) Promoter CpG content analysis of E13.5 XY ECKO and DCKO overlapping or DCKO only promoters. High, intermediate and low CpG content promoters were defined as described in the methods. F) Percentage of methylated CG sites with 4X coverage in E10.5 XX PGCs as measured by WGBS (n=2 replicates). G) Representative WGBS tracks from E11.5 XX PGCs and E11.5 H3K27me3 ChIP-seq tracks (Liu et al., 2014) at representative overlapping DEGs from ECKO and DCKO embryos (Hargan-Calvopina et al., 2016). H) Representation of co-immunoprecipitation in serum+LIF mouse ESCs following pulldown with an anti-EED antibody (05-132). Input is collected prior to the pulldown, IP is the EED bound fraction and IgG is a negative control reciprocal pulldown with a non-specific mouse antibody (5415) (blots from n=3 independent replicate pull downs for EED (05-132), EZH2 (5246) and DNMT1 (ab87654), n=2 independent replicates for UHRF1 (sc373750)). I) Co-immunoprecipitation in EpiLCs following pulldown with an anti-EED antibody (05-132) (blots from n=3 independent replicates for EED (05-132), DNMT1 (ab87654) UHRF1 (sc373750), n=2 independent replicates for EZH2 (5246)). All replicate and uncropped blots are in document S1. All antibodies identified by their catalogue number listed in table S3. See also Figure S5.

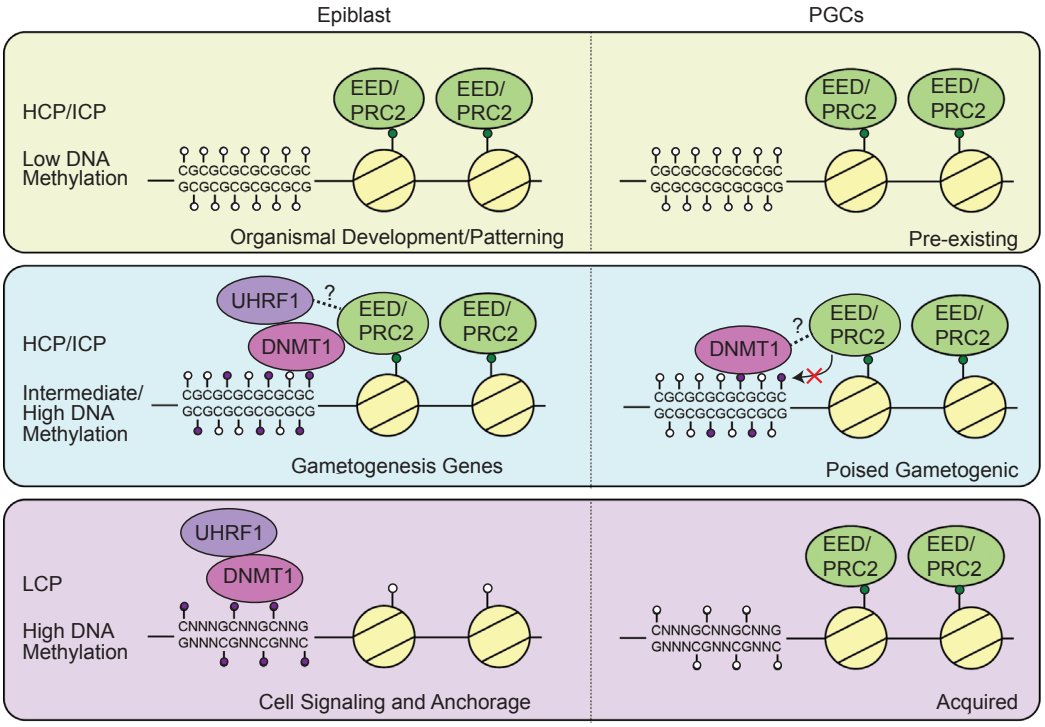

Figure 6: Model for EED and DNMT1 Co-regulation of Gametogenesis Genes. Promoters that exhibit H3K27me3 in the epiblast and in PGCs (pre-existing H3K27me3) have low levels of DNA methylation. These genes are involved in organismal development. Promoters with detectable H3K27me3 in PGCs but not in the epiblast (acquired H3K27me3) begin with high levels of DNA methylation in the epiblast which reverts to low DNA methylation in PGCs. These genes are involved in cell signaling and anchorage. This study identified a new set of poised gametogenic promoters that begin with H3K27me3 and high levels of DNA methylation in the epiblast. These promoters continue to have detectable H3K27me3 and DNA methylation in PGCs. We propose that the maintenance of this signature in the epiblast is regulated by DNMT1/EED interactions. In PGCs, EED is not required to maintain DNA methylation at gametogenesis genes (red cross). Dotted line in the epiblast represents a potential interaction between UHRF1 in the epiblast as an alternative interacting partner with EED/PRC2. Dotted line between DNMT1 and EED/PRC2 in PGCs represents a theoretical interaction which has yet to be validated.

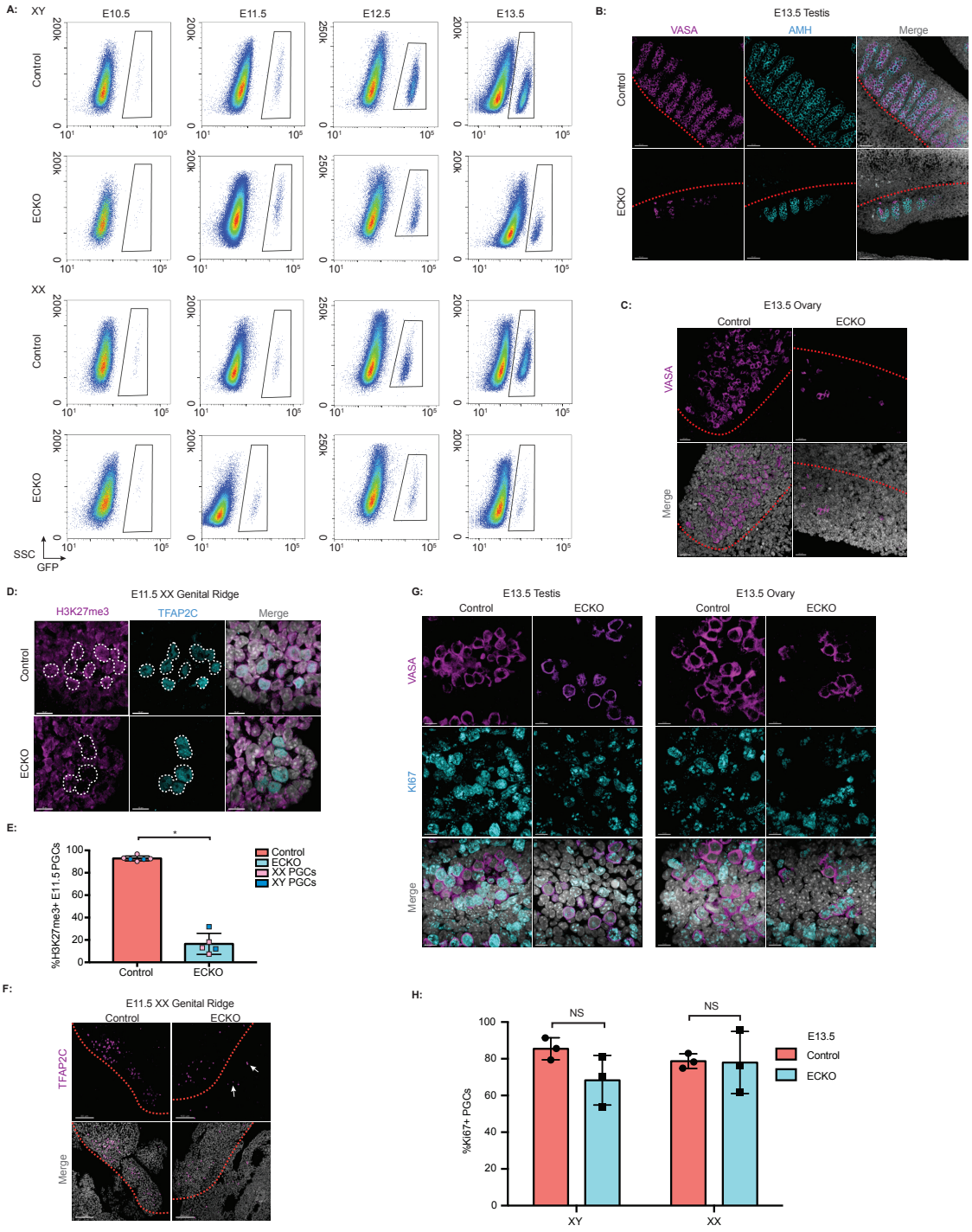

Figure S1: ECKO embryos lose H3K27me3 in PGCs by E11.5 A) Flow plot representations of dissociated control and ECKO AGM and gonads isolated from XY and XX embryos at E10.5, E11.5, E12.5 and E13.5. PGCs are GFP+. B) Representative IF images of AMH in testes at E13.5. VASA marks PGCs and AMH marks the testis cords. Red dotted lines outline the gonad. Scale bar is 50 mm. C) Representative IF images of E13.5 ovaries. VASA marks PGCs. Scale bar is 20 mm. D) Representative IF images for H3K27me3 at E11.5. TFAP2C marks PGCs. Scale bar is 10

mm. E) Ratio of H3K27me3+ PGCs from D. XY and XX embryos pooled and labeled as blue and pink respectively. F) Representative IF images genital ridges at E11.5. TFAP2C marks PGCs. Red dotted lines outline the genital ridge and arrows mark PGCs outside the genital ridge. Scale bar is 100 mm. G) Representative IF images of Ki67 at E13.5. VASA marks PGCs. Scale bar is 10 mm. H) Ratio of Ki67+ PGCs from G. Significance was calculated using T-test in all panels. * is $p \leq 0.05$. All error bars are ± standard deviation. For all IF, n=3-7 embryos. See also Figure 1.

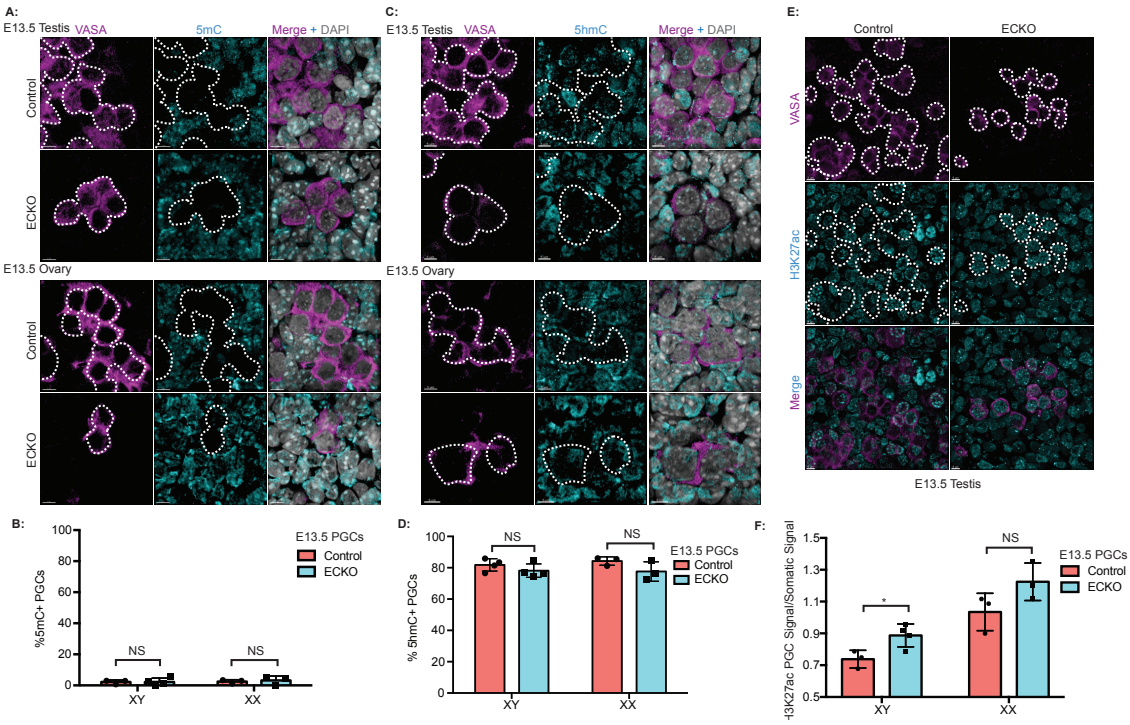

Figure S2: Global epigenetic remodeling in PGCs following deletion of EED. A) Representative IF images for 5mC at E13.5 in embryonic gonads. VASA marks PGCs. Scale bar is 5 mm. B) Ratio of 5mC+ PGCs from A. C) Representative IF images for 5hmC at E13.5. VASA marks PGCs. Scale bar is 5 mm. D) Ratio of 5hmC+ from C. E) Representative IF images for H3K27ac at E13.5. VASA marks PGCs. Scale bar is 5 mm. F) Ratio of PGC nuclear H3K27ac signal relative to gonadal somatic signal from E. White dashed lines outline PGCs in all panels. Significance was calculated using T-test in all panels. * is $p<0.05$. All error bars are ± standard deviation. For all IF, n=3-4 embryos. See also Figure 1.

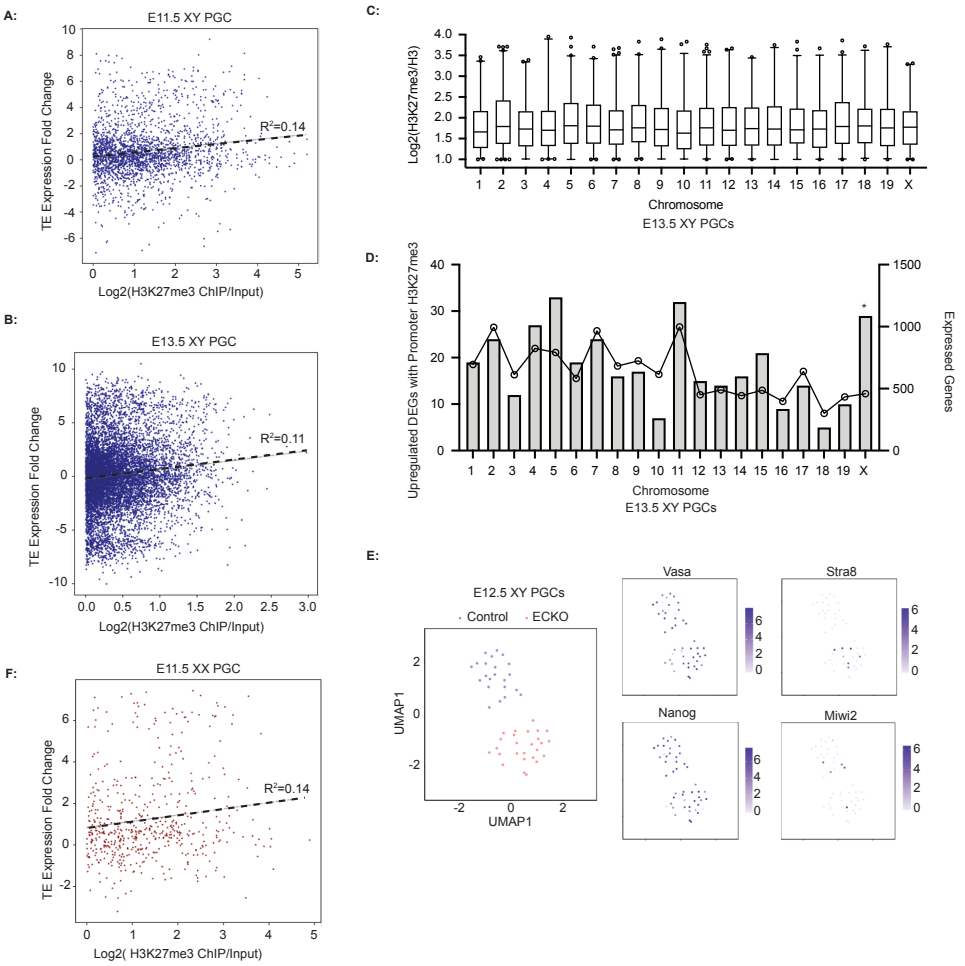

Figure S3: Loss of EED alters expression of genes but not transposons in PGCs. A) Scatter plot of TE expression from E11.5 XY PGC RNA-seq relative to the enrichment of H3K27me3 at E11.5 (Sachs et al., 2013). Dotted line represents the line of best of fit with the R^2 displayed on the graph. B) Scatter plot of TE expression in PGCs from the E13.5 testis relative to the enrichment of H3K27me3 at E13.5 (Liu et al., 2014). Dotted line represents the line of best of fit with the R^2 displayed on the graph. C) H3K27me3 log2 fold change (H3K27me3/H3) abundance (Liu et al., 2014) at E13.5 in XY PGCs. D) Analysis of gene expression by chromosome at E13.5. Line plot (right Y axis) represents all detectable genes on the chromosome and the bar plot (left Y axis) represents all significantly upregulated genes with H3K27me3 marked promoters (Liu et al., 2014). * is $p<0.01$ as determined by a Hypergeometric test as described in the methods. E) UMAP of single GFP+ sorted PGCs from the testis at E12.5. Feature plots for the germline marker *Ddx4 (Vasa)*, the meiotic differentiation gene *Stra8*, the pro-spermatogonial gene *Miwi2* (*Piwil4)* and the pluripotent gene *Nanog* are highlighted. F) Scatter plot of TE expression from E11.5 XX PGCs relative to the enrichment of H3K27me3 at E11.5 (Sachs et al., 2013) within the TE. Dotted line represents the line of best of fit with the R^2 displayed on the graph. See also Figures 2 and 3.

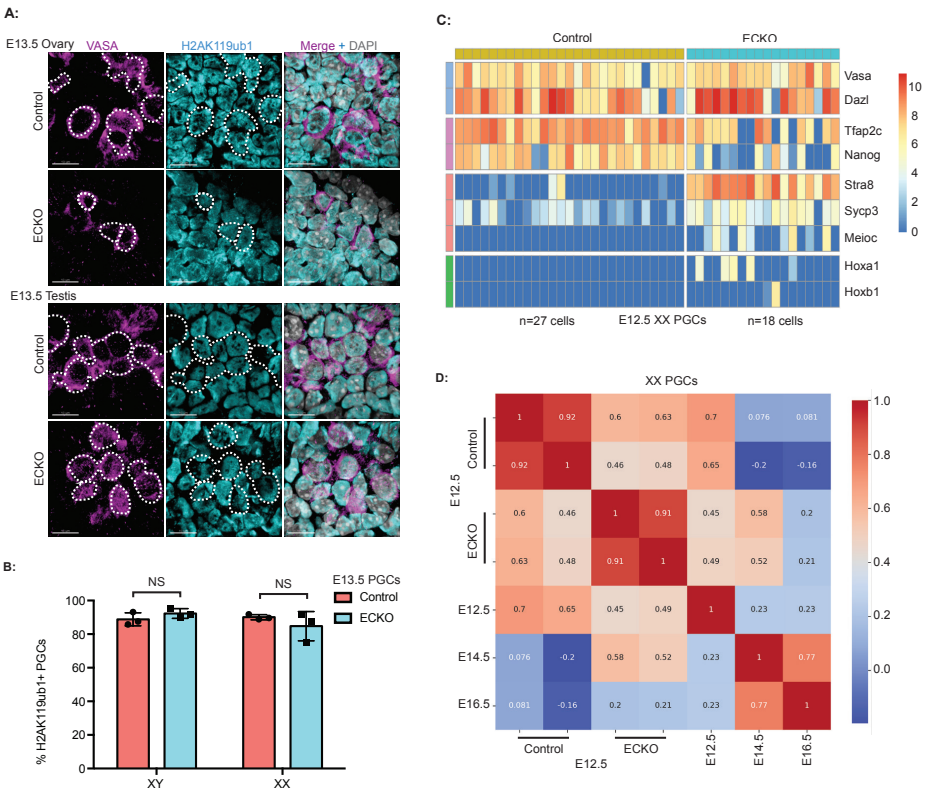

Figure S4: Ovarian ECKO PGCs precociously differentiate. A) Representative IF images for H2Ak119ub1 at E13.5. VASA marks the PGCs. White dashed lines outline PGCs. Scale bar is 10 mm. n=3 embryos. B) Ratio of H2AK119ub1+ PGCs from A. Significance was calculated using T-test. * is $p \leq 0.05$. All error bars are ± standard deviation. C) k-means hierarchical clustering and heatmap of selected PGC marker genes in single cell RNA-Seq data of E12.5 sorted XX PGCs. Selected genes were clustered into rows; Blue is germline identity genes, Purple is PGC genes, Red is meiotic genes and Green is somatic genes. Color is assigned based on log normalized read counts. Cell number for each condition is below the plot. D) Correlation plot between E12.5 sorted GFP+ XX PGCs analyzed by SMART-Seq compared to 10X Genomics single cell RNA-Seq of PGCs from wild-type gonads at E12.5, E14.5 and E16.5 (Zhao et al., 2020). See also Figure 3.

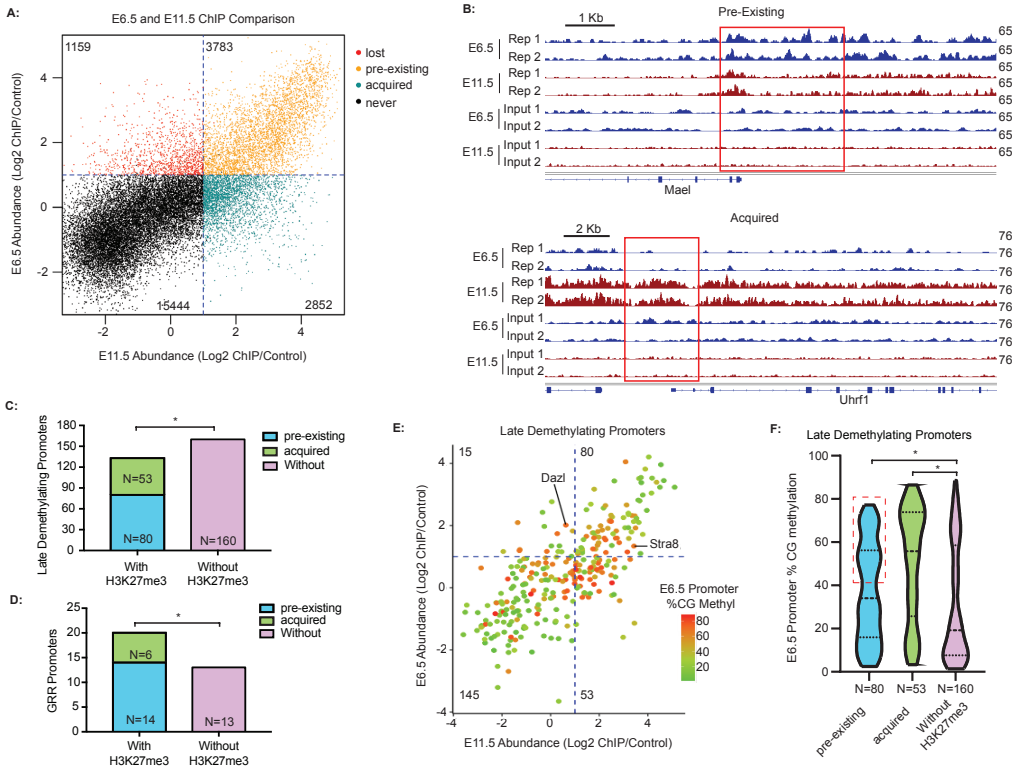

Figure S5: Late demethylating promoters are enriched for both H3K27me3 and DNA methylation. A) Scatterplot for promoter log2 normalized H3K27me3 CPM values at E6.5 (Yang et al., 2018) and E11.5 (Sachs et al., 2013). Dotted lines represent a 2-fold enrichment above input. All promoters with an FDR > 0.05 at both time points were categorized as Never. B) Genome browser tracks of a representative pre-existing (*Mael*) and acquired (*Uhrf1*) promoter. Red boxes outline promoter regions (-2 to +0.5 kb of TSS). C) Late demethylating promoters categorized with pre-existing or acquired H3K27me3 (Seisenberger et al., 2012). D) GRR promoters categorized with pre-existing or acquired H3K27me3 (Hill et al., 2018). E) Scatterplot of late demethylating promoters for log2 normalized CPM values at E6.5 (Yang et al., 2018) and E11.5 (Sachs et al., 2013). Dotted lines represent a 2-fold enrichment above input. All promoters with an FDR > 0.05 in both time points were categorized as Never. Promoter %CG methylation at E6.5 (Seisenberger et al., 2012). Dazl and Stra8 are labeled. F) %CG methylation at E6.5 (Seisenberger et al., 2012) for the late demethylating promoters in the pre-existing, acquired or without H3K27me3 at E11.5 (never and lost) categories. Pre-existing promoters with high (≥40%) E6.5 CG methylation are boxed in red. See also Figure 4.

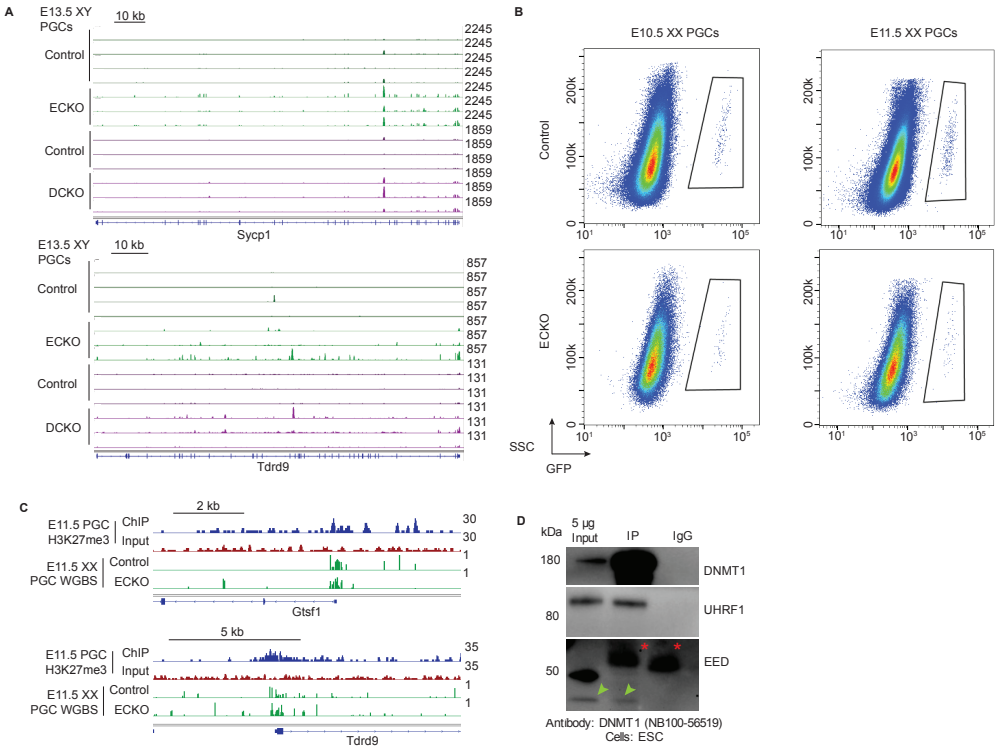

Figure S6: Overlapping ECKO and DCKO DEGs show similar regulation. A) Representative overlapping upregulated DEG RNA-sequencing tracks from ECKO and DCKO (Hargan-Calvopina et al., 2016.) B) Representative flow plots from E10.5 and E11.5 XX PGCs isolation via FACs for WGBS. C) Representative WGBS tracks at E11.5 in XX PGCs and E11.5 H3K27me3 ChIP-seq tracks (Liu et al., 2014) at overlapping upregulated ECKO and DCKO DEGs. D) Representation of co-immunoprecipitation in serum+LIF mouse ESCs following pulldown with an anti-DNMT1 antibody (NB100-56519). Input is collected prior to the pulldown, IP is the DNMT1 bound fraction and IgG is a negative control reciprocal pulldown with a non-specific mouse antibody (5415) (blots from n=3 independent replicate pull downs for EED (05-132), EZH2 (5246) and DNMT1 (NB100-56519), n=2 independent replicates for UHRF1 (sc373750)). * is the heavy chain of the pulldown antibody and arrowhead is the short isoform of EED. All replicate and uncropped blots are in document S1. All antibodies identified by their catalogue number listed in table S3. See also Figure 5.

Table S1: Differentially expressed gene analysis. All ECKO and DCKO DEGs and DEG promoter H3K27m3 analysis as defined in the methods. Related to Figures 2, 3, 5, S3, S4, S6 and STAR methods.

Table S2: Gene classification. All identified genes and their respective promoters used in this paper are shown with their relevant classifications. E6.5 and E11.5 %CG methylation values and late demethylating promoter classification is from (Seisenberger et al., 2012). Promoter H3k27me3

abundance is from (Yang et al., 2018) (E6.5), (Sachs et al., 2013) (E11.5) and (Liu et al., 2014) (E13.5). H3K27me3 categorization is from this manuscript. CpG content is as defined by (Mohn et al., 2008; Weber et al., 2007). GRR are from (Hill et al., 2018). All DCKO DEGs are from (Hargan-Calvopina et al., 2016) and ECKO DEGs are from this manuscript. Related to Figures 2, 3, 4, 5, S3, S4, S5, S6 and STAR methods.

Table S3: Antibodies used. All antibodies used in this manuscript.

Antibodies	Source	Identifier
Goat Polyclonal anti-MVH	R&D Systems	Cat# AF2030; RRID AB_2277369
Mouse Monoclonal anti-AP-2gamma (TFAP2C)	Santa Cruz	Cat# SC12762; RRID AB_667770
Rabbit Polyclonal anti-H3K27me3	Millipore	Cat# 07-449-MI; RRID AB_310624
Mouse Monoclonal anti-5mC	Aviva Biosciences	Cat# AMM99021; RRID AB_387479
Rabbit Monoclonal anti-H2AK119ub1	Cell Signaling Technologies	Cat# 8240T; RRID AB_10891618
Rabbit Polyclonal anti-cPARP	Cell Signaling Technologies	Cat# 9544; RRID AB_2160724
Mouse Monoclonal anti-KI67	BD Biosciences	Cat# 556003; RRID AB_396287
Mouse Monoclonal anti-AMH	Bio-Rad	Cat# MCA2246T; RRID AB_226470
Rabbit Polyclonal anti-H3K27ac	Abcam	Cat# ab4729; RRID AB_2118291
Rabbit Polyclonal anti-5hmC	Active Motif	Cat# 39069; RRID AB_10013602
Mouse Monoclonal anti-SYCP3 (SCP3)	Abcam	Cat# ab97672; RRID AB_10678841
Rabbit Polyclonal anti-PIWL2 (MILI)	Abcam	Cat# ab36764; RRID AB_777284
Donkey Polyclonal anti-Mouse Alexa Fluor 488	Jackson ImmunoResearch	Cat# 715-546-150; RRID AB_2340849
Donkey Polyclonal anti-Rabbit Alexa Fluor 488	Jackson ImmunoResearch	Cat# 711-545-152; RRID AB_2313584
Donkey Polyclonal anti-Rabbit Alexa Fluor 594	Jackson ImmunoResearch	Cat# 711-585-152; RRID AB_2340621
Donkey Polyclonal anti-Goat Alexa Fluor 594	Jackson ImmunoResearch	Cat# 705-586-147; RRID AB_2340434
Rabbit Monoclonal anti-DNMT1	Abcam	Cat# ab188453; RRID AB_2877711
Mouse Monoclonal anti-EED	Millipore	Cat# 05-132-0MI; RRID AB_1586999
Rabbit Monoclonal anti-EZH2	Cell Signaling Technologies	Cat# 5246s; RRID AB_10694683
Mouse Monoclonal anti-UHRF1	Santa Cruz	Cat#sc373750; RRID AB_10947236
Mouse Monoclonal anti-DNMT1	Novus Biologicals	Cat#NB100-56519; RRID AB_838131
Rabbit Polyclonal IgG Control	Abcam	Cat#ab27478; RRID AB_2616600
Mouse Polyclonal IgG Control	Cell Signaling Technologies	Cat#5415; RRID AB_10829607
Rat Monoclonal anti-Mouse HRP	Abcam	Cat#ab131368; RRID AB_2895114
Veriblot for IP Detection Reagent HRP	Abcam	Cat#ab131366; RRID AB_2892718

Table S4: PCR primers. Sequences of all primers used in this manuscript.

Primer Name	Primer	Purpose	Sequence
SMCX-1	Forward	Genotyping	CCGCTGCCAAATTCTTTGG
SMCY-1	Reverse	Genotyping	TGAAGCTTTTGGCTTTGAG
Blimp1-Cre Transgene	Forward	Genotyping	GCCGAGGTGCGCGTCAGTAC
Blimp1-Cre Transgene	Reverse	Genotyping	CTGAACATGTCCATCAGGTTCTTG
Oct4 Control	Forward	Genotyping	GATCACCTGGGGTTTGAGAA
Oct4 Control	Reverse	Genotyping	CAAGGCAAGGGAGGTAGACA
Oct4 Transgene	Forward	Genotyping	CAAGGCAAGGGAGGTAGACA
Oct4 Transgene	Reverse	Genotyping	AGGAACTGCTTCCTTCACGA
EED fl/fl	Forward	Genotyping	GGGACGTGCTGACATTTTCT
EED fl/fl	Reverse	Genotyping	CTTGGGTGGTTTGGCTAAGA

Table S5: Sequencing summary. Summary of all bulk RNA sequencing, single cell Smart-seq RNA sequencing, WGBS and ChIP-sequencing comparison used in this study. Related to STAR methods.

Document S1: Summary of replicates and uncropped Western blots. Related to Figures 5 and S6.

2

Document S1: Summary crops; EED (05-132) Pulldowns in EpiLCs

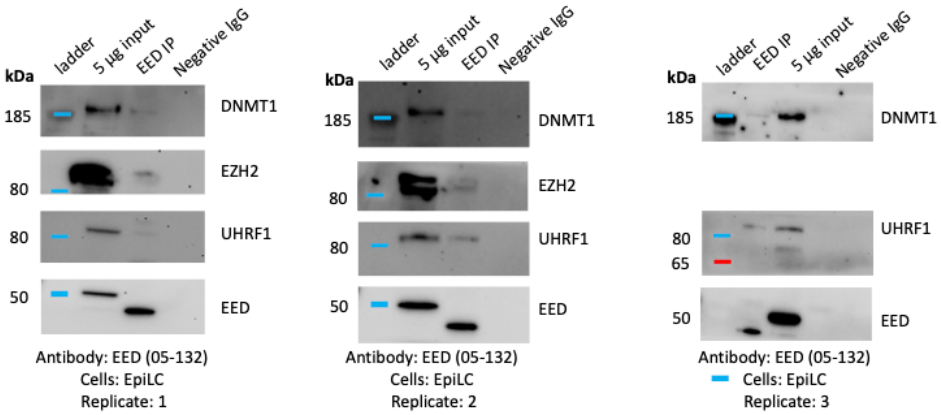

DNMT1, EED and EZH2 in Figure 5I

UHRF1 in Figure 5I

3

Document S1: Summary crops; EED (05-132) Pulldowns in ESCs

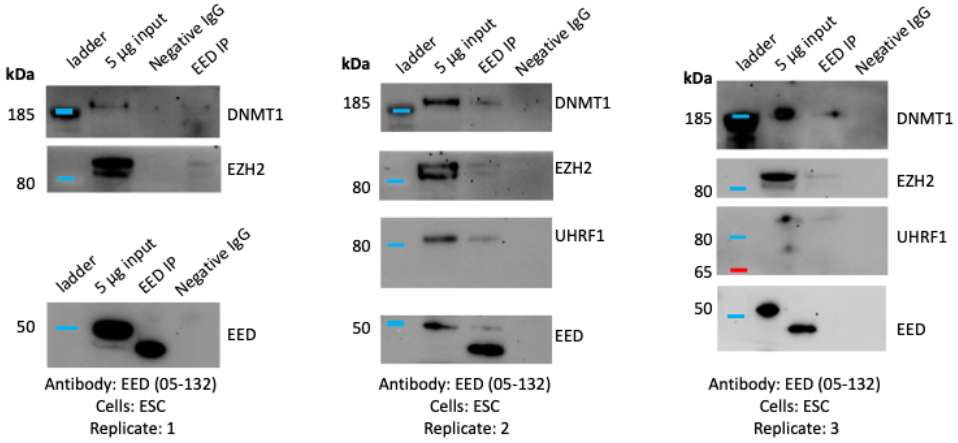

Figure 5H

4

Document S1: Summary crops; DNMT1 (ab188453) Pulldowns in ESCs

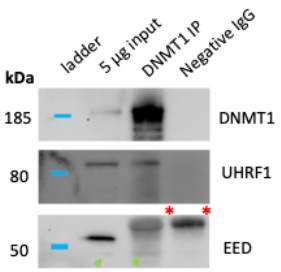

Antibody: DNMT1 (ab188453)
Cells: ESC
Replicate: 1

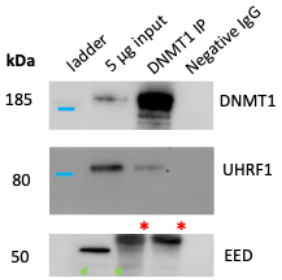

Antibody: DNMT1 (ab188453)
Cells: ESC
Replicate: 2

In Figure S6D

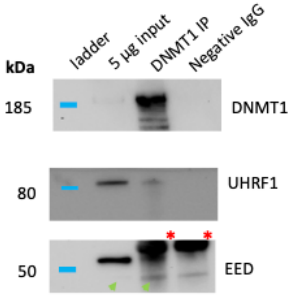

Antibody: DNMT1 (ab188453)
Cells: ESC
Replicate: 3

* = Heavy Chain
◂ = EED Band

5

Document S1: Summary crops; DNMT1 (NB100-56519) Pulldowns in ESCs

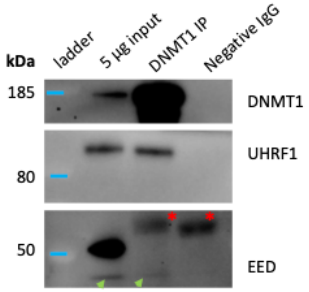

Antibody: DNMT1 (NB100-56519)
Cells: ESC
Replicate: 1

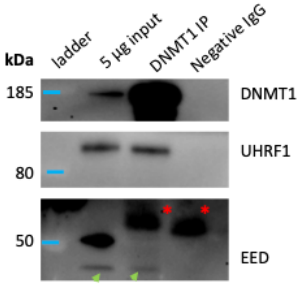

Antibody: DNMT1 (NB100-56519)
Cells: ESC
Replicate: 2

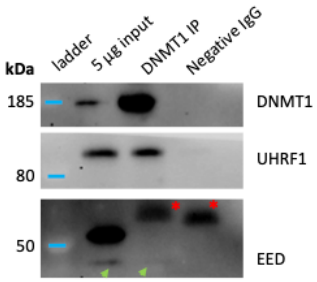

Antibody: DNMT1 (NB100-56519)
Cells: ESC
Replicate: 3

* = Heavy Chain
◂ = EED Band

Document S1: EpiLC EED (Millipore 05-132) Pulldown Replicate 1 Blots (Summary Blot 1)

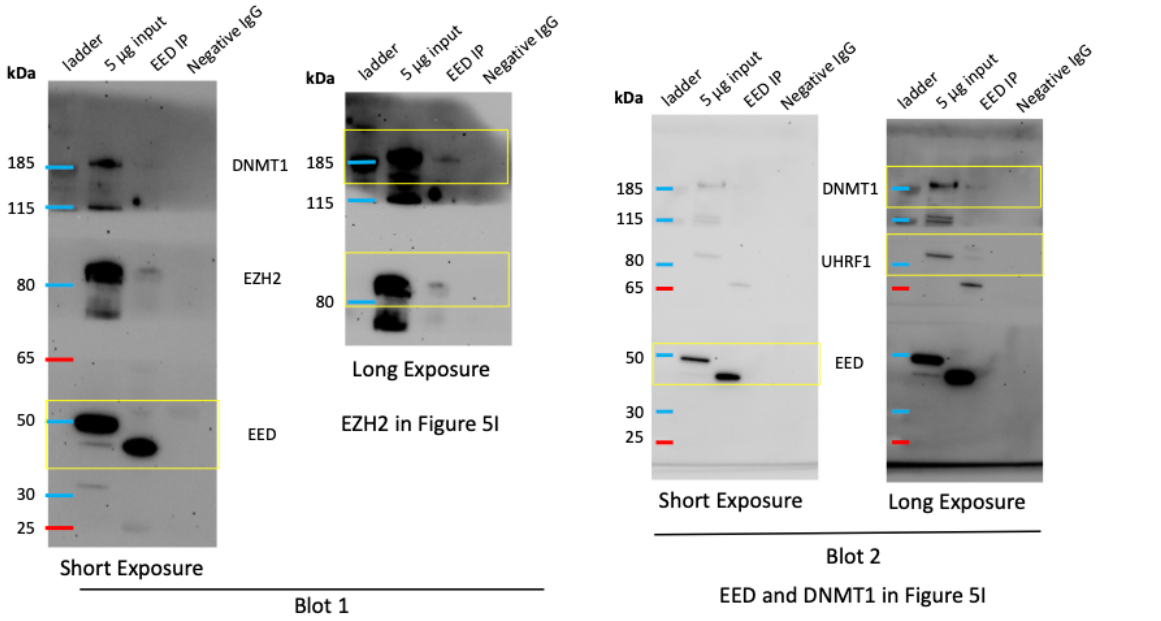

Document S1: EpiLC EED (Millipore 05-132) Pulldown Replicate 2 Blots (Summary Blot 2)

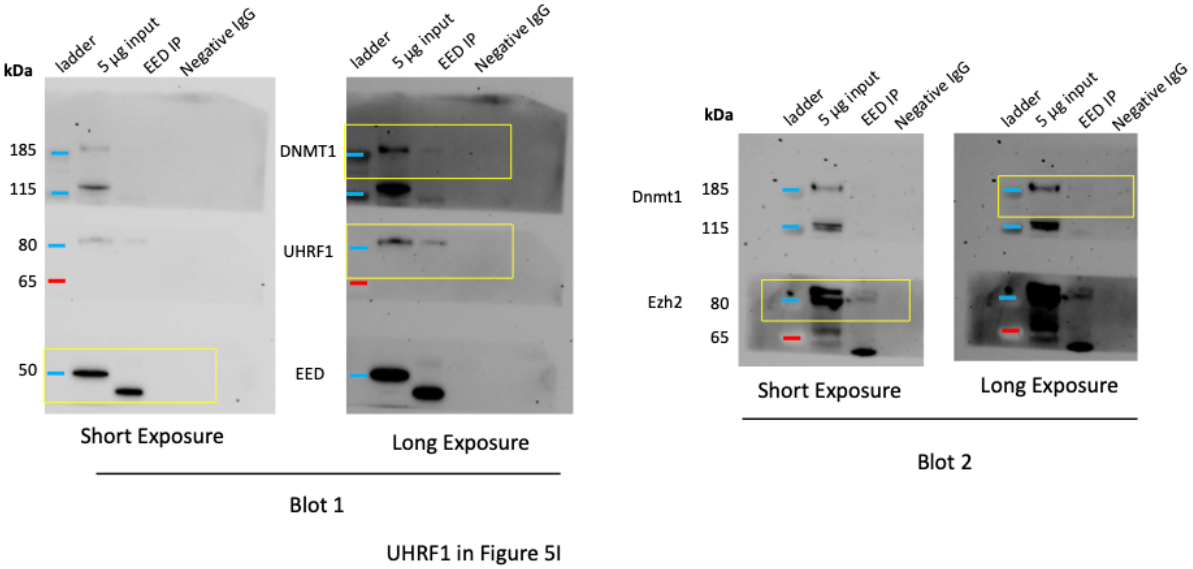

8

Document S1: EpiLC EED (Millipore 05-132) Pulldown Replicate 3 Blots (Summary Blot 3)

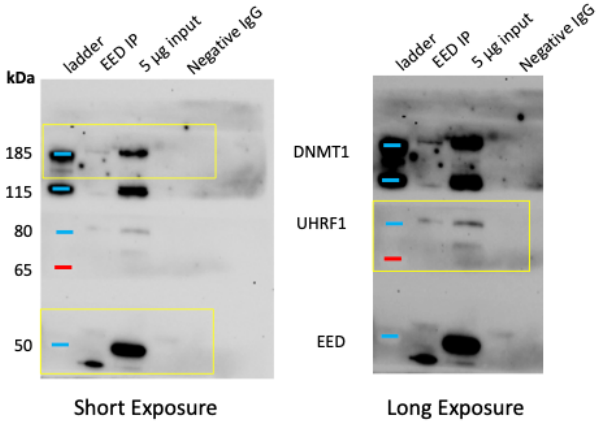

9

Document S1: ESC EED (Millipore 05-132) Pulldown Replicate 1 Blots (Summary Blot 4)

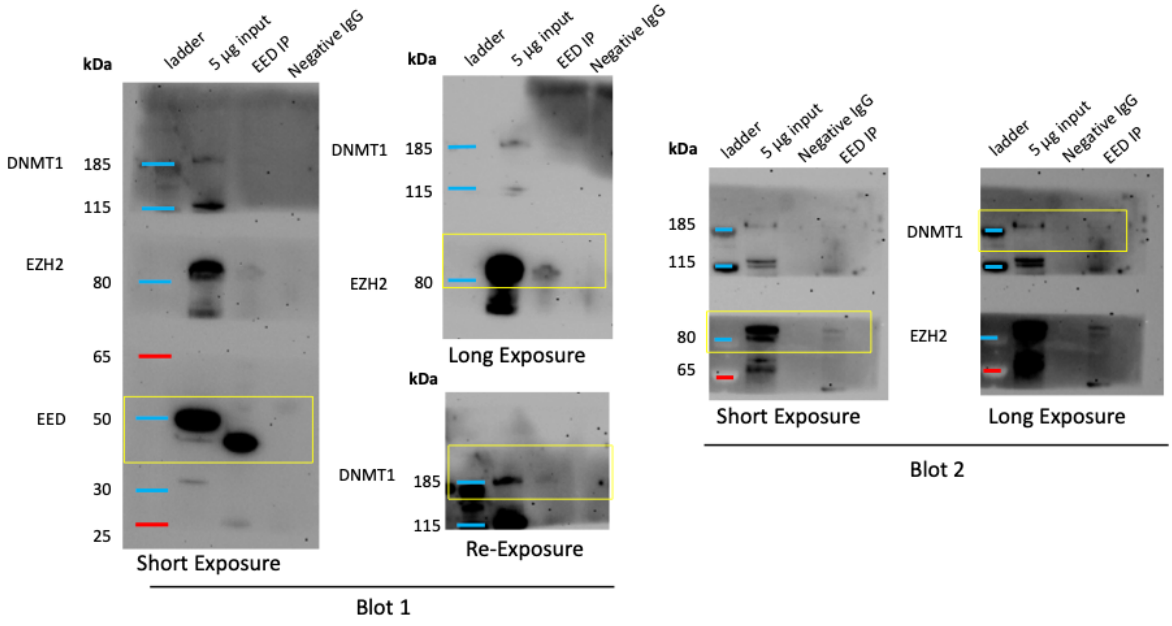

Document S1: ESC EED (Millipore 05-132) Pulldown Replicate 2 Blots (Summary Blot 5)

10

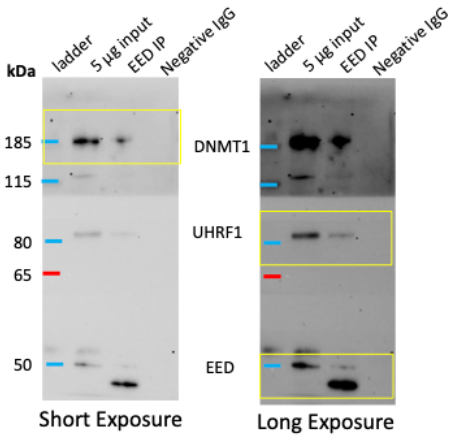

Blot 1

UHRF1 and EED in Figure 5H

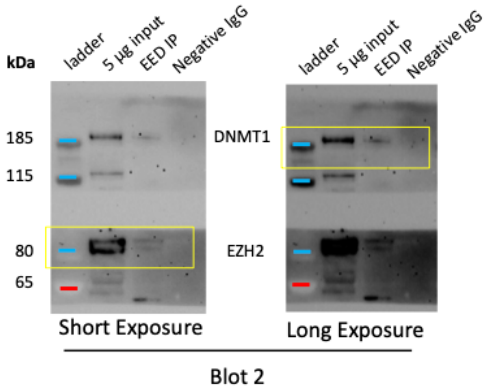

Blot 2

EZH2 and DNMT1 in Figure 5H

Document S1: ESC EED (Millipore 05-132) Pulldown Replicate 3 Blots (Summary Blot 6)

11

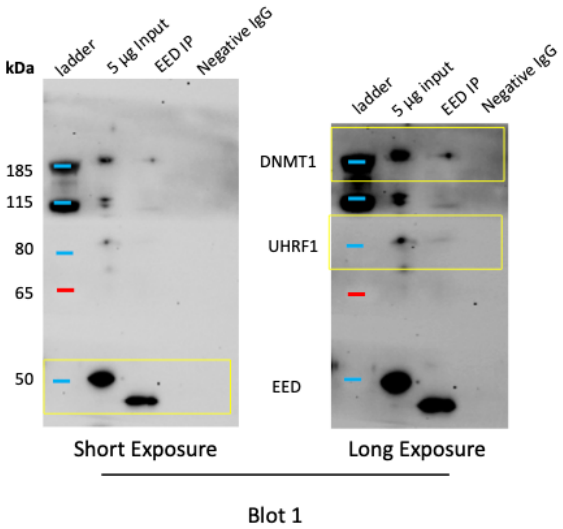

Blot 1

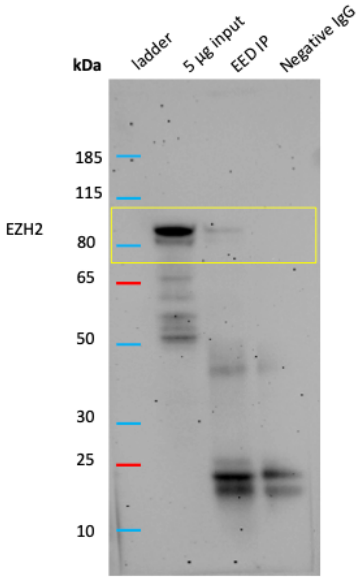

Blot 2

Document S1: ESC DNMT1 (Abcam ab188453) Pulldown Replicate 1 and 2 Blots

12

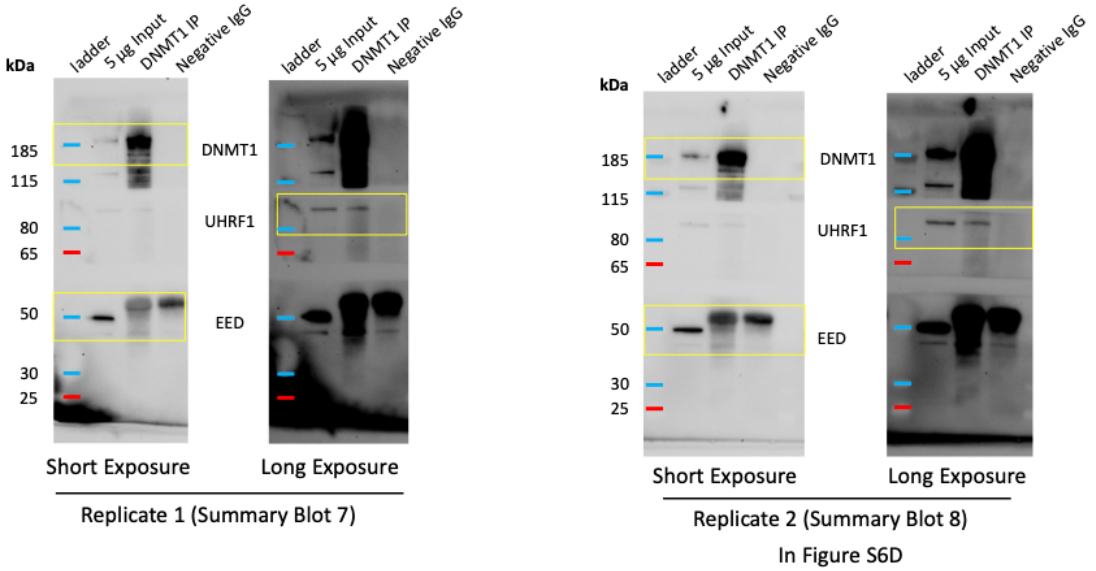

Document S1: ESC DNMT1 (Abcam ab188453) Pulldown Replicate 3 Blots (Summary Blot 9)

13

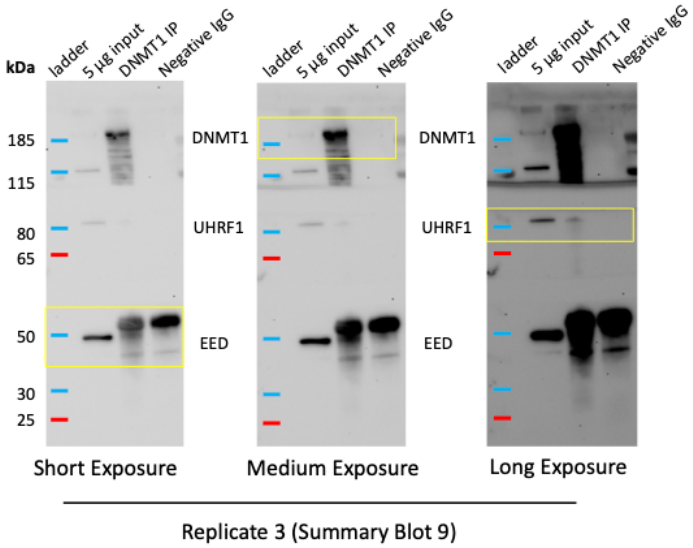

Document S1: ESC DNMT1 (NB100-56519) Pulldown Replicate 1 Blots (Summary Blot 10)

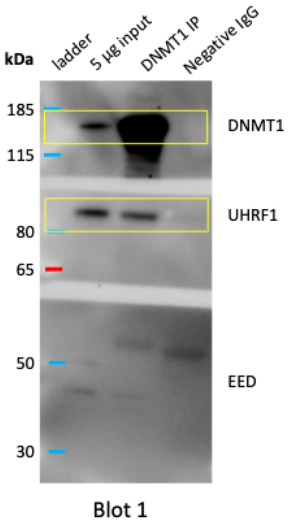

Blot 1

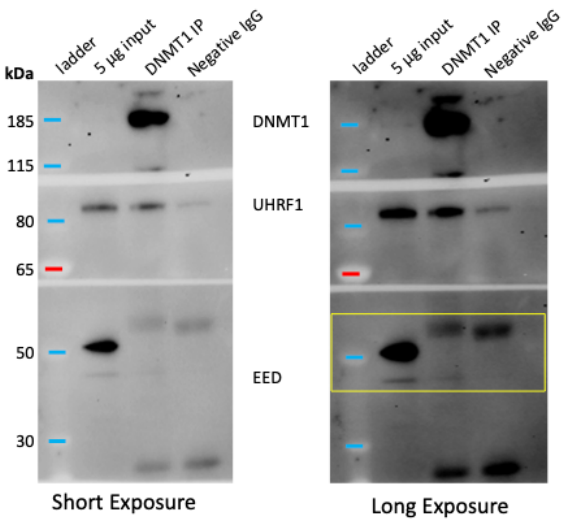

Blot 2

Document S1: ESC DNMT1 (NB100-56519) Pulldown Replicate 2 Blots (Summary Blot 11)

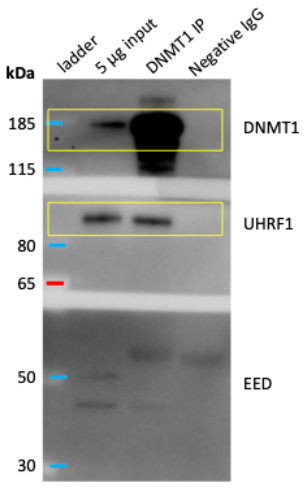

Blot 1

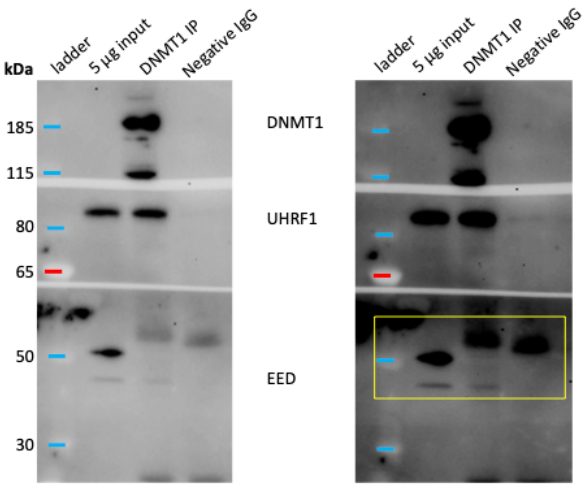

Blot 2

Document S1: ESC DNMT1 (NB100-56519) Pulldown Replicate 3 Blots (Summary Blot 12)

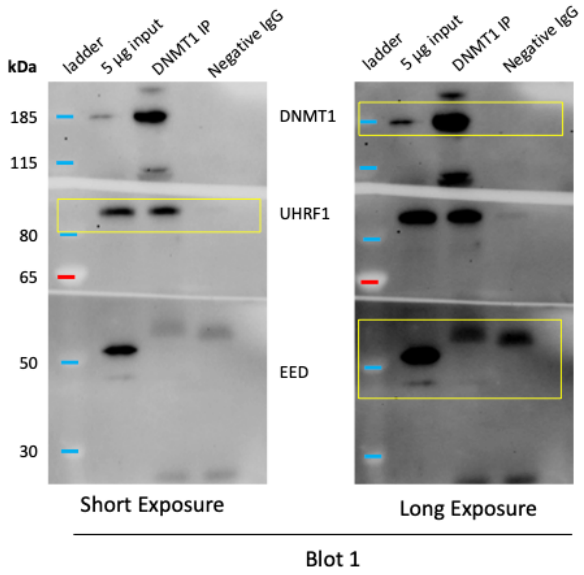

References

Anders, S., Pyl, P.T., and Huber, W. (2015). HTSeq—a Python framework to work with high-throughput sequencing data. Bioinformatics *31*, 166–169.

Aravin, A.A., Sachidanandam, R., Bourc'his, D., Schaefer, C., Pezic, D., Toth, K.F., Bestor, T., and Hannon, G.J. (2008). A piRNA pathway primed by individual transposons is linked to de novo DNA methylation in mice. Mol. Cell *31*, 785–799.

Baltus, A.E., Menke, D.B., Hu, Y.-C., Goodheart, M.L., Carpenter, A.E., de Rooij, D.G., and Page, D.C. (2006). In germ cells of mouse embryonic ovaries, the decision to enter meiosis precedes premeiotic DNA replication. Nat Genet *38*, 1430–1434.

Bartke, T., Vermeulen, M., Xhemalce, B., Robson, S.C., Mann, M., and Kouzarides, T. (2010). Nucleosome-Interacting Proteins Regulated by DNA and Histone Methylation. Cell *143*, 470–484.

Boulares, A.H., Yakovlev, A.G., Ivanova, V., Stoica, B.A., Wang, G., Iyer, S., and Smulson, M. (1999). Role of Poly(ADP-ribose) Polymerase (PARP) Cleavage in Apoptosis CASPASE 3-RESISTANT PARP MUTANT INCREASES RATES OF APOPTOSIS IN TRANSFECTED CELLS. J. Biol. Chem. *274*, 22932–22940.

Bracken, A.P., Dietrich, N., Pasini, D., Hansen, K.H., and Helin, K. (2006). Genome-wide mapping of Polycomb target genes unravels their roles in cell fate transitions. Genes Dev. *20*, 1123–1136.

Broad Institute (2020). Picard Toolkit. Broad Institute, Github Repository. http://broadinstitute.github.io/picard/

Cao, Q., Wang, X., Zhao, M., Yang, R., Malik, R., Qiao, Y., Poliakov, A., Yocum, A.K., Li, Y., Chen, W., et al. (2014). The central role of EED in the orchestration of polycomb group complexes. Nat Commun *5*, 3127.

Chen, F., Zhang, Q., Deng, X., Zhang, X., Chen, C., Lv, D., Li, Y., Li, D., Zhang, Y., Li, P., et al. (2018). Conflicts of CpG density and DNA methylation are proximally and distally involved in gene regulation in human and mouse tissues. Epigenetics *13*, 721–741.

Dewannieux, M., Dupressoir, A., Harper, F., Pierron, G., and Heidmann, T. (2004). Identification of autonomous IAP LTR retrotransposons mobile in mammalian cells. Nature Genetics *36*, 534–539.

Dobin, A., Davis, C.A., Schlesinger, F., Drenkow, J., Zaleski, C., Jha, S., Batut, P., Chaisson, M., and Gingeras, T.R. (2013). STAR: ultrafast universal RNA-seq aligner. Bioinformatics *29*, 15–21.

Endoh, M., Endo, T.A., Shinga, J., Hayashi, K., Farcas, A., Ma, K.-W., Ito, S., Sharif, J., Endoh, T., Onaga, N., et al. (2017). PCGF6-PRC1 suppresses premature differentiation of mouse embryonic stem cells by regulating germ cell-related genes. ELife *6*, e21064.

Gerdes, J., Schwab, U., Lemke, H., and Stein, H. (1983). Production of a mouse monoclonal antibody reactive with a human nuclear antigen associated with cell proliferation. Int. J. Cancer *31*, 13–20.

Ginsburg, M., Snow, M.H., and McLaren, A. (1990). Primordial germ cells in the mouse embryo during gastrulation. Development *110*, 521–528.

Guibert, S., Forné, T., and Weber, M. (2012). Global profiling of DNA methylation erasure in mouse primordial germ cells. Genome Res *22*, 633–641.

Guo, W., Fiziev, P., Yan, W., Cokus, S., Sun, X., Zhang, M.Q., Chen, P.-Y., and Pellegrini, M. (2013). BS-Seeker2: a versatile aligning pipeline for bisulfite sequencing data. BMC Genomics *14*, 774.

Hackett, J.A., Sengupta, R., Zylicz, J.J., Murakami, K., Lee, C., Down, T.A., and Surani, M.A. (2013). Germline DNA Demethylation Dynamics and Imprint Erasure Through 5-Hydroxymethylcytosine. Science *339*, 448–452.

Haggerty, C., Kretzmer, H., Riemenschneider, C., Kumar, A.S., Mattei, A.L., Bailly, N., Gottfreund, J., Giesselmann, P., Weigert, R., Brändl, B., et al. (2021). Dnmt1 has de novo activity targeted to transposable elements. Nat Struct Mol Biol *28*, 594–603.

Hajkova, P., Erhardt, S., Lane, N., Haaf, T., El-Maarri, O., Reik, W., Walter, J., and Surani, M.A. (2002). Epigenetic reprogramming in mouse primordial germ cells. Mech. Dev. *117*, 15–23.

Hargan-Calvopina, J., Taylor, S., Cook, H., Hu, Z., Lee, S.A., Yen, M.-R., Chiang, Y.-S., Chen, P.-Y., and Clark, A.T. (2016). Stage-Specific Demethylation in Primordial Germ Cells Safeguards against Precocious Differentiation. Dev. Cell *39*, 75–86.

Hayashi, K., Ohta, H., Kurimoto, K., Aramaki, S., and Saitou, M. (2011). Reconstitution of the mouse germ cell specification pathway in culture by pluripotent stem cells. Cell *146*, 519–532.

Heeringen, S.J. van, Akkers, R.C., Kruijsbergen, I. van, Arif, M.A., Hanssen, L.L.P., Sharifi, N., and Veenstra, G.J.C. (2014). Principles of nucleation of H3K27 methylation during embryonic development. Genome Res. *24*, 401–410.

Hill, P.W.S., Leitch, H.G., Requena, C.E., Sun, Z., Amouroux, R., Roman-Trufero, M., Borkowska, M., Terragni, J., Vaisvila, R., Linnett, S., et al. (2018). Epigenetic reprogramming enables the primordial germ cell-to-gonocyte transition. Nature *555*, 392–396.

Huang, D.W., Sherman, B.T., and Lempicki, R.A. (2009). Bioinformatics enrichment tools: paths toward the comprehensive functional analysis of large gene lists. Nucleic Acids Res *37*, 1–13.

Huang, T.-C., Wang, Y.-F., Vazquez-Ferrer, E., Theofel, I., Requena, C.E., Hanna, C.W., Kelsey, G., and Hajkova, P. (2021). Sex-specific chromatin remodelling safeguards transcription in germ cells. Nature 1–6.

Jadhav, U., Manieri, E., Nalapareddy, K., Madha, S., Chakrabarti, S., Wucherpfennig, K., Barefoot, M., and Shivdasani, R.A. (2020). Replicational Dilution of H3K27me3 in Mammalian Cells and the Role of Poised Promoters. Molecular Cell *78*, 141-151.e5.

Jameson, S.A., Natarajan, A., Cool, J., DeFalco, T., Maatouk, D.M., Mork, L., Munger, S.C., and Capel, B. (2012). Temporal Transcriptional Profiling of Somatic and Germ Cells Reveals Biased Lineage Priming of Sexual Fate in the Fetal Mouse Gonad. PLOS Genetics *8*, e1002575.

Kim, S., Günesdogan, U., Zylicz, J.J., Hackett, J.A., Cougot, D., Bao, S., Lee, C., Dietmann, S., Allen, G.E., Sengupta, R., et al. (2014). PRMT5 Protects Genomic Integrity during Global DNA Demethylation in Primordial Germ Cells and Preimplantation Embryos. Mol Cell *56*, 564–579.

King, A.D., Huang, K., Rubbi, L., Liu, S., Wang, C.-Y., Wang, Y., Pellegrini, M., and Fan, G. (2016). Reversible Regulation of Promoter and Enhancer Histone Landscape by DNA Methylation in Mouse Embryonic Stem Cells. Cell Rep *17*, 289–302.

Kiselev, V.Yu., Kirschner, K., Schaub, M.T., Andrews, T., Yiu, A., Chandra, T., Natarajan, K.N., Reik, W., Barahona, M., Green, A.R., et al. (2017). SC3 - consensus clustering of single-cell RNA-Seq data. Nat Methods *14*, 483–486.

Kobayashi, H., Sakurai, T., Miura, F., Imai, M., Mochiduki, K., Yanagisawa, E., Sakashita, A., Wakai, T., Suzuki, Y., Ito, T., et al. (2013). High-resolution DNA methylome analysis of primordial germ cells identifies gender-specific reprogramming in mice. Genome Res *23*, 616–627.

Kuzmichev, A., Nishioka, K., Erdjument-Bromage, H., Tempst, P., and Reinberg, D. (2002). Histone methyltransferase activity associated with a human multiprotein complex containing the Enhancer of Zeste protein. Genes Dev *16*, 2893–2905.

Langmead, B., and Salzberg, S.L. (2012). Fast gapped-read alignment with Bowtie 2. Nat. Methods *9*, 357–359.

Lengner, C.J., Camargo, F.D., Hochedlinger, K., Welstead, G.G., Zaidi, S., Gokhale, S., Scholer, H.R., Tomilin, A., and Jaenisch, R. (2007). Oct4 Expression Is Not Required for Mouse Somatic Stem Cell Self-Renewal. Cell Stem Cell *1*, 403–415.

Lesch, B.J., Dokshin, G.A., Young, R.A., McCarrey, J.R., and Page, D.C. (2013). A set of genes critical to development is epigenetically poised in mouse germ cells from fetal stages through completion of meiosis. Proc Natl Acad Sci U S A *110*, 16061–16066.

Li, H., Handsaker, B., Wysoker, A., Fennell, T., Ruan, J., Homer, N., Marth, G., Abecasis, G., Durbin, R., and 1000 Genome Project Data Processing Subgroup (2009). The Sequence Alignment/Map format and SAMtools. Bioinformatics *25*, 2078–2079.

Li, Y., Zheng, H., Wang, Q., Zhou, C., Wei, L., Liu, X., Zhang, W., Zhang, Y., Du, Z., Wang, X., et al. (2018). Genome-wide analyses reveal a role of Polycomb in promoting hypomethylation of DNA methylation valleys. Genome Biology *19*, 18.

Liao, Y., Smyth, G.K., and Shi, W. (2014). featureCounts: an efficient general purpose program for assigning sequence reads to genomic features. Bioinformatics *30*, 923–930.

Liu, M., Zhu, Y., Xing, F., Liu, S., Xia, Y., Jiang, Q., and Qin, J. (2020). The polycomb group protein PCGF6 mediates germline gene silencing by recruiting histone-modifying proteins to target gene promoters. J. Biol. Chem. *295*, 9712–9724.

Liu, Q., Wang, G., Li, Q., Jiang, W., Kim, J., Wang, R., Zhu, S., Wang, X., Yan, L., Yi, Y., et al. (2019). Polycomb group proteins EZH2 and EED directly regulate androgen receptor in advanced prostate cancer. Int. J. Cancer *145*, 415–426.

Liu, S., Brind'Amour, J., Karimi, M.M., Shirane, K., Bogutz, A., Lefebvre, L., Sasaki, H., Shinkai, Y., and Lorincz, M.C. (2014). Setdb1 is required for germline development and silencing of H3K9me3-marked endogenous retroviruses in primordial germ cells. Genes Dev. *28*, 2041–2055.

Lopes, S.M.C. de S., Hayashi, K., Shovlin, T.C., Mifsud, W., Surani, M.A., and McLaren, A. (2008). X Chromosome Activity in Mouse XX Primordial Germ Cells. PLOS Genetics *4*, e30.

Mallol, A., Guirola, M., and Payer, B. (2019). PRDM14 controls X-chromosomal and global epigenetic reprogramming of H3K27me3 in migrating mouse primordial germ cells. Epigenetics & Chromatin *12*, 38.

Martin, M. (2011). Cutadapt removes adapter sequences from high-throughput sequencing reads. EMBnet.Journal *17*, 10–12.

McCarrey, J.R., and Dilworth, D.D. (1992). Expression of Xist in mouse germ cells correlates with X–chromosome inactivation. Nature Genetics *2*, 200–203.

McCarthy, D.J., Campbell, K.R., Lun, A.T.L., and Wills, Q.F. (2017). Scater: pre-processing, quality control, normalization and visualization of single-cell RNA-seq data in R. Bioinformatics *33*, 1179–1186.

Mendenhall, E.M., Koche, R.P., Truong, T., Zhou, V.W., Issac, B., Chi, A.S., Ku, M., and Bernstein, B.E. (2010). GC-Rich Sequence Elements Recruit PRC2 in Mammalian ES Cells. PLOS Genetics *6*, e1001244.

van Mierlo, G., Dirks, R.A.M., De Clerck, L., Brinkman, A.B., Huth, M., Kloet, S.L., Saksouk, N., Kroeze, L.I., Willems, S., Farlik, M., et al. (2019). Integrative Proteomic Profiling Reveals PRC2-Dependent Epigenetic Crosstalk Maintains Ground-State Pluripotency. Cell Stem Cell *24*, 123-137.e8.

Mohn, F., Weber, M., Rebhan, M., Roloff, T.C., Richter, J., Stadler, M.B., Bibel, M., and Schübeler, D. (2008). Lineage-Specific Polycomb Targets and De Novo DNA Methylation Define Restriction and Potential of Neuronal Progenitors. Molecular Cell *30*, 755–766.

Montgomery, N.D., Yee, D., Montgomery, S.A., and Magnuson, T. (2007). Molecular and functional mapping of EED motifs required for PRC2-dependent histone methylation. J Mol Biol *374*, 1145–1157.

Mozzetta, C., Pontis, J., Fritsch, L., Robin, P., Portoso, M., Proux, C., Margueron, R., and Ait-Si-Ali, S. (2014). The Histone H3 Lysine 9 Methyltransferases G9a and GLP Regulate Polycomb Repressive Complex 2-Mediated Gene Silencing. Molecular Cell *53*, 277–289.

Murphy, P.J., Cipriany, B.R., Wallin, C.B., Ju, C.Y., Szeto, K., Hagarman, J.A., Benitez, J.J., Craighead, H.G., and Soloway, P.D. (2013). Single-molecule analysis of combinatorial epigenomic states in normal and tumor cells. PNAS *110*, 7772–7777.

Napoles, M. de, Nesterova, T., and Brockdorff, N. (2007). Early Loss of Xist RNA Expression and Inactive X Chromosome Associated Chromatin Modification in Developing Primordial Germ Cells. PLOS ONE *2*, e860.

de Napoles, M., Mermoud, J.E., Wakao, R., Tang, Y.A., Endoh, M., Appanah, R., Nesterova, T.B., Silva, J., Otte, A.P., Vidal, M., et al. (2004). Polycomb Group Proteins Ring1A/B Link Ubiquitylation of Histone H2A to Heritable Gene Silencing and X Inactivation. Developmental Cell *7*, 663–676.

Ng, J.-H., Kumar, V., Muratani, M., Kraus, P., Yeo, J.-C., Yaw, L.-P., Xue, K., Lufkin, T., Prabhakar, S., and Ng, H.-H. (2013). In vivo epigenomic profiling of germ cells reveals germ cell molecular signatures. Dev. Cell *24*, 324–333.

Ohinata, Y., Payer, B., O'Carroll, D., Ancelin, K., Ono, Y., Sano, M., Barton, S.C., Obukhanych, T., Nussenzweig, M., Tarakhovsky, A., et al. (2005). Blimp1 is a critical determinant of the germ cell lineage in mice. Nature *436*, 207–213.

Pasini, D., Malatesta, M., Jung, H.R., Walfridsson, J., Willer, A., Olsson, L., Skotte, J., Wutz, A., Porse, B., Jensen, O.N., et al. (2010). Characterization of an antagonistic switch between histone H3 lysine 27 methylation and acetylation in the transcriptional regulation of Polycomb group target genes. Nucleic Acids Res *38*, 4958–4969.

Prokopuk, L., Stringer, J.M., Hogg, K., Elgass, K.D., and Western, P.S. (2017). PRC2 is required for extensive reorganization of H3K27me3 during epigenetic reprogramming in mouse fetal germ cells. Epigenetics & Chromatin *10*, 7.

Prokopuk, L., Hogg, K., and Western, P.S. (2018). Pharmacological inhibition of EZH2 disrupts the female germline epigenome. Clinical Epigenetics *10*, 33.

Quinlan, A.R., and Hall, I.M. (2010). BEDTools: a flexible suite of utilities for comparing genomic features. Bioinformatics *26*, 841–842.

Richardson, S.R., Gerdes, P., Gerhardt, D.J., Sanchez-Luque, F.J., Bodea, G.-O., Muñoz-Lopez, M., Jesuadian, J.S., Kempen, M.-J.H.C., Carreira, P.E., Jeddeloh, J.A., et al. (2017). Heritable L1 retrotransposition in the mouse primordial germline and early embryo. Genome Res. *27*, 1395–1405.

Robinson, M.D., McCarthy, D.J., and Smyth, G.K. (2010). edgeR: a Bioconductor package for differential expression analysis of digital gene expression data. Bioinformatics *26*, 139–140.

Rothbart, S.B., Krajewski, K., Nady, N., Tempel, W., Xue, S., Badeaux, A.I., Barsyte-Lovejoy, D., Martinez, J.Y., Bedford, M.T., Fuchs, S.M., et al. (2012). Association of UHRF1 with H3K9 methylation directs the maintenance of DNA methylation. Nat Struct Mol Biol *19*, 1155–1160.

Sachs, M., Onodera, C., Blaschke, K., Ebata, K.T., Song, J.S., and Ramalho-Santos, M. (2013). Bivalent Chromatin Marks Developmental Regulatory Genes in the Mouse Embryonic Germline in Vivo. Cell Rep *3*, 1777–1784.

Saitou, M., and Yamaji, M. (2012). Primordial Germ Cells in Mice. Cold Spring Harb Perspect Biol *4*, a008375.

Sangrithi, M.N., Royo, H., Mahadevaiah, S.K., Ojarikre, O., Bhaw, L., Sesay, A., Peters, A.H.F.M., Stadler, M., and Turner, J.M.A. (2017). Non-Canonical and Sexually Dimorphic X Dosage Compensation States in the Mouse and Human Germline. Developmental Cell *40*, 289-301.e3.

Schuettengruber, B., Bourbon, H.-M., Di Croce, L., and Cavalli, G. (2017). Genome Regulation by Polycomb and Trithorax: 70 Years and Counting. Cell *171*, 34–57.

Seisenberger, S., Andrews, S., Krueger, F., Arand, J., Walter, J., Santos, F., Popp, C., Thienpont, B., Dean, W., and Reik, W. (2012). The Dynamics of Genome-wide DNA Methylation Reprogramming in Mouse Primordial Germ Cells. Mol Cell *48*, 849–862.

Seki, Y., Hayashi, K., Itoh, K., Mizugaki, M., Saitou, M., and Matsui, Y. (2005). Extensive and orderly reprogramming of genome-wide chromatin modifications associated with specification and early development of germ cells in mice. Dev. Biol. *278*, 440–458.

Soh, Y.Q.S., Mikedis, M.M., Kojima, M., Godfrey, A.K., Rooij, D.G. de, and Page, D.C. (2017). Meioc maintains an extended meiotic prophase I in mice. PLOS Genetics *13*, e1006704.

Stringer, J.M., Forster, S.C., Qu, Z., Prokopuk, L., O'Bryan, M.K., Gardner, D.K., White, S.J., Adelson, D., and Western, P.S. (2018). Reduced PRC2 function alters male germline epigenetic programming and paternal inheritance. BMC Biology *16*, 104.

Sugimoto, M., and Abe, K. (2007). X Chromosome Reactivation Initiates in Nascent Primordial Germ Cells in Mice. PLOS Genetics *3*, e116.

Traut, W., Endl, E., Scholzen, T., Gerdes, J., and Winking, H. (2002). The temporal and spatial distribution of the proliferation associated Ki-67 protein during female and male meiosis. Chromosoma *111*, 156–164.

Wang, Q., Yu, G., Ming, X., Xia, W., Xu, X., Zhang, Y., Zhang, W., Li, Y., Huang, C., Xie, H., et al. (2020). Imprecise DNMT1 activity coupled with neighbor-guided correction enables robust yet flexible epigenetic inheritance. Nature Genetics *52*, 828–839.

Weber, M., Hellmann, I., Stadler, M.B., Ramos, L., Pääbo, S., Rebhan, M., and Schübeler, D. (2007). Distribution, silencing potential and evolutionary impact of promoter DNA methylation in the human genome. Ng *39*, 457–466.

Western, P.S., Miles, D.C., Bergen, J.A. van den, Burton, M., and Sinclair, A.H. (2008). Dynamic Regulation of Mitotic Arrest in Fetal Male Germ Cells. STEM CELLS *26*, 339–347.

Wickham, H. (2016). ggplot2: Elegant Graphics for Data Analysis (Springer International Publishing).

Wu, H., D'Alessio, A.C., Ito, S., Xia, K., Wang, Z., Cui, K., Zhao, K., Eve Sun, Y., and Zhang, Y. (2011). Dual functions of Tet1 in transcriptional regulation in mouse embryonic stem cells. Nature *473*, 389–393.

Yamaguchi, S., Hong, K., Liu, R., Inoue, A., Shen, L., Zhang, K., and Zhang, Y. (2013). Dynamics of 5-methylcytosine and 5-hydroxymethylcytosine during germ cell reprogramming. Cell Res. *23*, 329–339.

Yang, X., Hu, B., Hou, Y., Qiao, Y., Wang, R., Chen, Y., Qian, Y., Feng, S., Chen, J., Liu, C., et al. (2018). Silencing of developmental genes by H3K27me3 and DNA methylation reflects the discrepant plasticity of embryonic and extraembryonic lineages. Cell Res *28*, 593–596.

Yokobayashi, S., Liang, C.-Y., Kohler, H., Nestorov, P., Liu, Z., Vidal, M., van Lohuizen, M., Roloff, T.C., and Peters, A.H.F.M. (2013). PRC1 coordinates timing of sexual differentiation of female primordial germ cells. Nature *495*, 236–240.

Yu, M., Riva, L., Xie, H., Schindler, Y., Moran, T.B., Cheng, Y., Yu, D., Hardison, R., Weiss, M.J., Orkin, S.H., et al. (2009). Insights into GATA-1-mediated gene activation versus repression via genome-wide chromatin occupancy analysis. Mol. Cell *36*, 682–695.

Zhao, W., Tong, H., Huang, Y., Yan, Y., Teng, H., Xia, Y., Jiang, Q., and Qin, J. (2017). Essential Role for Polycomb Group Protein Pcgf6 in Embryonic Stem Cell Maintenance and a Noncanonical Polycomb Repressive Complex 1 (PRC1) Integrity. J. Biol. Chem. *292*, 2773–2784.

Zhao, Z.-H., Ma, J.-Y., Meng, T.-G., Wang, Z.-B., Yue, W., Zhou, Q., Li, S., Feng, X., Hou, Y., Schatten, H., et al. (2020). Single-cell RNA sequencing reveals the landscape of early female germ cell development. The FASEB Journal *34*, 12634–12645.

Zheng, H., Huang, B., Zhang, B., Xiang, Y., Du, Z., Xu, Q., Li, Y., Wang, Q., Ma, J., Peng, X., et al. (2016). Resetting Epigenetic Memory by Reprogramming of Histone Modifications in Mammals. Molecular Cell *63*, 1066–1079.

Chapter 5

Conclusion and Future Perspectives

Given the prevalence of infertility and current limitations in treatment options, it is essential that we study the mechanisms regulating hPGC specification and epigenetic reprogramming. One of the most promising new advances for infertility treatment is the recently published *in vitro* gametogenesis protocol which has allowed for the complete recapitulation of the XX mouse germline *in vitro* (Hikabe et al., 2016). While there has been some preliminary work translating this technique into human cell culture, the cells fail to progress into mature oocytes suggesting a problem in either the specification or epigenetic reprogramming of the hPGCLCs (Yamashiro et al., 2018). Given the practical and ethical limitations in assessing these processes in human embryos, we rely upon the *in vitro* hPGCLC differentiation method as well as mPGC-specific conditional knockout mice in order to study the mechanisms of hPGC specification and epigenetic reprogramming, respectively.

In chapter 2, we discussed our use of CRISPR/Cas9 gene editing to characterize the transcription factor network which specifies hPGCs by creating null mutants in human embryonic stem cells which were then differentiated into hPGCLCs. Through this, we identified that unlike mPGCs, EOMES is required for hPGCLC induction (Chen et al., 2017). This technique provides a robust way to identify and validate key regulators of hPGC specification which can potentially be used as a diagnostic or therapeutic target.

While the hPGCLC method is sufficient to study the specification of hPGCs, it fails to properly undergo the epigenetic reorganization necessary for further germline development (Sasaki et al., 2015). Therefore, in order to properly assess epigenetic reprogramming in hPGCs, we turned to the mouse embryo as a model organism. Using the Cre-lox system with a *Blimp1* promoter driven *Cre*, we created mPGC-specific conditional knockout mice in order to assess the role of a gene of interest in germline development without altering expression in other tissue

(Ohinata et al., 2005). In chapter 3, we explored the role of UHRF1 and identified that while its cofactor DNMT1 has been shown to have a key role in regulating the timing of sex-specific differentiation in PGCs, it is doing so independent of UHRF1 (Hargan-Calvopina et al., 2016). This raises questions over what is directing DNMT1 to maintain DNA methylation at the late demethylating promoters of gametogenesis genes (Kagiwada et al., 2013; Seisenberger et al., 2012). Recently, DNMT1 was confirmed to have *de novo* methyltransferase activity in "neighborhoods" of dense DNA methylation (Wang et al., 2020). Since the late demethylating promoters contain heavily methylated CG islands, it is possible that this higher than average density of methylated cytosines attracts or holds DNMT1 at these sites for a longer period of time allowing for a slower DNA demethylation (Hill et al., 2018; Seisenberger et al., 2012). Additionally, it is also possible that there is another cofactor which directs DNMT1 to these loci which has yet to be identified. Indeed, in chapter 4 we identified an interaction between DNMT1 and EED/PRC2 using Epiblast-like cells, an *in vitro* model of the post-implantation epiblast which mPGCs are specified from (Hayashi et al., 2011). However, closer examination of the late demethylating promoters revealed no change in the maintenance of DNA methylation following conditional knockout of EED, confirming that, much like UHRF1, PRC2 is not directing DNMT1 to these loci.

Looking more broadly, much like DNMT1 (Hargan-Calvopina et al., 2016) and PRC1 (Yokobayashi et al., 2013), EED/PRC2 was found to regulate the timing of exit from the mPGC stage of the germline. Given that all of these epigenetic regulators converge on and repress gametogenesis genes such as *Stra8*, a key protein in driving XX germline differentiation, the possibility for an expansive epigenetic regulatory network is intriguing (Hargan-Calvopina et al., 2016; Yokobayashi et al., 2013). It has recently been shown that PRC1.6, a subcomplex of

PRC1, is essential to maintain repression of the gametogenesis genes in mouse embryonic stem cells (Endoh et al., 2017). Given the ability for PRC2 and PRC1 to recognize the other's downstream histone mark, H3K27me3 and H2AK119ub1 respectively, and establish a polycomb mediated repressive feedback loop, it is possible that PRC1.6 may be directing PRC2 to the gametogenesis promoters (Boyer et al., 2006; Bracken et al., 2006). PRC1.6 has also been shown to interact with G9A/GLP (Liu et al., 2020) and SETDB1 (Mochizuki et al., 2021) to direct deposition of their repressive marks, H3K9me1/2 and H3K9me3 respectively, to gametogenesis promoters *in vitro*. Additionally, we identified a subset of gametogenesis genes which are marked by both DNA methylation and H3K27me3 within the E6.5 post-implantation mouse epiblast which is maintained through the first stage of DNA demethylation suggesting a coordinated role in regulating mPGC differentiation (Sachs et al., 2013; Seisenberger et al., 2012; Yang et al., 2018). With all of these epigenetic regulatory pathways converging onto the same subset of gametogenesis genes, it is reasonable to suspect that they may be working as part of a greater regulatory network to finely tune gene expression during mPGC differentiation. This presents not only an exciting avenue for future research which can be pursued both in a mouse model to explore the potential co-maintenance of these marks during mPGC differentiation as well as to assess whether targeted inhibition of these pathways in hPGCLCs allows for a more accurate recapitulation of hPGC differentiation *in vitro*.

Altogether, this work furthers our understanding of the mechanisms driving both hPGC specification and the subsequent epigenetic regulatory networks which direct germline differentiation. This is critical to better understand the underlying causes of infertility, improve diagnosis of germline disorders and to further the development of treatment options such as IVG.

References

Boyer, L.A., Plath, K., Zeitlinger, J., Brambrink, T., Medeiros, L.A., Lee, T.I., Levine, S.S., Wernig, M., Tajonar, A., Ray, M.K., et al. (2006). Polycomb complexes repress developmental regulators in murine embryonic stem cells. Nature *441*, 349–353. https://doi.org/10.1038/nature04733.

Bracken, A.P., Dietrich, N., Pasini, D., Hansen, K.H., and Helin, K. (2006). Genome-wide mapping of Polycomb target genes unravels their roles in cell fate transitions. Genes Dev. *20*, 1123–1136. https://doi.org/10.1101/gad.381706.

Chen, D., Liu, W., Lukianchikov, A., Hancock, G.V., Zimmerman, J., Lowe, M.G., Kim, R., Galic, Z., Irie, N., Surani, M.A., et al. (2017). Germline competency of human embryonic stem cells depends on eomesodermin. Biol Reprod *97*, 850–861. https://doi.org/10.1093/biolre/iox138.

Endoh, M., Endo, T.A., Shinga, J., Hayashi, K., Farcas, A., Ma, K.-W., Ito, S., Sharif, J., Endoh, T., Onaga, N., et al. (2017). PCGF6-PRC1 suppresses premature differentiation of mouse embryonic stem cells by regulating germ cell-related genes. ELife *6*, e21064. https://doi.org/10.7554/eLife.21064.

Hargan-Calvopina, J., Taylor, S., Cook, H., Hu, Z., Lee, S.A., Yen, M.-R., Chiang, Y.-S., Chen, P.-Y., and Clark, A.T. (2016). Stage-Specific Demethylation in Primordial Germ Cells Safeguards against Precocious Differentiation. Dev. Cell *39*, 75–86. https://doi.org/10.1016/j.devcel.2016.07.019.

Hayashi, K., Ohta, H., Kurimoto, K., Aramaki, S., and Saitou, M. (2011). Reconstitution of the mouse germ cell specification pathway in culture by pluripotent stem cells. Cell *146*, 519–532. https://doi.org/10.1016/j.cell.2011.06.052.

Hikabe, O., Hamazaki, N., Nagamatsu, G., Obata, Y., Hirao, Y., Hamada, N., Shimamoto, S., Imamura, T., Nakashima, K., Saitou, M., et al. (2016). Reconstitution *in vitro* of the entire cycle of the mouse female germ line. Nature *539*, 299–303. https://doi.org/10.1038/nature20104.

Hill, P.W.S., Leitch, H.G., Requena, C.E., Sun, Z., Amouroux, R., Roman-Trufero, M., Borkowska, M., Terragni, J., Vaisvila, R., Linnett, S., et al. (2018). Epigenetic reprogramming enables the primordial germ cell-to-gonocyte transition. Nature *555*, 392–396. https://doi.org/10.1038/nature25964.

Kagiwada, S., Kurimoto, K., Hirota, T., Yamaji, M., and Saitou, M. (2013). Replication-coupled passive DNA demethylation for the erasure of genome imprints in mice. The EMBO Journal *32*, 340–353. https://doi.org/10.1038/emboj.2012.331.

Liu, M., Zhu, Y., Xing, F., Liu, S., Xia, Y., Jiang, Q., and Qin, J. (2020). The polycomb group protein PCGF6 mediates germline gene silencing by recruiting histone-modifying proteins to target gene promoters. J. Biol. Chem. *295*, 9712–9724. https://doi.org/10.1074/jbc.RA119.012121.

Mochizuki, K., Sharif, J., Shirane, K., Uranishi, K., Bogutz, A.B., Janssen, S.M., Suzuki, A., Okuda, A., Koseki, H., and Lorincz, M.C. (2021). Repression of germline genes by PRC1.6 and SETDB1 in the early embryo precedes DNA methylation-mediated silencing. Nat Commun *12*, 7020. https://doi.org/10.1038/s41467-021-27345-x.

Ohinata, Y., Payer, B., O'Carroll, D., Ancelin, K., Ono, Y., Sano, M., Barton, S.C., Obukhanych, T., Nussenzweig, M., Tarakhovsky, A., et al. (2005). Blimp1 is a critical determinant of the germ cell lineage in mice. Nature *436*, 207–213. https://doi.org/10.1038/nature03813.

Sachs, M., Onodera, C., Blaschke, K., Ebata, K.T., Song, J.S., and Ramalho-Santos, M. (2013). Bivalent Chromatin Marks Developmental Regulatory Genes in the Mouse Embryonic Germline in Vivo. Cell Rep *3*, 1777–1784. https://doi.org/10.1016/j.celrep.2013.04.032.

Sasaki, K., Yokobayashi, S., Nakamura, T., Okamoto, I., Yabuta, Y., Kurimoto, K., Ohta, H., Moritoki, Y., Iwatani, C., Tsuchiya, H., et al. (2015). Robust In Vitro Induction of Human Germ Cell Fate from Pluripotent Stem Cells. Cell Stem Cell *17*, 178–194. https://doi.org/10.1016/j.stem.2015.06.014.

Seisenberger, S., Andrews, S., Krueger, F., Arand, J., Walter, J., Santos, F., Popp, C., Thienpont, B., Dean, W., and Reik, W. (2012). The Dynamics of Genome-wide DNA Methylation Reprogramming in Mouse Primordial Germ Cells. Mol Cell *48*, 849–862. https://doi.org/10.1016/j.molcel.2012.11.001.

Wang, Q., Yu, G., Ming, X., Xia, W., Xu, X., Zhang, Y., Zhang, W., Li, Y., Huang, C., Xie, H., et al. (2020). Imprecise DNMT1 activity coupled with neighbor-guided correction enables robust yet flexible epigenetic inheritance. Nature Genetics *52*, 828–839. https://doi.org/10.1038/s41588-020-0661-y.

Yamashiro, C., Sasaki, K., Yabuta, Y., Kojima, Y., Nakamura, T., Okamoto, I., Yokobayashi, S., Murase, Y., Ishikura, Y., Shirane, K., et al. (2018). Generation of human oogonia from induced pluripotent stem cells in vitro. Science *362*, 356–360. https://doi.org/10.1126/science.aat1674.

Yang, X., Hu, B., Hou, Y., Qiao, Y., Wang, R., Chen, Y., Qian, Y., Feng, S., Chen, J., Liu, C., et al. (2018). Silencing of developmental genes by H3K27me3 and DNA methylation reflects the discrepant plasticity of embryonic and extraembryonic lineages. Cell Res *28*, 593–596. https://doi.org/10.1038/s41422-018-0010-1.

Yokobayashi, S., Liang, C.-Y., Kohler, H., Nestorov, P., Liu, Z., Vidal, M., van Lohuizen, M., Roloff, T.C., and Peters, A.H.F.M. (2013). PRC1 coordinates timing of sexual differentiation of female primordial germ cells. Nature *495*, 236–240. https://doi.org/10.1038/nature11918.